Efficient Ranking-Based Methodologies in the Optimal Design of Large-Scale Chemical Processes under Uncertainty

by

Sami Saeed Bahakim

A thesis
presented to the University of Waterloo
in fulfillment of the
thesis requirement for the degree of
Master of Applied Science
in
Chemical Engineering

Waterloo, Ontario, Canada, 2014

AUTHOR'S DECLARATION

I hereby declare that I am the sole author of this thesis. This is a true copy of the thesis, including any required final revisions, as accepted by my examiners.

I understand that my thesis may be made electronically available to the public.

Abstract

Chemical process design is still an active area of research since it largely determines the optimal and safe operation of a new process under various conditions. The design process involves a series of steps that aims to identify the most economically attractive design typically using steady-state optimization. However, optimal steady-state designs may fail to comply with the process constraints when the system under analysis is subject to uncertainties in the inputs (e.g. the composition of a reactant in a feedstream) or in the system's parameters (e.g. the activation energy in a chemical reaction). This has motivated the development of systematic methods that explicitly account for uncertainty in optimal process design. In this work, a new efficient approach for the optimal design under uncertainty is presented. The key idea is to approximate the process constraint functions and outputs using Power Series Expansions (PSE)-based functions. A ranking-based approach is adopted where the user can assign priorities or probabilities of satisfaction for the different process constraints and process outputs considered in the analysis. The methodology was tested on a reactor-heat exchanger system, the Tennessee Eastman plant, which is an industrial benchmark process, and a post-combustion CO_2 capture plant, which is a large-scale chemical plant that has recently gained attention and significance due to its potential to mitigate CO_2 emissions from fossil-fired power plants. The results show that the present method is computationally attractive since the optimal process design is accomplished in shorter computational times when compared to the stochastic programming approach, which is the standard method used to address this type of problems.

Furthermore, it has been shown that process dynamics play an important role while searching for the optimal process design of a system under uncertainty. Therefore, a stochastic-based simultaneous design and control methodology for the optimal design of chemical processes under uncertainty that incorporates an advanced model-based scheme such as Model Predictive Control (MPC) is also presented in this work. The key idea is to determine the time-dependent variability of the system that will be accounted for in the process design using a stochastic-based worst-case variability index. A case study of an actual wastewater treatment industrial plant has been used to test the proposed methodology. The MPC-based simultaneous design and control approach provided more economical designs when compared to a decentralized multi-loop PI control strategy, thus showing that this method is a practical approach to address the integration of design and control while using advanced model-based control strategies.

Acknowledgements

First and foremost, I would like to express my sincere gratitude to my supervisor Professor Luis Ricardez-Sandoval for his continuous support and guidance during my entire Master's program. In addition to the great deal of technical knowledge I have acquired under his supervision, I have also learned how to communicate efficiently, how to conduct myself professionally, and how to approach any challenge with fortitude and determination. I would also like to thank Professor Ali Elkamel, for his assistance during my early days in Master's studies.

I would also like to extend my thanks the readers of my thesis, Professor Mark Pritzker and Professor Nasser Mohieddin Abukhdeir.

I would also like to thank my colleagues, Jingde Li, Jennifer Charry-Sanchez, Shabnam Rasoulian, David Evans, Hussein Sahraei, Darinel Valencia-Marquez and Bhushan Patil for the helpful discussions, and to all my friends at Waterloo for making my time here a very enjoyable experience.

Finally, I would like express my deepest gratitude to my parents and my brothers who have always been there for me. As I move on to the next chapter of my life, it is comforting to know that, regardless of wherever life takes me, I will always have a loving family to lean on.

Dedicated to my beloved parents

Table of Contents

List of Figures

List of Tables

Nomenclature

List of English symbols

a	Constraint limits
A_{cl}	Cross-sectional area of clarifier
A_{cond}	Heat transfer area of condenser
A_{HX}	Heat transfer area of cross heat-exchanger
A_t	Heat exchanger transfer area
C	Number of disturbances
C_{A0}	Initial concentration of reactant A
C_{A1}	Concentration of A remaining in the product stream
C_{abs}	Cost of absorber
CC	Capital Costs
$CCap$	Carbon Capture
C_{cond}	Cost of condenser
C_{HX}	Cost of cross heat-exchanger
CMF	Cumulative distribution function
c_o	Concentration of dissolved oxygen
C_p	Heat capacity of the recycled flow
C_{pw}	Heat capacity of the cooling water
C_{reb}	Cost of reboiler utility operation
c_s	oxygen specific saturation
C_{steam}	Cost of steam utility
$CSTR$	Continuous Stirred Tank Reactor
C_{strp}	Cost of stripper
$\mathbf{d}$	Design variables
D_{abs}	Diameter of absorber

DC	Dynamic Costs
$\mathbf{d}^l, \mathbf{d}^u$	Lower and upper bounds for design variables
D_{strp}	Diameter of stripper
E	Activation energy
eig	Eigenvalues
F_0	Reactor feed flowrate
F_2	Recycle stream flowrate
F_c	Cost correction factor
F_d	Design factor
F_{in}	Inlet flowrate of flue gas stream
fk	Aeration turbine speed
fk_d	fraction of death biomass (to substrate)
F_m	Material factor
F_p	Pressure factor
GA	Genetic Algorithm
$\mathbf{h}$	Process constraints
H	Heat of reaction
H_{abs}	Height of absorber
H_{strp}	Height of stripper
$\mathbf{J}$	Nonlinear dynamic process model (open-loop)
$\mathbf{J}_{\text{closed}}$	Closed-loop dynamic process model
k	Sampling period
k_0	Rate constant
k_{01}	Oxygen demand constant
k_c	Specific cellular activity
k_d	Biomass death rate
k_{la}	Oxygen transfer into the water constant
k_s	Saturation constant

L	Number of uncertain parameters
lb	Height of the *bth* layer in the clarifier
ld	Height of the *dth* layer in the clarifier
L_{min}	Reactor's minimum allowable liquid level
lr	Height of the *rth* layer in the clarifier
M	Control horizon
M&S	Marshall & Swift equipment index
$\mathbf{M}^{(i)}$	i^{th} order sensitivity term
MC	Monte Carlo
MEA	Methanolamine solvent
m_i	i^{th} measurements in the TE plant
MPC	Model Predictive Control
n_{ran}	Number of random samples
N	Number of sampled realizations in system's uncertainty/disturbance
OC	Operating Costs
$\mathbf{p}$	Model parameters
$\mathbf{p}\sim$	Uncertain model parameters
Pb_h	Probability of constraint satisfaction
PDF	Probability Distribution Function
p_G	Desired production of product G
p_H	Desired production of product H
PI	Proportional Integral
P_{max}	Reactor's maximum allowable pressure
PSE	Power Series Expansion
q	Expansion order
Q_{cond}	Condenser heat duty
Q_{HE}	Amount of heat transferred
Q_{reb}	Reboiler heat duty

R	Gas constant
R	Prediction horizon
ROR	Rate of return
s	Substrate concentration inside the bioreactor
$SB\text{-}WCV$	Stochastic-based worst-case variability
s_i	Substrate concentration in the input wastewater stream
s_{ir}	Substrate concentration entering the bioreactor
SQP	Sequential Quadratic Programming
t	Time
T_0	Feed temperature
T_1	Reactor temperature
T_2	Recycle stream temperature
TE	Tennessee Eastman
T_{in}	Inlet temperature of flue gas stream
T_{lean}	Lean solvent temperature
T_{reb}	Reboiler temperature
T_{w1}	Cooling water inlet temperature
T_{w2}	Cooling water exit temperature
$\mathbf{u}$	Model inputs or manipulated variables
U	Overall heat transfer coefficient
$\mathbf{u}^{\sim}$	Uncertain model inputs
$\mathbf{u}^l, \mathbf{u}^u$	Lower and upper bounds for model inputs
V	Reactor volume
V_b	Bioreactor volume
vs	Rate of settling for activated sludge
W	Cooling water flowrate
w	Bioreactor outlet flow

w_1	Exit stream flowrate
w_2	Recycle flowrate
w_i	Flowrate of input wastewater stream
w_p	Purge stream flowrate
w_r	Treated water flowrate
$\mathbf{x}$	State variables
X	Conversion of reactant A
$\mathbf{y}$	Model outputs
$\mathbf{z}$	Steady state process model

List of Greek symbols

$\boldsymbol{\theta}$	System's uncertain variables
$\boldsymbol{\alpha}$	Probability distribution parameters
ξ_h	Extreme possible value at user-defined Pb_h
$\boldsymbol{\eta}$	Set of decision variables
$\Re$	Set of real numbers
ΔH_{vap}	Steam's heat of vaporization
Θ	Conversion factor
φ	% of CO_2 capture
ζ	Purity of CO_2 in the product stream
$\boldsymbol{\varepsilon}$	Process inputs
$\boldsymbol{\varsigma}$	Variables that can be adjusted for control
$\boldsymbol{\rho}$	Input variables that are kept constant
$\boldsymbol{\lambda}$	Disturbances
$\boldsymbol{\nu}$	Unmeasured disturbances
$\boldsymbol{\omega}$	Measured disturbances
$\boldsymbol{\delta}$	Process outputs

$\boldsymbol{\gamma}$	Controlled output variables
$\boldsymbol{\chi}$	Output variables that are not in closed-loop
$\boldsymbol{\kappa}$	Optimization design parameters and operating conditions
$\boldsymbol{\Lambda}$	Controller tuning parameters
$\boldsymbol{\Gamma}$	MPC input weights
$\boldsymbol{\Omega}$	MPC output weights
ϕ	Cost function
Π	User-predefined confidence levels
$\boldsymbol{\gamma}_{sp}$	Output set-points
ψ_z^*	SB-WCV index at a specified user-defined probability level
$\boldsymbol{\psi}$	Set of SB-WCV indexes
$\mathbf{g}(\boldsymbol{\psi})$	Worst variability distribution function
$\mathbf{\Delta u}$	Control moves
μ	Mean value
σ	Standard deviation
β	Biomass concentration inside the bioreactor
β_i	Biomass concentration in the input wastewater stream
β_{ir}	Biomass concentration entering the bioreactor
β_b	Biomass concentration in the clarifier, layer *b*
β_d	Biomass concentration in the clarifier, layer *d*
β_r	Biomass concentration in the clarifier, layer *r*
ϑ	specific growth rate
μ_y	fraction of converted substrate to biomass

Subscripts

abs	Absorber
cl	Clarifier

cond	Condenser
HX	Cross heat exchanger
lean	Lean amine solvent
max	Maximum
min	Minimum
reb	Reboiler
strp	Stripper
vap	Vaporization

Chapter 1
Introduction

Chemical process design is an essential task performed to achieve the desired throughput and quality of the final products in the face of safety, environmental, operational and physical constraints at minimum cost. The design process involves a series of steps that aims to identify the most economically attractive design typically using steady-state optimization [1,2]. Although chemical processes have been traditionally designed using this approach, the designs obtained from those analyses may fail to comply with the process constraints when it is subjected to uncertainties in the inputs (e.g., the composition of a reactant in a feedstream) or in the system's parameters (e.g., the activation energy in a chemical reaction). The resulting instances of infeasibility or constraint violations due to the presence of uncertainties will have adverse effects on the process economics. For example, a chemical process whose equipment sizing and operating conditions have been designed based on optimal steady-state design economics may be subjected to uncertainty in the composition of raw materials. This may result in products that may not meet the clients' minimum products' specifications and thus have no market for these goods or can only gain low profit margins because of their low quality. Therefore, the design obtained from steady-state calculations at the nominal operating conditions may no longer be 'optimal' when operating under uncertainty. Since uncertainties are inevitable and inherent in almost every process, the typical approach used to address this problem is to add overdesign factors, e.g., adding an additional (percentage) volume to a storage tank will aim to accommodate the uncertainty in the system at the expense of increasing the costs for this process. However, the main limitation with this approach is that there is no systematic method to assign overdesign factors and is typically done from process experience, using process heuristics or even arbitrarily. Moreover, this practice of overdesigning a process to ensure feasibility under uncertainty has been proven to be costly, especially in the design of an expensive process unit or when uncertain parameters only affect specific equipment or process units. This has motivated the development of systematic methods that explicitly account for uncertainty in the calculation of the optimal process design. The aim of these methods is to assess the effect of the uncertainty on the process outputs (or constraints), and then adjust the design of the plant (such as equipment sizes and operating conditions) to accommodate those uncertainties and maintain the operability of the plant within its feasible limits and close to its process design goals. The designs obtained from those

analyses are expected to specify the most economically attractive process that complies with the process constraints in the presence of uncertainty. Several methods have been proposed in the literature to address the optimal design of chemical processes under uncertainty, e.g., stochastic programming, multi-scenario optimization and chance-constrained programming. Each of the methods proposed in the literature has its own benefits and limitations in terms of computational efficiency, conservatism of the designs, ease of implementation, and its applicability to large-scale nonlinear chemical processes. The development of practical computationally-efficient methods that can be applied to design industrially-relevant chemical plants is still an active area of research that has received great attention due to its relevance to the field. It is the aim of this study to develop a new practical approach to address the optimal design of large-scale chemical processes under uncertainty. The benefits of the proposed method have been evaluated using two industrial benchmark chemical processes.

The Tennessee Eastman (TE) process is a widely studied industrial problem published by the Tennessee Eastman Company as a process simulation for academic research. A mathematical model describing the process plant is not explicitly given for this process; instead, a FORTRAN code has been provided for process simulations with no clear description of the actual process or chemical species being used. The process consists of a reactor, recycle compressor, partial condenser and flash separator with a recycle loop to produce two liquid products (labelled as G and H) and by-product F using four gaseous reactants, A, C, D and E. Hence, the Tennessee Eastman plant serves as a suitable design problem as it tests the applicability of the method to be developed in this study for large-scale systems. In addition, although this plant has been widely used by the academic community to test or validate different techniques or methods proposed in the field of process systems, the optimal steady-state design under uncertainty of this plant has not been reported in the open literature to the author's knowledge.

Another industrially-relevant process that has received attention in recent years due to its significance to reduce greenhouse gas emissions is post-combustion CO_2 capture plants. The effect of greenhouse gases on the global climate, also known as global warming, has become more drastic in recent decades and brought concerns to scientists and the general public about its possible threats to the environment [3]. Carbon dioxide (one of the greenhouse gases) has a significant impact on global warming [4,5] and is sometimes considered the principal contributor among all the other greenhouse

gases [6]. A large source of CO_2 emissions to the environment are from power plants using fossil fuel combustion sources such as coal and natural gas. In general, coal-based power plants release twice the amount of CO_2 per unit of electricity generated than natural gas-based power plants [7,8]. Currently, fossil fuels are the primary source of energy due to its availability, abundance, energy density and existing infrastructure for distribution and delivery, making it a more reliable and economically attractive option than newer alternative sources such as nuclear or renewables [9–11]. This has motivated approaches to mitigate and control CO_2 emissions for the continuous use of fossil fuel energy. CO_2 capture and storage is considered to be an effective option for reducing the amount of CO_2 released to the environment [12–14] and has been implemented on various chemical processes, e.g., coal gasification, natural gas production, and fertilization [15]. As with any other chemical process, CO_2 capture is subject to inherent uncertainties in its input streams or system parameters. This may have a direct effect on its performance such as meeting the target CO_2 removal amounts or it may also alter the process operation causing undesired variability in operating variables such as temperature or pressure, which may lead to a plant shutdown in extreme cases. Since any plant is subject to uncertainties, the design of its process equipment is essential to ensure that the plant is operational under these uncertain circumstances. Input variables having their own ranges of variability will affect the process differently and thus require specific designs to operate feasibly. Therefore, a study of the effect of process uncertainties on the optimal design of a post-combustion CO_2 capture plant can provide useful new insights. To the author's knowledge, such studies have not yet been performed for this process.

A key limitation in optimal process design is that it is usually performed using steady-state optimization calculations, although it has been shown that process dynamics does play an important role while searching for the optimal process design of a system under uncertainty. The selection of the optimal process design while taking into account the process dynamic performance, also referred to as *simultaneous design and control* or *integration of design and control*, has been suggested by both academia and industry [16–22]. Unlike the traditional sequential design approach which obtains optimal process designs first based on steady-state analysis and then only designs the process controls from dynamic analysis, the concept of integration of design and control aims to account for both steady-state and dynamic analysis in one single step to obtain both optimal process design and controllability characteristics simultaneously. The key idea is that processes designed based on steady-state economics may not provide suitable controllability of the outputs in the face of

disturbances. For example, a case study presented by Luyben [23] of a temperature-controlled reaction in a jacketed CSTR, assesses two different configurations: using a single large reactor or two smaller reactors in series. Steady-state economics suggested that using the two smaller reactors in series is more profitable as the capital costs are lower. However, dynamic response analysis of both configurations to a step disturbance in the heat of reaction showed that the larger single reactor provided better controllability of the reactor's temperature. Hence, this illustrates the importance of taking process dynamics into account at the design stage. To obtain the optimal design and control of a process, knowledge of the disturbances is important to determine its effect on the dynamic response of the system, and thus adjust the sizing of equipment and aggressiveness of the control strategy to accommodate those disturbances. While some processes are subject to disturbances that follow a specific time-dependent behaviour, e.g., an oscillatory behaviour, there are processes for which the occurrence of a particular realization of the disturbances is stochastic or random. For the latter case, a probabilistic description is a suitable explanation of its behavior. Although methodologies exist for the integration of process design and control, most of the methods have assumed that the disturbances follow a certain class of time-dependent functions, e.g., a sinusoidal function with uncertain (critical) parameters [21,24], or a series of step changes with unknown (but bounded) magnitudes [25,26], or calculated from a worst-case scenario formulation [27,28]; very few methodologies have assumed that the disturbance follows a probabilistic-based behavior [29]. Probabilistic-based simultaneous design and control have not been widely explored, though it offers more economical optimal designs by reducing the conservativeness associated with the current approaches available in the literature. On the other hand, model-based control strategies such as Model Predictive Control (MPC) have matured enough and gained wide interest in the industrial applications due to its superior features over conventional feedback controllers. MPC offers optimal and multivariable control of systems and explicitly considers and can maintain in principle the dynamic operability of the manipulated and controlled variables within their feasible limits. As part of this research study, a new methodology for integration of design and control under the effect of stochastic-based disturbances using MPC has been developed.

1.1 Research objectives and contribution

The research carried out in this work aims to achieve the following:

i. Develop a practical and efficient method for the optimal design of large-scale chemical processes under uncertainty. A ranking-based approach will be adopted whereby the user can assign priorities or probabilities of satisfaction for the different process constraints and model outputs considered in the analysis. The user-defined ranking structure will determine the level of conservatism of the designed plant.

ii. Implement the method developed in this work to address the optimal design under uncertainty of a post-combustion CO_2 capture plant. This contribution will demonstrate the applicability of the proposed approach for large-scale chemical processes. This method will be used to study the effect of process uncertainties in the input flue gas stream on the design of CO_2 capture plants.

iii. Develop a method to integrate design and an advanced control strategy under dynamic uncertainty. In contrast to the method proposed in the first objective outlined above, which aims to specify optimal steady-state designs under uncertainty, a key characteristic of the method proposed in this point is that it will explicitly take into account the time-dependent variability of the disturbances and the dynamic operability of the process while searching for the optimal process design . A model-based Model Predictive Control (MPC) will be implemented as the control strategy in addition to the probabilistic ranking-based feature to test the compliance of the process constraints in the analysis. The proposed method will be tested using an industrial wastewater treatment plant located in Manresa, Spain.

1.2 Outline of thesis

This thesis is organized in six chapters as follows:

Chapter 2 presents the literature review on the key subjects covered in this work. The studies relevant to the different methods and approaches to the optimal process design under uncertainty are reviewed. Several studies carried out to address the optimal CO_2 capture process plants with and without uncertainty are also summarized in this chapter. Further, a review on the simultaneous design and control strategies that have been proposed in the literature is discussed at the end of this chapter.

Chapter 3 presents a novel approach for the optimal design of chemical processes in the presence of uncertainty. This includes a ranking-based approach whereby the user can assign priorities or probabilities of satisfaction for the different process constraints and model outputs considered in the analysis. The key idea in this work is to approximate the process constraint functions and process outputs using Power Series Expansion (PSE)-based functions. The method was initially tested on a reactor-heat exchanger system and the Tennessee Eastman process.

Chapter 4 presents a study on the effect of process uncertainty on the optimal design of a CO_2 capture plant. Such a study is important since the presence of uncertainties can affect the process operations leading to lower plant performance or may even deem the process inoperable. The ranking-based probabilistic method presented in Chapter 3 is used for the optimal design of the CO_2 capture plant under uncertainty. In this work, uncertainty is assumed in three input variables affecting the operation of a CO_2 capture plant, namely the CO_2 content, temperature and flow rate of the flue gas stream. Several case scenarios considering single and simultaneous uncertainties are investigated.

A stochastic-based simultaneous design and control methodology for chemical processes under uncertainty is presented in Chapter 5. The key novelties of the proposed method include the use of a multivariable advanced Model Predictive Control (MPC) scheme in the analysis and the computation of a stochastic-based worst-case variability (SB- WCV) index, which accounts for the probabilistic nature of the disturbances. A case study of an actual wastewater treatment industrial plant is presented and used to test the proposed method and compare its performance to that obtained using the

sequential design approach and then a simultaneous design and control method using conventional PI-based control schemes.

Chapter 6 summarizes the key research outcomes of the present study and discusses the future research avenues that can be further explored in this area.

Chapter 2

Literature Review

The field of optimal process design under uncertainty has gained wide interest among researchers due to the fact that these uncertainties may cause serious operational problems if not accounted for at the design stage. In addition, the presence of uncertainty is almost inherent in every process due to lack of knowledge or imprecise measurements, making it a general design issue and not just specific to certain processes. This chapter presents a review on the different methods and approaches published in the literature for optimal design of chemical processes under uncertainty. Similarly, a comprehensive review on the design of CO_2 capture plants is presented since this specific process plant will be used to study the effect of uncertainties on its optimal design. Further, the methodologies that have been proposed in the literature for optimal design and control of chemical processes under uncertainty are revised with special emphasis on those approaches that have described disturbances using a stochastic (probabilistic-based) approach.

2.1 Optimal process design under uncertainty

The problem of optimal process design under uncertainty can be conceptually posed as follows:

$$\begin{array}{ll} \text{minimize} & \text{Expected Total Annualized Cost } (\Phi) \\ \text{Subject to} & \text{Process model, Process Design Equatons} \\ & \text{Process constraints (equality or inequality)} \\ & \text{Design limits} \end{array} \qquad (2.1)$$

The objective function consists of the total economic costs of the process that are typically annualized and defined in terms of the process' capital and operating costs. Since uncertainty will be accounted for in this problem, the expected value of the total capital (CC) and operating (OC) costs becomes the objective function to be minimized. A mathematical model (**z**) describing the process is usually available or derived from first-order principles (mechanistic) or from experimental data (empirical modelling). Uncertainty in the process inputs (**u**) or in the model parameters (**p**) will result in

variability in the outputs (**y**) and states (**x**) of the system, and thus in the evaluations of the process feasibility constraints which may include safety, environmental or operational constraints. Problem (2.1) aims to find a process design (**d**) and process operation (**u**) that remains feasible with respect to the process constraints (**h**) under each realization of uncertainty ($\boldsymbol{\theta}$) which includes both input and parameter uncertainty. Based on the above, the mathematical description of problem (2.1) is as follows:

$$\begin{aligned} \min_{\boldsymbol{\eta}=[\mathbf{d},\mathbf{u}]} \ & \Phi = E[\mathrm{CC}(\mathbf{d},\mathbf{x},\mathbf{u},\boldsymbol{\theta}) + \mathrm{OC}(\mathbf{d},\mathbf{x},\mathbf{u},\boldsymbol{\theta})] \\ \text{s.t.} \quad & \mathbf{z}(\mathbf{d},\mathbf{p},\mathbf{x},\mathbf{y},\mathbf{u},\boldsymbol{\theta}) = \mathbf{0} \\ & \mathbf{h}(\mathbf{d},\mathbf{x},\mathbf{u},\boldsymbol{\theta}) \le \mathbf{0} \\ & \mathbf{d}^l \le \mathbf{d} \le \mathbf{d}^u \\ & \mathbf{u}^l \le \mathbf{u} \le \mathbf{u}^u \end{aligned} \tag{2.2}$$

The uncertain inputs and model parameters ($\boldsymbol{\theta}$) are typically assumed to follow some known probability distributions from process knowledge or heuristics. However, usually they are random and assumed to follow a particular probabilistic description.

A popular method used to account for uncertainty in process design is referred to as the stochastic programming approach [30–32]. This method evaluates the system's optimal design by performing extensive simulations of the actual plant's model (**z**) due to multiple realizations in the uncertain parameters ($\boldsymbol{\theta}$). The sampling of the uncertain realizations is usually based on the Monte Carlo sampling method [33]. Different approaches that employ the stochastic programming approach are available in literature, e.g., the stochastic branch and bound method [34,35] and the scenario-based simulation method, which assigns likelihood of occurrence (probability) to each uncertain scenario [36]. The multi-scenario optimization approach is a stochastic programming method that has also been proposed for optimal process design under uncertainty [37–42]. In this method, two stages are considered: the design stage and the operation stage. Selection of the first (design, **d**) stage aims to minimize the expected value of the costs incurred due to the operating conditions specified in the second (operation, **u**) stage in the presence of uncertainty. Scenarios of the uncertain realizations are introduced into the second stage of the formulation, where a feasible solution will be able to handle each scenario by manipulating the operating variables (**u**) of the process. For continuous uncertain domains, discrete sampling is required in the multi-scenario optimization approach. The more uncertain realizations (scenarios) included in the analysis, the more accurate the results are expected

to be at the expense of higher computational costs. The latter is a key limitation of this approach to address the optimal design of large-scale process systems [43].

The multi-scenario approach is suitable when process reliability, i.e., full compliance of the process constraints, is critical since it requires feasibility for all the possible uncertain scenarios at minimum cost. However, there are cases where the compliance of specific process constraints is critical (safety-related) whereas violation in other process constraints may be allowed with no actual risk to the process operation or products quality. For example, a slight variation in the liquid level of a storage tank away from its corresponding feasible limits due to uncertainties in the process may cause no serious implications to the plant's economics. On the other hand, the variability in a reactor's working temperature outside its feasible limits due to uncertainty in the system parameters, e.g., reaction rate kinetic parameters, has a significant impact on the plant's economics because it directly affects the products' throughput and quality. Since compliance of the process constraints normally require larger (more expensive) designs, it may sometimes be more economical to allow violation of less critical constraints (e.g. tank liquid level) under uncertainty, than to design a robust process that satisfies the constraints at all times. In the latter case, it is therefore desired to develop a ranking-based design approach that ensures feasibility of the critical higher ranked constraints (e.g. reactor temperature) at all times but allows less ranked (non-critical) constraints to be partially violated with the aim of achieving more economical but yet feasible operational process designs.

A systematic method that implements the ranking-based approach is chance constrained programming [44]. The conceptual formulation of this approach is as follows:

$$
\begin{aligned}
\min_{\boldsymbol{\eta}=[\mathbf{d},\mathbf{u}]} \ & \Phi = E[\mathrm{CC}(\mathbf{d},\mathbf{x},\mathbf{u},\boldsymbol{\theta}) + \mathrm{OC}(\mathbf{d},\mathbf{x},\mathbf{u},\boldsymbol{\theta})] + \varpi \,\mathrm{var}[\mathrm{CC}(\mathbf{d},\mathbf{x},\mathbf{u},\boldsymbol{\theta}) + \mathrm{OC}(\mathbf{d},\mathbf{x},\mathbf{u},\boldsymbol{\theta})] \\
\text{s.t.} \quad & \mathbf{z}(\mathbf{d},\mathbf{p},\mathbf{x},\mathbf{y},\mathbf{u},\boldsymbol{\theta}) = \mathbf{0} \\
& \mathrm{P}\{\mathbf{h}(\mathbf{d},\mathbf{x},\mathbf{u},\boldsymbol{\theta}) \le \mathbf{0}\} \ge \Pi_h \\
& \mathrm{P}\{\mathbf{d}^l \le \mathbf{d} \le \mathbf{d}^u\} \ge \Pi_d \\
& \mathrm{P}\{\mathbf{u}^l \le \mathbf{u} \le \mathbf{u}^u\} \ge \Pi_u
\end{aligned}
\qquad (2.3)
$$

In this method, the objective function aims to minimize the expected value and variance of the cost function whereas the constraints are redefined as minimum probability of satisfaction $\mathrm{P}\{\cdot\}$ held by the actual physical and process constraints under uncertainty. ϖ is a weighting factor that specifies the importance of the variability in the cost function due to random realizations in the uncertain

parameters ($\boldsymbol{\theta}$); Π_h, Π_d and Π_u are user-predefined confidence levels between 0 and 1. To calculate the probabilities of constraint satisfaction $P\{\cdot\}$, monotonic relationships between individual uncertain variables and its corresponding constrained variables are used to map the output boundaries according to the region of the uncertain inputs. This information is then used in a multivariate integration to compute the probabilities in the limited region of the uncertain inputs. This chance-constrained programming is therefore transformed into a deterministic equivalent optimization problem. The main challenge with this approach is the need to evaluate multiple integrals to compute expected values (and/or variances) for the objective function and constraints (at a given probability limit Π) in the presence of uncertainty. Li et al. [45–47] developed a chance-constrained based methodology that addressees several industrial problems, i.e., production planning, process design and operation, optimal control. Ostrovsky et al. [48–50] developed a different approach to transform chance constraints into deterministic constraints using the concept of uncertainty regions. This method searches for the optimal form (or shape) and location of the 'uncertain space', which is a decision variable in the optimization formulation by assuring that the uncertain variables fall within this region with a high probability (close to unity). This approximation in the uncertainty region reduces the computational costs in the evaluation of multiple integrals. Despite the progress made in this area, the need to evaluate multivariate integrals to compute the statistic operations and probabilistic constraints $P\{\cdot\}$, and the computational effort associated with this calculation, are the main challenges faced towards the application of these methodologies for large-scale industrial chemical plants.

In summary, the computational challenges associated with both stochastic programming and chance-constrained programming approaches hinder their applicability to design large-scale chemical processes under uncertainty. As a result, there have been continuous efforts to develop more efficient methodologies for the optimal design of process under uncertainty.

2.2 Post-combustion CO_2 capture plant

Several approaches have been proposed to capture CO_2 including pre-combustion [51], post-combustion [52–55] and oxy-combustion method [56,57]. Post-combustion using chemical absorption with amine solvents is by far the most common and developed technique to capture CO_2 from flue gas having low CO_2 concentrations. This method is preferred over the other two approaches

since it can be implemented in existing fossil-fired power plants without major changes in equipment configurations that would be more costly [3,54,58,59]. One such method is chemical absorption. A common approach is to react the CO_2 in the flue gas with an amine solvent to form an intermediate compound which decomposes with the application of heat to regenerate the solvent. Monoethanolamine (MEA) is the most widely used amine solvent for this purpose due to its high reactivity with CO_2 [60]. Typically, the carbon capture unit includes an absorption column in which CO_2 in the entering flue gas stream is captured by the MEA solvent, a stripping column with a reboiler at its bottom to heat the CO_2-rich solvent and regenerate it, and a condenser is typically located at the top of the stripper to recover a CO_2-rich gas stream. Heat exchangers are also included in the plant layout to maintain the temperature requirements for this process. A specific description of this process is presented in Chapter 4.

Several studies have been performed to optimize the design and operation of MEA-based CO_2 capture plants [58,59,61–66]. The focus of those studies is to search for the process operations (e.g., amine solvent inlet concentration and temperature, stripper operating pressure and CO_2 loading) and design decisions (e.g., number of stages for the absorber and stripper columns) that minimize the plant economics. The resulting optimal CO_2 capture plant design is expected to satisfy its process and target constraints (e.g. CO_2 emission, CO_2 removal) under nominal operating conditions. However, in the presence of uncertainties in the process inputs, these designs may fail to comply with the desired targets or process constraints. In a practical context, uncertainty is inherent in every process. Hence, efforts to account for uncertainty at the design stage have been suggested and widely studied in the field of process systems engineering [67–71]. In the context of CO_2 capture plants, the effect of uncertainties in the prices of fuel and CO_2 on the investment behavior of choosing between coal, gas and nuclear power plants has been studied by Yang et al [72]. The option of installing a carbon capture unit has been considered in the analysis of coal and gas power plants. In another study by Geske and Herold [73], uncertainties in CO_2 price and technology development (thermal efficiency and capital costs) have been considered in the analysis of installing a CO_2 capture plant to an already existing plant. Several other studies have investigated the effect of uncertainty in the prices of key economic parameters (e.g. fuel, electricity, CO_2) on the optimal planning of power generation plants coupled with CO_2 capture when considering different technologies or timing of investments [74–79]. Nonetheless, those studies have targeted the effects of financial and risk uncertainties on higher-level decisions of planning, investment and technology selection rather than on the effect of process-level

uncertainties on process operation and equipment design. To the author's knowledge, no study in the literature has investigated the latter case.

2.3 Simultaneous design and control methodologies

The design of chemical processes has been traditionally performed following a sequential approach where the process design parameters such as the equipment sizes and the process operating conditions are first estimated from the steady-state optimization of the process economics. Once the optimal steady-state design has been specified, process controllability is then addressed by assessing the dynamic response of the plant in closed-loop in the presence of disturbances and model parameter uncertainty. To achieve the required control performance, this second stage of the conventional design method involves the selection of suitable control structures, control algorithms and their corresponding tuning parameters that can meet the process design goals. However, the process design parameters and operating conditions specified in the first stage of the design analysis will impose a limitation on the control system's ability to maintain the feasible and flexible operation of the process in the presence of disturbances or parametric uncertainty [2,80,81]. To accommodate such conditions, overdesign factors can be added to the process design parameters which may lead to the specification of expensive process designs. Hence, the selection of the optimal process design while considering the process dynamic performance in the analysis, also referred to as *simultaneous design and control* or *integration of design and control*, has been suggested by both academia and industry as an attractive alternative to overcome the issues associated with the traditional (sequential) design approach [16–22]. The problem of simultaneous process design and control under uncertainty can be conceptually posed as follows:

$$\begin{array}{ll} \text{minimize} & \text{Expected Total Annualized Cost}: \Phi(t) \\ \text{Subject to} & \text{Dynamic Process Model, Process Design Equatons} \\ & \text{Control Scheme Equations} \\ & \text{Inequality Path Constraints, End Point Constraints} \\ & \text{Design Limits} \end{array} \tag{2.4}$$

Similar to problem (2.1), the objective function in problem (2.4) aims to minimize the total annualized costs. However, since simultaneous design and control problems consider the effect of

time-varying disturbances $\boldsymbol{\theta}(t)$ on the process, the expected value of the cost function is computed with respect to the time domain. Similarly, a dynamic process model ($\mathbf{J}(t)$) usually consisting of differential equations with respect to time are used here rather than steady state models. Besides the introduction of the transient time domain into the problem, a key difference with problem (2.1) is that control scheme equations, and its tuning parameters (Λ), are considered in the calculations. The mathematical description of problem (2.4) is as follows:

$$\begin{aligned}
&\min_{\boldsymbol{\eta}=[\mathbf{d},\mathbf{u},\Lambda]} \Phi = E[\mathrm{CC}(\mathbf{d},\mathbf{x}(t),\mathbf{u}(t),\boldsymbol{\theta}(t),\Lambda) + \mathrm{OC}(\mathbf{d},\mathbf{x}(t),\mathbf{u}(t),\boldsymbol{\theta}(t),\Lambda)] \\
&\text{s.t.} \quad \mathbf{J}(\mathbf{d},\mathbf{p}(t),\mathbf{x}(t),\mathbf{y}(t),\mathbf{u}(t),\boldsymbol{\theta}(t),\Lambda) = \mathbf{0} \\
&\qquad \mathbf{h}(\mathbf{d},\mathbf{x}(t),\mathbf{u}(t),\boldsymbol{\theta}(t),\Lambda) \le \mathbf{0} \\
&\qquad \mathbf{d}^l \le \mathbf{d} \le \mathbf{d}^u \\
&\qquad \mathbf{u}^l \le \mathbf{u}(t) \le \mathbf{u}^u
\end{aligned} \tag{2.5}$$

The process design **d**, the manipulated variables **u** and the controller tuning parameters Λ are optimized to obtain the most economical process that remain dynamically feasible in the face of time-varying disturbances $\boldsymbol{\theta}(t)$.

Most of the methodologies developed for the simultaneous design and control of chemical processes have considered conventional feedback Proportional-Integral (PI) controllers in their analysis [18,25,82–85]. Although plant-wide control is still an active area of research [86–89], advanced model-based control strategies such as Model Predictive Control (MPC) has matured enough after almost three decades of implementation where it has been widely used and recognized in both the industry [90] and in the academia [91–94], making it one of the most significant advances in process control in the last decades [95]. While maintaining the control objectives on spec, the implementation of MPC ensures optimal control action through the optimization framework that is incorporated in its algorithm. MPC also has the advantage to handle constraints in the manipulated and controlled variables explicitly in its algorithm. In addition, it has been shown that MPC may provide better control performance than conventional feedback controllers [96,97]. Hence, it is desired to incorporate MPC in the simultaneous design and control methodology despite some of the computational challenges that are avoided while using conventional feedback controllers, e.g., the need to identify an internal MPC model and solve an optimization problem at each time step. Previous works in the literature that implemented MPC control algorithms in the context of simultaneous design and control are available [21,98–102].

Most of the optimization-based approaches reported in literature for simultaneous design and control follow the same key idea: determine (or specify) the critical realizations in the disturbances and in the uncertain system's parameters that produce the largest deviations in the controlled variables and therefore demand significant efforts from the control system to maintain the process on spec in the presence of these conditions. This is often termed as the *worst-case scenario*, and the variability in the system due to this scenario is called the *worst-case process variability*. This worst-case scenario is then used by the simultaneous design and control methodologies to evaluate the process economics and constraints considered in the formulation. An optimal design and control scheme is referred to as the configuration that can accommodate the worst-case scenario (or critical scenarios identified *a priori*) in a safe and acceptable fashion without violating constraints in the control action movements or in the critical operating variables of the system. The challenge and difference in the approaches available in literature is in the method used to compute this worst-case scenario, e.g., using open-loop controllability indexes [81,82,103–105], from a formal dynamic optimization formulation [16,25,83,106,107], or from the implementation of robust control tools [27,71,99,108–110]. Recent comprehensive reviews on the current techniques and methods on integration of design and control are available [111–113].

Following a worst-case estimation method and then backing off to the closest optimum dynamically feasible and stable design as proposed by the previous methods may often lead to conservative (expensive) designs. This is because these methods use the worst-case (or the critical scenarios) to evaluate the dynamic performance of the system and estimate the optimal feasible design that accommodates this largest variability without considering how often this largest (worst-case) variability may occur during operation, nor considering the level of significance of each process constraint. For example, a large variability in the liquid level in a storage tank (which may cause an overflow) may be tolerated more than the variability in a reactor's temperature that could have more serious effects on the product's quality and the process economics. Therefore, it may be more profitable to allow for the water tank to overflow sometimes rather than overdesign the plant (increased costs), especially if the worst-case scenario causing this overflow is a rare occurrence. The need for a methodology that incorporates the probability of occurrence of worst-case process variability, and ranks variables and systems according to their safety or commercial significance, is motivated by the economic savings it can offer: specify less conservative (economically attractive)

yet dynamically feasible process designs. To date there are very few studies that present stochastic-based approaches for integration of design and control. A recent method presented in the literature for optimal design that has adopted the ranking-based approach was proposed by Ricardez-Sandoval [29]. This work makes use of simulations using Monte Carlo sampling methods to obtain the distribution of the process constraints under uncertainty. A user defined probability limit is assigned to each constraint, which in turn sets the ranking or importance of that constraint. However, the analysis was limited to a simple case study of a CSTR tank, implementing conventional feedback controllers. To the author's knowledge, an approach that implements advanced control strategies such as MPC is still an active area of research and has not been studied for disturbances that follow probabilistic-based (stochastic) descriptions.

2.4 Uncertainty sampling methods

Many of the methods described in this chapter require sampling of uncertain variables from probability distribution functions (PDFs). The Monte-Carlo (MC) sampling technique is one of the most popular methods used for sampling from a probability distribution, which generates n_{ran} pseudorandom numbers to approximate a standard uniform distribution. Then, to obtain the specific values for each random variable, the n_{ran} samples are inverted over the cumulative distribution of the specified PDF for that variable. Another sampling technique called the Latin hypercube sampling (LHS) uses stratification sampling that may provide more accurate estimates of the distribution function [114]. The range of the uncertain variable is divided into intervals of equal probability and a single value is sampled from each interval. In the case of multidimensional uncertainty, the n_{ran} samples obtained for one stochastic variable is randomly paired with all the other randomly sampled n_{ran} values of the other random variables. Florian [115] has proposed an efficient sampling scheme through an improved variant of the LHS which was called the Updated Latin Hypercube Sampling, that results in a substantial decrease of the variance in the estimates of statistical parameters (such as the mean value) using moderate number of simulations. Another sampling approach named the Antithetic Variates (AV) method [116], has been shown to reduce the mean squared error (bias) of an estimated statistical function when compared to the use of independent random sampling (such as MC), but it is not as efficient as the Latin Hypercube Sampling technique [117]. Johnson et al [118] proposed a sampling method based on Maximin designs, which spreads the sampling region around the entire domain space by maximizing the minimum distance between any two samples. Efficient

sampling methods nowadays make use of low-discrepancy sequences instead of random sampling as is the case with the Monte Carlo and Latin hypercube techniques. These methods, typically referred to as quasi-Monte Carlo methods, usually converge faster than techniques employing random or pseudorandom sequences. The Halton and Hammersley sequences are two such low-discrepancy sequences that have been used in several applications. Diwekar et al [119] have implemented an efficient sampling technique based on the use of the Hammersley Sampling Sequence (HSS), and showed that it requires considerably less sample points to estimate the statistical properties within a pre-specified tolerance than the Monte Carlo (or Latin hypercube) sampling methods when performing optimization under uncertainty. Other works that have implemented this more efficient sampling technique have been reported [120–122]. The sampling methods described thus far normally choose the set of samples *a priori* running the experiment or simulation, categorized as space-filling design methods. Another class of techniques called adaptive sampling adjusts the grid of the samples according to the complexity of the design space. For example, in variance-reduction sampling strategies, further sampling points are chosen from the region with high variance so that more samples are obtained to improve the accuracy of the estimate and reduce its variance. Adaptive multiple additive regression trees (AMART) [123] and the tree Gaussian process (TGP) [124] are sampling techniques based on the adaptive sampling method.

In this work, most of the sampling is carried out using the well-known Monte Carlo method, while at some instances the more efficient Halton method will be used to evaluate the computational performance of the proposed methods.

Chapter 3
Optimal design of large-scale chemical processes under uncertainty: A ranking-based approach

This chapter presents a practical ranking-based method to address the optimal design and operation of large-scale processes under uncertainty. The organization of this chapter is as follows: an overview of the goals and benefits of the proposed methodology is given in Section 3.1. Next, Section 3.2 presents the mathematical framework proposed to compute the distributions in the constraints from knowledge of the uncertainty distribution of the model inputs and model parameters. The systematic method to address the optimal design under uncertainty is presented in Section 3.3. The approach proposed in this work has been tested using different case studies, which are presented in Section 3.4. The method is initially tested using a case study that involves the design of a reactor and heat exchanger system. This case study was evaluated under different scenarios, to analyze the benefits and limitations of the new approach. A second case study involving the optimal operation of the Tennessee Eastman plant [125] demonstrates the computational benefits and accuracy of the present approach to address the optimal design and operation of large-scale systems under uncertainty. Section 3.5 summarizes the methodology and work presented in this chapter. The content of this chapter has been published in the AIChE Journal [126] (see Appendix).

3.1 Overview of proposed method

The approach used for the proposed method employs Power Series Expansions (PSE) to express the actual process constraints and model outputs in terms of the uncertain parameters considered in the analysis. The resulting PSE analytical expressions are then used to compute the distributions of the process constraints and outputs (i.e. frequency histograms) based on the different (probabilistic-based) realizations of the uncertain parameters. Accordingly, the feasibility in the process constraints is evaluated at a given (user-defined) probability of satisfaction from knowledge of their corresponding probability distributions. The effect of the system uncertainty on the cost function can also be assessed in a similar manner to the process constraints. Different process design alternatives can be assessed when the feasibility in the constraints is set to different probability of satisfaction

limits, i.e., a ranking-based design. Thus, the present approach aids the user in the decision-making process under uncertainty. The computational benefits and the accuracy in the calculations while using the present ranking-based design methodology are evaluated using two case studies, i.e., a reactor-heat exchanger system and the Tennessee Eastman (TE) process. The PSE method is a general and practical approach that can be readily implemented to approximate the behavior of nonlinear process models using sensitivity analysis. These features make this approach an attractive and practical alternative, especially for large-scale processes since their corresponding PSE-based functions can be readily estimated using established numerical methods, e.g. finite differences. However, the key benefit of this approach is the significant reduction in the computational costs associated with running multiple simulations of the system to estimate the process output distributions under uncertainty.

Pintarič et al.[127] recently proposed an approach to design flexible process flowsheets for systems under uncertainty by performing first-order sensitivity analysis to identify the critical scenarios that may produce the worst-case realizations in the uncertain parameters. These critical points, together with an identified central basic point, were used to evaluate the process constraints, which were found to be sufficient to ensure the design flexibility. In this work, the objective function is evaluated only at the central basic point, with no need to evaluate a multidimensional integral. While this approach is computationally attractive, especially when dealing with a large number of uncertainties, it aims to identify robust (conservative) process designs since the process constraints are satisfied for the entire space of the uncertain parameters. This differs from the method presented here since the design attained by the proposed method in this chapter is subject to a probability of satisfaction in the process constraint functions and model outputs (i.e. a ranking-based approach) and therefore allows the specification of more economically attractive designs. In Section 3.4, the present approach is compared to that of Pintarič et al. to evaluate its computational benefits.

3.2 Process design under probabilistic-based uncertainty

This section presents a method for the optimal design of process systems under uncertainty in the model parameters or in the model inputs. The present analysis assumes that a process model **z** describing the behavior of the system under analysis is available for simulations and is described as follows:

$$\mathbf{z}(\mathbf{d},\mathbf{p},\mathbf{x},\mathbf{y},\mathbf{u},\boldsymbol{\theta}) = \mathbf{0} \tag{3.1}$$

where **d** is the vector of design variables, **p** represents the model parameters whereas **x**, **y** and **u** are the state variables, the model outputs and inputs, respectively. The model parameters in **p** and model inputs in **u** that are uncertain are defined as $\mathbf{p}^{\sim}$ and $\mathbf{u}^{\sim}$ and will grouped in a single vector and referred from heretofore to as the system uncertainty **θ**, i.e.,

$$\boldsymbol{\theta} = [\mathbf{p}^{\sim}, \mathbf{u}^{\sim}] \tag{3.2}$$

This work assumes that each uncertain model input or model parameter can be described according to a particular probability density function (PDF), i.e.,

$$\begin{aligned} &\boldsymbol{\theta} = [\theta_1, \theta_2, ..., \theta_l, ..., \theta_L] \\ &\theta_l \sim \mathrm{PDF}(\boldsymbol{\alpha}_l) \end{aligned} \tag{3.3}$$

where the l^{th} uncertain variable included in $\boldsymbol{\theta}$ follows a specific PDF with distribution parameters $\boldsymbol{\alpha}_l$. The choice of the type of PDF to describe each uncertain parameter comes from process experience (when designing plants similar to an existing one) or historical data of the plant (when using the same input uncertainty source and such details are available). In the latter case, the distribution of the input uncertainty can be characterized by fitting the best PDF that describes the available data. When no such information is available, the PDFs of the uncertain variables are typically described using Gaussian or uniform probability distribution functions; however, the present method is not restricted to these functions and assumes that each uncertain parameter, such as θ_l, can be described using any symmetric or non-symmetric probability distribution function, e.g. lognormal, exponential. Note that the description presented in (3.3) does not assign specific values for the uncertain variables. Hence, an appropriate sampling technique such as the Monte Carlo sampling method is needed to obtain the different realizations in **θ**. Monte Carlo (MC) sampling in the proposed approach chooses *N* independent sample points randomly from the known PDFs (with distribution parameters $\boldsymbol{\alpha}_l$) of the uncertain variables θ_l. This is typically a standard task using available off-the-shelf computing software. Unlike the stochastic programming method, the present approach does not simulate the plant model **z** for all *N* uncertain realizations to compute the variability in the constraints due to **θ**.

Instead, the present method represents the process constraint functions and model outputs using a Power Series Expansion (PSE) function. Then, *N* Monte Carlo sampling points representing the uncertain parameters' distribution are generated and used as inputs to simulate the corresponding PSE functions. The simulation results, describing the variability in the constraint functions and the model outputs due to θ_l, are then used to evaluate the feasibility and economics of the current design under analysis. As it will be shown in the next sections, the evaluation of the constraints and model outputs using PSE functions is a much less intensive task than simulating the actual process model (**z**) *N* times, especially for large complex models. The procedure to obtain the PSE constraint functions is described next.

3.2.1 PSE method: analytical approximation of the process constraints

The process constraints are typically described as a function of the system parameters, state variables as well as the model inputs and outputs, i.e.

$$\mathbf{h}(\mathbf{p},\mathbf{x},\mathbf{y},\mathbf{u},\boldsymbol{\theta}) \le \mathbf{0} \tag{3.4}$$

where the vector of process constraints **h** usually impose a safety, physical or operational limitation on the process to be designed. The key idea is to compute analytical expressions for each of the process constraint functions included in **h** due to the potential realizations in $\boldsymbol{\theta}$ using Power Series Expansion (PSE) functions. Therefore, the actual nonlinear constraint function *h* is represented in the present analysis as follows:

$$\begin{aligned} h(\boldsymbol{\theta}) &= h(\bar{\boldsymbol{\theta}}) + \mathbf{M}^{(1)}(\boldsymbol{\theta}-\bar{\boldsymbol{\theta}}) + \frac{1}{2}(\boldsymbol{\theta}-\bar{\boldsymbol{\theta}})^T \mathbf{M}^{(2)}(\boldsymbol{\theta}-\bar{\boldsymbol{\theta}}) + \ldots \\ \mathbf{M}^{(1)} &= \left.\frac{\partial h}{\partial \boldsymbol{\theta}}\right|_{\boldsymbol{\theta}=\bar{\boldsymbol{\theta}}} \\ \mathbf{M}^{(2)} &= \left.\frac{\partial^2 h}{\partial \boldsymbol{\theta}^2}\right|_{\boldsymbol{\theta}=\bar{\boldsymbol{\theta}}} \\ E[\boldsymbol{\theta}] &= \bar{\boldsymbol{\theta}} \end{aligned} \tag{3.5}$$

where $\mathbf{M}^{(i)}$ refers to the i^{th} sensitivity term of the process constraint function *h*, i.e., $\mathbf{M}^{(1)}$ and $\mathbf{M}^{(2)}$ represent the Jacobian and Hessian matrices of the process constraint function *h*, respectively.

Similarly, $\bar{\boldsymbol{\theta}}$ represents the nominal (mean) value of the uncertain parameters $\boldsymbol{\theta}$. The PSE constraint function in (3.5) is shown only up to an expansion order of 2, but it can be easily expanded to any higher order *q*. The constraint function h is assumed to be (*q*+1) times totally differentiable with respect to $\boldsymbol{\theta}$. When a constraint h is a function of a single uncertain variable θ, h simplifies to the following expression:

$$h(\theta) = h(\bar{\theta}) + \sum_{j=1}^{q} \frac{1}{j!} \left(\frac{\partial^j h}{\partial \theta^j} \right) \Bigg|_{\theta=\bar{\theta}} (\theta - \bar{\theta})^j \tag{3.6}$$

As shown in (3.5), the PSE-based expansion used to describe the constraint functions is easier to evaluate since it is explicitly defined in terms of the system uncertain parameters $\boldsymbol{\theta}$. Therefore, the PSE constraint functions can be used to evaluate the process constraints **h** due to multiple realizations in the uncertain parameters $\boldsymbol{\theta}$ with minimum computational effort. If an analytical expression of the sensitivity terms $\mathbf{M}^{(1)}, \mathbf{M}^{(2)}, \ldots$etc. is available, then it may be derived and computed analytically. Otherwise, they will be approximated numerically which will require computing the constraint value at several points by simulating the actual process model at those points. By substituting the *N* sampled uncertainty realizations $\boldsymbol{\theta}_N \in \Re^{N \times L}$ into each PSE-based process constraint expression similar to that shown in (3.5), a set of estimates of each constraint function *h* corresponding to each realization of the *N* sampled uncertain variables is obtained, i.e. $h(\boldsymbol{\theta}_N) \in \Re^{N \times 1}$. The set of estimates collected in $h(\boldsymbol{\theta}_N)$ are then used to generate a frequency histogram that describes the distribution (variability) of the constraint function *h* due to $\boldsymbol{\theta}$. The accuracy of the estimated distribution of the process constraints (depicted by the histogram) improves as *N* becomes larger and as the number of expansion terms considered in the PSE-based constraint function for *h* is increased. While increasing the order of the expansion improves the analytical approximation of the process constraint, it also increases the computational cost due to evaluation of higher order terms in the PSE-based expansion. Therefore, the choice of the expansion order in the PSE is problem specific since it depends on many aspects of the system under analysis, e.g., the degree of nonlinearity of the system, the size of the process model, the method used to compute the terms in the expansion, i.e. analytical or numerical [128], the probability distribution function assigned to the system's uncertain parameters $\boldsymbol{\theta}$. These particular aspects of the method are further analyzed with the case studies presented in this work. Higher order PSE expansions may be required to represent systems with strong nonlinearities. In

those cases, the computational costs of the present method will increase, especially when many uncertain parameters are considered in the analysis, since the proposed method relies on the calculation of the sensitivities to the uncertain parameters.

In the present approach, the distribution of each of the process constraints included in $\mathbf{h}$ will be used as a tool to implement a ranking-based design approach. The significance of a process constraint is specified by assigning it a probability limit (Pb_h), i.e., each constraint included in the analysis is ranked using Pb_h based on its significance. This probability of satisfaction indicates how often a particular constraint is expected to meet its corresponding feasible limit. Thus, to ensure a feasible process design, the variability in the process constraints $\mathbf{h}$ cannot violate their pre-specified limits (Pb_h) due to the different realizations in $\boldsymbol{\theta}$. Using the assigned Pb_h limit and $h(\boldsymbol{\theta}_N)$ obtained from the PSE-based constraint function, an estimate of the extreme possible value of the process constraint function ξ_h that occurs $(100 \times Pb_h)$% of the time can be evaluated as follows:

$$\begin{aligned} Pb_h &= CMF(\xi_h, h(\boldsymbol{\theta}_N)) = P(h \le \xi_h) \\ \xi_h &= \{\xi_h : CMF(\xi_h, h(\boldsymbol{\theta}_N)) = Pb_h\} = CMF^{-1}(Pb_h, h(\boldsymbol{\theta}_N)) \end{aligned} \tag{3.7}$$

where *CMF* is the cumulative probability function of the process constraint function, $P(h \le \xi_h)$ denotes the probability that h is less than ξ_h. Figure 3.1 presents a schematic representation of the PSE-based constraint function *h* evaluated at a given probability Pb_h. If the extreme possible value of the constraint ξ_h (calculated at a given Pb_h) satisfies the process restrictions specified in (3.4), a feasible process design is obtained with a $(100 \times Pb_h)$% guarantee that constraint *h* is satisfied. Based on the above, the constraints (3.4) under system uncertainty are evaluated in the present analysis using the constraint function extreme estimates (ξ_h) at a user-defined probability of satisfaction (Pb_h), i.e.,

$$\xi_h(CMF, h(\boldsymbol{\theta}_N), Pb_h) \le 0 \qquad \Leftrightarrow \qquad P\big(h(\mathbf{p}, \mathbf{x}, \mathbf{y}, \mathbf{u}, \boldsymbol{\theta}) \le 0\big) \ge Pb_h \tag{3.8}$$

The expression on the right-hand side in (3.8) denotes the probability of the actual nonlinear constraint functions obtained with the actual nonlinear plant model **z** whereas the extreme estimate on the left-hand side is obtained from the PSE-based constraint function shown in (3.5) followed by a probabilistic inference.

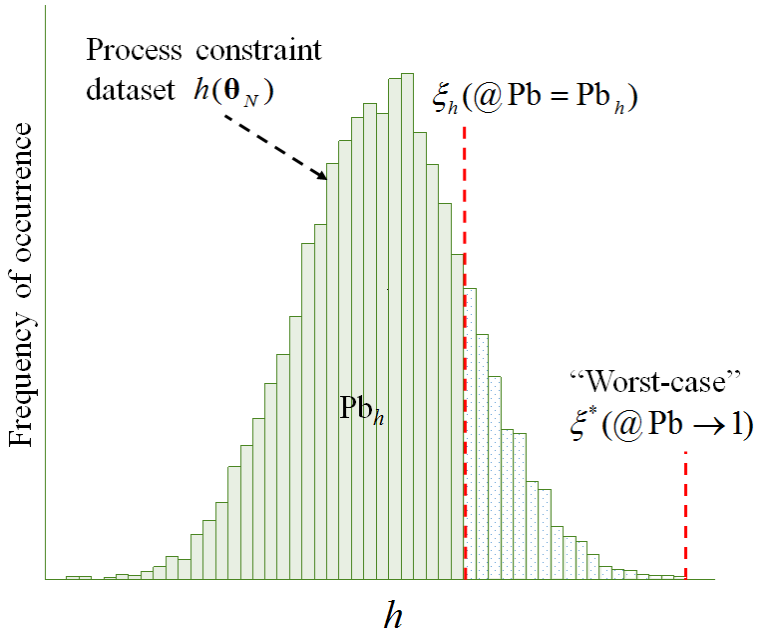

Figure 3.1 Schematic representation of the constraint function's distributional analysis.

Since ξ_h is only an estimate of the constraint at a given probability limit Pb_h, h can still take values beyond ξ_h with a probability of (1- Pb_h). In the proposed approach, the probability of constraint satisfaction Pb_h , which determines the rank assigned to each constraint, represents an input to the present method, i.e., it is a user-defined input parameter. Thus, higher probabilities should be assigned to those constraints that are considered to be critical. Setting $\mathrm{Pb}_h \to 1$ implies that the design will satisfy the constraints almost every time, this is often termed the worst-case scenario approach (see Figure 3.1). While the worst-case scenario ensures that the design remains feasible for almost all the realizations in $\boldsymbol{\theta}$, this robust design is typically conservative and expensive. The subscript in Pb_h suggests that different probabilities can be assigned for each process constraint enabling a ranking-based design. The latter will assist in achieving less conservative (economically attractive) designs but at the same time keeping the critical constraints within specification (at a given probability of occurrence). Therefore, the selection of a suitable ranking structure is problem-specific since it depends on the goals to be attained by the design, e.g., process economics and process safety. The analysis described above for the process constraints can also be implemented in the same fashion to

evaluate the variability in the model outputs and state variables that are included in the plant's cost function.

3.3 Optimal design under uncertainty

Based on the above developments, the optimal design of a chemical system under uncertainty can be formulated as follows:

$$
\begin{aligned}
&\min_{\boldsymbol{\eta}=[\mathbf{d},\mathbf{u}]} \Phi = \mathrm{CC}(\mathbf{d},\boldsymbol{\theta}) + \mathrm{OC}(\mathbf{x},\mathbf{y},\mathbf{u},\boldsymbol{\theta}) \\
&\quad \text{s.t.} \\
&\quad \mathbf{z}(\mathbf{d},\mathbf{p},\mathbf{x},\mathbf{y},\mathbf{u},\boldsymbol{\theta}) = \mathbf{0} \\
&\quad \xi_h(CMF, h(\boldsymbol{\theta}_N), \mathrm{Pb}_h) \le 0 \qquad\qquad h \in \mathbf{h} \\
&\quad \mathbf{d}^l \le \mathbf{d} \le \mathbf{d}^u \\
&\quad \mathbf{u}^l \le \mathbf{u} \le \mathbf{u}^u
\end{aligned}
\tag{3.9}
$$

The above problem aims to minimize the economic cost of the process, usually described in terms of the capital (CC) and operating (OC) costs, by selecting feasible process designs **d** and operating conditions (i.e. model inputs **u**). The feasibility criteria follow a ranking-based approach where each function *h* can take different values of Pb_h, which becomes the minimum probability of satisfaction for a constraint. Despite the stochastic nature of this process design formulation, i.e., each uncertain parameter is described with a specific PDF shown in (3.3), the implementation of the PSE-based approach proposed here to evaluate the process constraints and cost function under uncertainty in the parameters **θ** reduces problem (3.9) into a deterministic nonlinear constrained optimization problem that can be solved using available NLP solvers such as Sequential Quadratic Programming (SQP) [129]. The outcome of the present formulation returns an optimal process design that accommodates uncertainty in the parameters **θ** up to a user-defined probability of constraints satisfaction (Pb_h). Figure 3.2 summarizes the main features of the proposed approach in comparison to the traditional stochastic programming method.

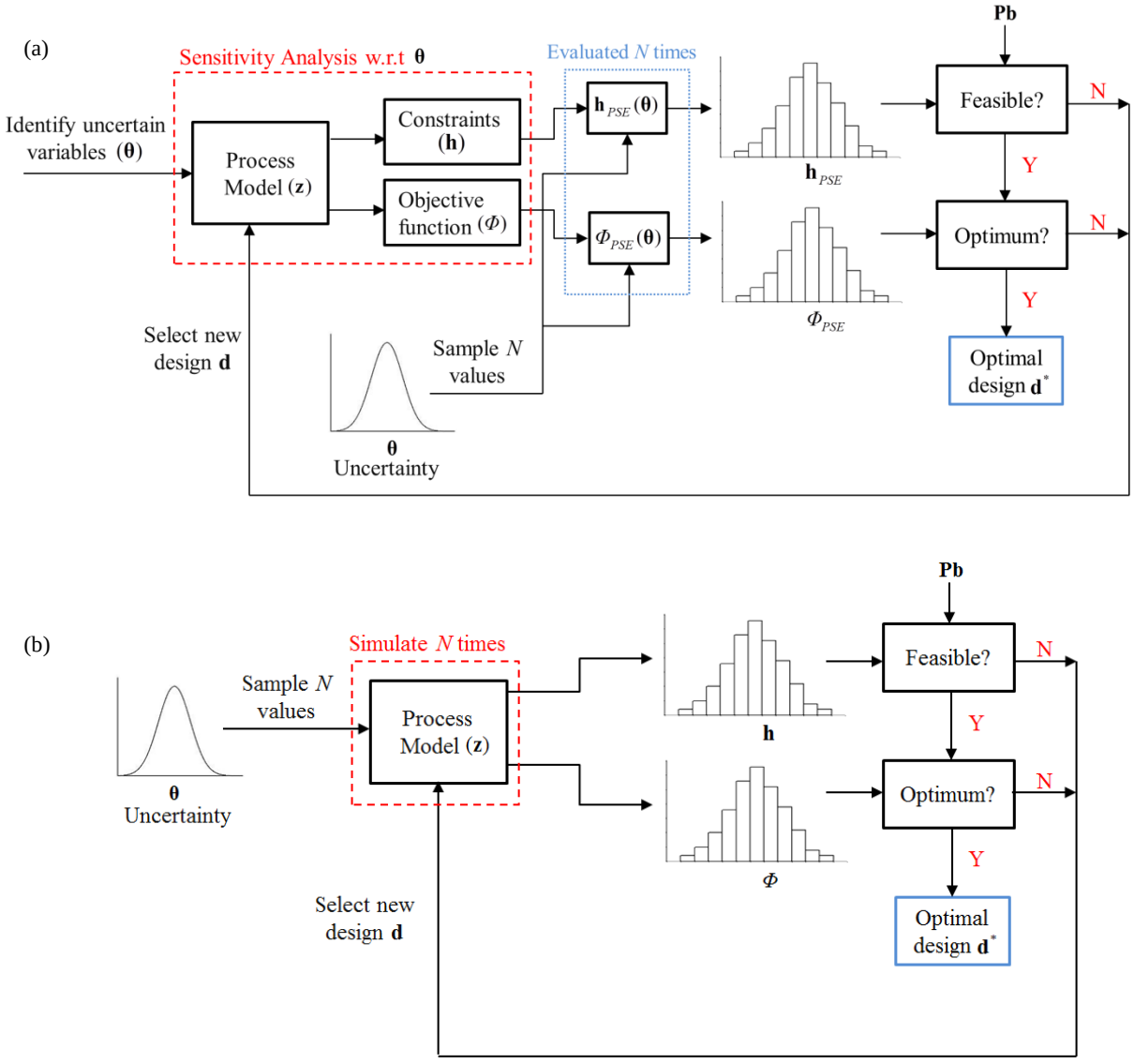

Figure 3.2 Schematic representation of the algorithms for the (a) proposed PSE-based approach in comparison to the (b) traditional stochastic programming method.

The most computational demanding part of each algorithm is represented by the blocks within the dashed box in Figure 3.2, which requires the simulation of the actual nonlinear process model $\mathbf{z}$. For the stochastic programming approach (Figure 3.2b), the sampled uncertain realizations are input into this computationally intensive block directly, demanding N complete simulations of the process model corresponding to each uncertain realization. On the other hand, the proposed approach utilizes

the process model for sensitivity analysis, which demands only a few simulations depending on the order of the PSE approximation to be used. The *N* sampled uncertain realizations are inputs into the PSE-based model, which can be simulated orders of magnitude faster than the actual process model (dashed box in Figure 3.2b) thus making the present ranking-based approach computationally attractive and suitable to address the optimal design or large-scale systems.

3.3.1 Remarks

In the present approach, the equality constraints are satisfied for the entire space of the uncertain parameters. That is, the equality constraints, which are typically the process model equations in an optimal process design problem, i.e., **z** in problem (3.9), need to be solved for the different realizations considered in the uncertain parameters. This specification enables the evaluation of the output variability under uncertainty using the process model equations, which are then used to compute the distribution of the process constraint functions and model outputs. The present approach can also account for structural (discrete) decisions in the analysis. The computation of the sensitivities in the present approach only requires that the process model is continuous. In problems involving discrete decisions, the discrete variables are fixed in advance and the sub-problems to be solved have continuous process models that impose no restriction in the use of PSE to approximate and compute the process constraints and model outputs.

Note that in the case where the uncertainty is bounded but its distribution is unknown, a uniform distribution assumption would be adopted as this kind of distribution is the most pessimistic, i.e., more realizations of the extreme values may occur. For a uniform distribution, any value within the specified bounds has equal probability of occurrence, unlike other distributions such as the normal distribution where the majority of realizations will be close to the mean value and only a rare occurrence for the extreme points. As a result, the uniform distribution assumption yields conservative designs and is adopted in the present methodology for those cases of unknown uncertainty distributions. In the next section, the application of the present approach to address the optimal process design and operation of two case studies under different scenarios is presented. The studies presented in the next section were performed on an Intel Core i7 3770 CPU @3.4GHz (8GB in RAM).

3.4 Case Studies

In this section, the proposed method will be tested on two case studies: a reactor-heat exchanger system and the Tennessee Eastman plant.

3.4.1 Case Study 1: Reactor-heat exchanger system

The first case study considered in the present analysis is a plug-flow reactor coupled with a heat-exchanger system as shown in Figure 3.3. This system has been previously studied for optimal process design [130]. A first order exothermic reaction is assumed for the production of product *B* from reactant *A* in the direct reaction: A→B. F_0, T_0 and C_{A0} are the flowrate, temperature and concentration of reactant *A*, respectively, of the feed stream to the reactor. The concentration of the reactant remaining in the product stream is denoted by C_{A1}. The variables T_1, T_2 and F_2 are the temperature of the contents in the reactor, and the temperature and flowrate of the recycled stream from the heat exchanger, respectively. The recycled stream is cooled down in the heat exchanger using cooling water supplied at a temperature T_{w1} and flowrate W to ensure that the reaction temperature T_1 does not exceed a maximum temperature limit.

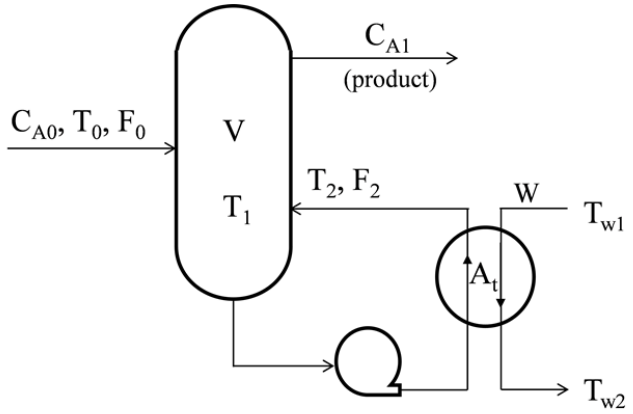

Figure 3.3 Flowsheet of a reactor-heat exchanger system.

The material and energy balances for the reactor and heat exchanger represent the process model for this system.

The steady-state mass and energy balances for the reactor are:

$$F_0(C_{A0} - C_{A1})/C_{A0} = Vk_0 \exp(-E/RT_1)C_{A1}$$
$$(-H)F_0(C_{A0} - C_{A1})/C_{A0} = F_0C_p(T_1 - T_0) + Q_{HE} \quad (3.10)$$

The steady-state energy balances for the heat exchanger system are:

$$Q_{HE} = F_2C_p(T_1 - T_2) = C_{pw}(T_{w2} - T_{w1})W$$
$$Q_{HE} = A_tU(0.5((T_1 - T_{w2}) + (T_2 - T_{w1}))) \quad (3.11)$$

where k_0, E and H are the rate constant, activation energy and heat of reaction, respectively. Q_{HE} is the rate of heat transferred to the heat exchanger, U is the overall heat transfer coefficient, whereas the heat capacity of the recycled flow and cooling water are represented by C_p and C_{pw}, respectively. The reactor is assumed to be perfectly insulated with negligible heat loss to the surroundings. The design parameters are the reactor volume V and heat exchanger transfer area A_t. In addition, X represents the conversion of reactant A. The state variables are C_{A1}, T_2, F_2 and W, which can be eliminated by analytic expressions using equations (3.10)-(3.11) as follows:

$$C_{A1} = C_{A0}(1 - X)$$
$$X = \frac{Vk_0C_{A0}\exp(-E/RT_1)}{F_0 + Vk_0C_{A0}\exp(-E/RT_1)}$$
$$T_2 = \frac{2(-H)F_0X}{A_tU} - \frac{2F_0C_p(T_1 - T_0)}{A_tU} - (T_1 - T_{w2}) + T_{w1} \quad (3.12)$$
$$F_2 = \frac{Q_{HE}}{C_p(T_1 - T_2)} \quad , \quad W = \frac{Q_{HE}}{C_{pw}(T_{w2} - T_{w1})}$$

The nominal values for the model parameters of this process are listed in Table 3.1 [130]. In this case study, uncertainty is assumed in two model inputs (F_0 and C_{A0}) and one model parameter (k_0). These uncertain parameters were assumed to follow a normal probability distribution with specific mean and variances, i.e.,

$$\begin{aligned}
&\boldsymbol{\theta}_{CS1} = [F_0, C_{A0}, k_0] \\
&F_0 \sim N(45.36, 1.506^2) \\
&C_{A0} \sim N(32.04, 1.266^2) \\
&k_0 \sim N(0.6242, 0.079^2)
\end{aligned} \tag{3.13}$$

As shown in (3.13), the expected values of these distributions correspond to the nominal operating conditions shown in Table 3.1 for each of these parameters. A variance of 5% of its mean is assumed for the feed flowrate F_0 and concentration C_{A0}, respectively, whereas a variance of 1% of its nominal value was assigned for the more sensitive parameter k_0. The goal of this process is to achieve a minimum of 90% conversion of reactant *A* while maintaining temperature constraints in the process units (see Table 3.1). The decision variables for this case study consist of the design parameters $\mathbf{d} = [V, A_t]$ and the operating variables $\mathbf{u} = [T_1, T_{w2}]$.

Table 3.1 Reactor-heat exchanger case study: model parameters and process constraints.

Model parameters [130]			**Process constraints**	
Variable	**Estimate**	**Units**	*c*1:	$0.9 - X \leq 0$
E/R	555.6	K	*c*2:	$X - 1 \leq 0$
H	-23,260	kJ/kg.mol	*c*3:	$T_2 - T_1 \leq 0$
U	1635	kJ/m^2.h.K	*c*4:	$311 - T_2 \leq 0$
C_p	167.4	kJ/kg.mol	*c*5:	$T_2 - 389 \leq 0$
C_{pw}	75.327	kJ/kg.mol	*c*6:	$T_{w1} - T_2 + 11.1 \leq 0$
F_0	45.36	kg.mol/h	*c*7:	$T_{w1} - T_{w2} \leq 0$
k_0	0.6242	m^3/kgmol.h	*c*8:	$T_{w2} - T_1 + 11.1 \leq 0$
C_{A0}	32.04	kg.mol/m^3	*c*9:	$311 - T_1 \leq 0$
T_0	333	K	*c*10:	$T_1 - 389 \leq 0$
T_{w1}	300	K	*c*11:	$301 - T_2 \leq 0$
			*c*12:	$T_{w2} - 355 \leq 0$

Using the PSE approximation method presented in the previous sections, the variability in the process constraints due to uncertainty in $\boldsymbol{\theta}_{CS1}$ are calculated for each set of values in the design variables **d** and **u** tested by the optimization algorithm. Using a probability of satisfaction of Pb_h=0.6827 for all

constraints, the extreme possible values (ξ_h) at that probability value can be estimated as shown in (3.7). For example, for constraint *c*1 in Table 3.1, the probabilistic form given in (3.8) is as follows:

$$\xi_{c1} \le 0 \qquad \Leftrightarrow \qquad \mathrm{P}(0.9 - X \le 0) \ge \mathrm{Pb}_h \tag{3.14}$$

The other process constraints shown in Table 3.1 are reformulated in a similar fashion. Based on the above, the optimal design problem shown in (3.9) is reformulated for the present case study as follows:

$$\begin{aligned}
&\min_{\boldsymbol{\eta}=[V,A_t,T_1,T_{w2}]} \Phi = 691.2V^{0.7} + 873.6A_t^{0.6} + 1.76W + 7.056F_2 \\
&\text{s.t.} \\
&\text{Process model} \qquad \text{eqns (3.10)} - \text{(3.11)} \\
&\xi_w \le 0 \qquad \forall w = c1, c2, \ldots, c12 \\
&V^l \le V \le V^u \qquad A_t^{\,l} \le A_t \le A_t^{\,u} \\
&T_1^{\,l} \le T_1 \le T_1^{\,u} \qquad T_{w2}^{\;\;l} \le T_{w2} \le T_{w2}^{\;\;u}
\end{aligned} \tag{3.15}$$

where the objective function is a combination of the capital and operating costs of the plant that was taken from the literature [130]. Problem (3.15) is solved with MATLAB SQP solver using different orders *q* for the PSE approximation and probability limits Pb_h.

As shown in Table 3.2(a), it is clear that the design obtained from the first order PSE approximation (*q*=1) is different from those obtained from higher order functions. Note that process designs obtained from a third-order (*q*=3) and a fourth-order (*q*=4) PSE approximation do not change significantly, which indicates convergence of the PSE approximation function at a given probability of satisfaction. This shows that the present methodology can account for the system nonlinearity using higher order PSE approximations to achieve accurate optimal designs. The expense of using higher orders in the PSE approximation can be observed in the increase of the computational time needed to solve the optimal design problem for these scenarios. In this case study, the maximum difference between the solutions obtained from orders *q*=3 and *q*=4 is only about 0.05% although the lower order identifies an optimal design in half the time than that needed by the fourth-order PSE approximation. Therefore, it is reasonable to select the PSE order to *q*=3 without losing accuracy in the results. Note that, although it is established that the solution of this case study converged using higher-order PSE functions, the design obtained from a first order PSE approximation is still feasible. An order of *q*=3

PSE is selected solely for the purpose of demonstrating the convergence property of using higher orders for systems with strong nonlinearities.

Table 3.2 Results for the reactor-heat exchanger system using different expansion orders and different probabilities of satisfaction..

(a) Optimal designs for different PSE orders (Pb_h=0.6827).				
Exp. Order	*q=1*	*q=2*	*q=3*	*q=4*
$V\ (m^3)$	90.77	92.13	91.65	91.70
$A_t\ (m^2)$	5.97	6.01	6.00	6.00
$T_1\ (K)$	389.00	389.00	389.00	389.00
$T_{w2}\ (K)$	329.63	329.61	329.61	329.60
Costs ($/yr)	19,757	19,933	19,871	19,878
CPU time (s)	1.03	3.91	12.40	29.81
(b) Optimal designs for different user-input probability Pb. (PSE method, q=3)				
Pb_h	*0.5*	*0.6827*	*0.9545*	*0.9973*
$V\ (m^3)$	86.56	91.65	104.69	116.42
$A_t\ (m^2)$	5.94	6.00	6.14	6.24
$T_1\ (K)$	389.00	389.00	389.00	389.00
$T_{w2}\ (K)$	329.57	329.61	329.69	329.75
Costs ($/yr)	19,205	19,871	21,519	22,941
CPU time (s)	10.29	12.40	16.55	15.45

Table 3.2(b) shows the optimal process design alternatives obtained when probability limits Pb_h are set to different values for all process constraints while using third-order PSE-based approximation functions (q=3). As expected, when a higher probability of constraint satisfaction is chosen, a larger reactor and heat transfer area in the heat exchanger are required, which leads to higher plant costs. For example, a 15% increase in total costs is needed to design a plant that will satisfy the constraints with a probability of 99.73% as opposed to the one that satisfies all the process constraints 68.27% of the time. As explained above, the choice of Pb_h is user-defined; its direct relation to profitability can be clearly assessed using the present ranking-based method. Note that the computational times for

different choices of Pb_h using third-order PSE approximation functions are similar. These designs have been validated through simulations of the actual plant model, i.e. Eqns (3.10)-(3.11), using 100,000 MC realizations in the 3 uncertain variables included in $\boldsymbol{\theta}_{CS1}$. Figure 3.4 shows that the minimum conversion rate constraint ($c1$) complies with their corresponding pre-specified probability limits, i.e., they satisfied the constraints close to the user-defined 99.73% and 68.27% values. The rest of the process constraints are validated in the same fashion and are not shown here for brevity.

To verify the accuracy of the results and the computational costs obtained using the present method, the present case study was also solved using a stochastic programming technique that uses the Monte Carlo sampling method applied to the actual process model. At each optimization step, random MC realizations of the uncertain parameters $\boldsymbol{\theta}_{CS1}$ are generated and used to simulate the complete process model. The results from the simulations are then used to obtain the output distributions and evaluate the compliance of the constraints and the cost function. For the present analysis, the actual plant model (3.10)-(3.11) is simulated for each realization and a histogram for the distribution of the constraints due to uncertainty in $\boldsymbol{\theta}_{CS1}$ is obtained. From these histograms, the extreme possible value at a given probability limit Pb_h is computed as shown in Figure 3.1; however, the distribution at each single function evaluation of the optimization algorithm is now obtained from actual simulations of the plant model rather than from the PSE approximation method. For the present analysis, 100,000 random MC sampling points are used in this approach. The optimal process design obtained at the user-defined probability limit Pb=0.9545 for all constraints is presented in Table 3.3(a). This result is in close agreement to that obtained by the new method shown in Table 3.2(b), i.e., the proposed method returned plant designs that are accurate within an error of less than 4%. Also, the new PSE-based method achieves a solution a few orders of magnitude faster than the Monte-Carlo based stochastic approach. Since sampling realizations of the uncertain parameters from their respective probability distributions is a requirement of stochastic programming, the efficiency of the sampling method used in the analysis is a factor that contributes towards the computational costs [119,131,132].

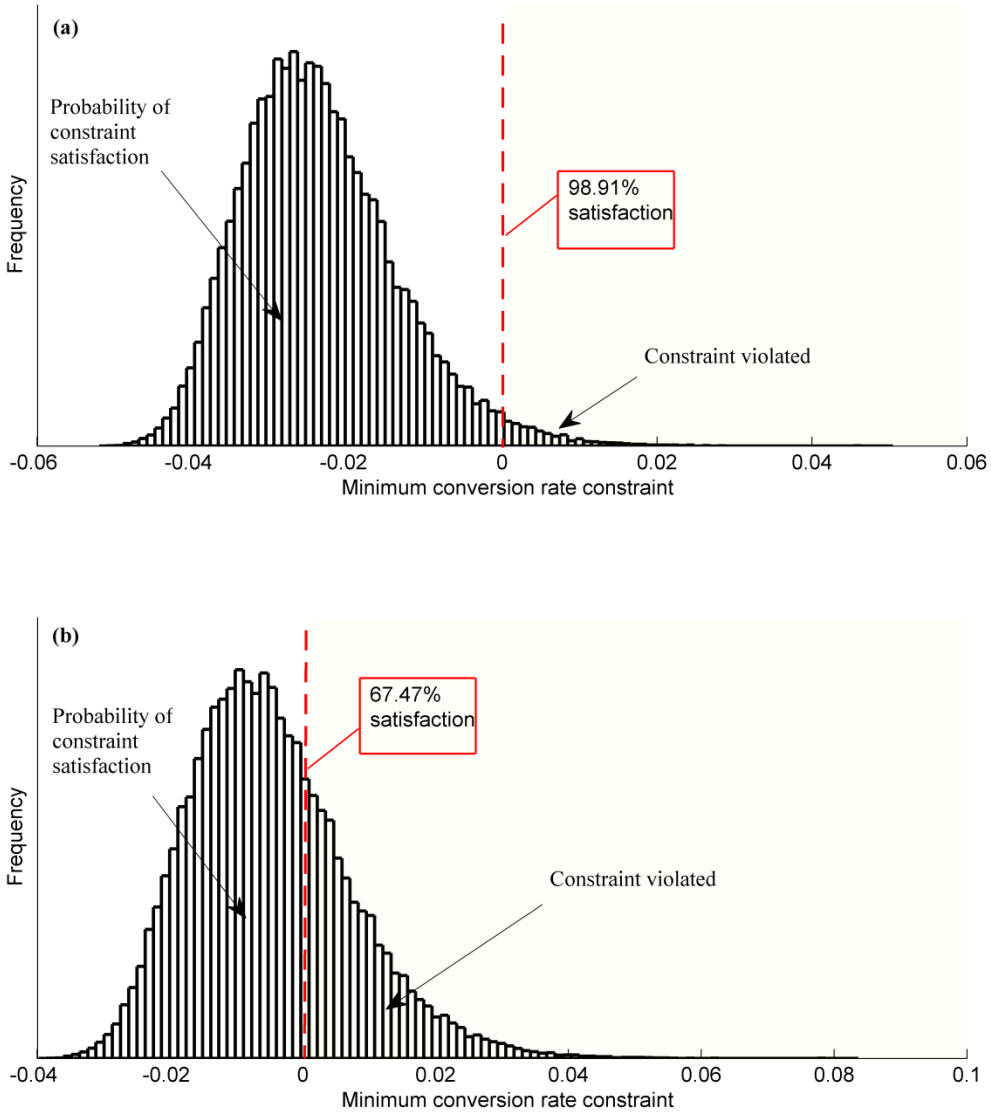

Figure 3.4 Frequency histogram of the minimum conversion rate constraint at probability limits (a) Pb=0.9973, (b) Pb=0.6827. Dashed line represents the maximum constraint limit.

To further demonstrate the computational benefits of the present approach, the present case study was also solved using the stochastic approach employing the Halton sampling technique [131], which is known to be more efficient than the standard MC sampling method. As shown in Table 3.3(a), it is clear that the Halton-based stochastic approach is more efficient than the MC-based approach since the computational costs are reduced by an order of magnitude due to fewer simulations needed to

attain the same convergence. However, the computational benefits of the present PSE-based approach are still striking when compared with the Halton-based stochastic approach (i.e. at least by one order of magnitude). It is important to note that, while stochastic programming approaches require simulation of the process model for each sampled point, the different sampling methods affect only the number of simulations N that are sufficient to obtain an accurate solution under the uncertainty conditions. On the other hand, the present PSE-method does not require sampling and so model simulations are done only a few times ($<<N$) depending on the order used to calculate the sensitivities. As such, regardless of the efficiency of the sampling technique, the proposed method is much less computationally intensive compared to stochastic programming approaches when handling large-scale problems.

Table 3.3 Results for the reactor-heat exchanger system using stochastic and ranking-based methods.

(a) Optimal design obtained using a stochastic approach that implements a different sampling technique (Pb_h=0.9545)		
Sampling method:	***Monte Carlo***	***Halton***
$V\ (m^3)$	108.06	107.50
$A_t\ (m^2)$	6.149	6.137
$T_1\ (K)$	388.98	388.91
$T_{w2}\ (K)$	333.29	330.74
Costs ($/yr)	21,885	21,872
CPU time(s)	3,369	914
(b) Ranking-based optimal design using PSE method with order (q=3).		
	Case A	*Case B*
$V\ (m^3)$	95.58	104.20
$A_t\ (m^2)$	6.05	6.14
$T_1\ (K)$	389.00	389.00
$T_{w2}\ (K)$	329.63	329.69
Costs ($/yr)	20,376	21,459
CPU time(s)	12.61	15.19

To further demonstrate the ranking-based feature of the present approach, two additional cases (A and B), with different probabilities of constraint satisfaction for the various process constraints, are considered. In this case, the constraints on the conversion rate (X) shown in Table 3.1 (i.e. $c1$ and $c2$) are assigned to 80% and 95% for cases A and B, respectively, whereas the recycled stream temperature (T_2) constraints, i.e., $c3$-$c6$ in Table 3.1, are set to 68% for both cases A and B. The remaining constraints (i.e. $c7$ to $c12$ in Table 3.1) are kept at high probabilities of satisfaction (99%). The optimal designs specified for cases A and B obtained using third-order PSE approximation functions are presented in Table 3.3(b). As shown, a different set of optimal designs are obtained compared to the case where equal probabilities are assigned to all constraints, e.g., Table 3.3(a). The results show that increasing the probability of satisfaction for the conversion rate constraints from 80% to 95% leads primarily to an increase in the volume of the reactor, and total plant costs by more than 5%. The histograms in Figure 3.5 obtained from simulations of the actual plant model using different MC realizations in $\boldsymbol{\theta}_{CS1}$ show that the minimum conversion rate constraint complies with the corresponding probability limits (Pb_{c1}) specified for case A and B, respectively.

As mentioned previously, the recent computationally attractive approach of Pintarič et al. [127] was developed for optimal process design under uncertainty. A comparison between this approach and the PSE-based method method can only be made for the worst-case scenario, i.e. robust designs that satisfy process constraints all the time without any ranking feature. One key feature of the method proposed in this work is that it can be used to approximate robust optimization process design under uncertainty by setting the probabilities of satisfaction on the process constraints to unity. As shown in Table 3.4, the computational times required by both approaches to achieve the optimal (robust) process design are comparable, indicating that the new approach is also computationally attractive for optimal (robust) process design under uncertainty. A first order PSE is sufficient to obtain an optimal feasible design while using this approach. This design satisfies the constraints at a very high probability of satisfaction, i.e., Pb_h=0.9999, which approximates the robust design obtained using the approach of Pintarič et al.

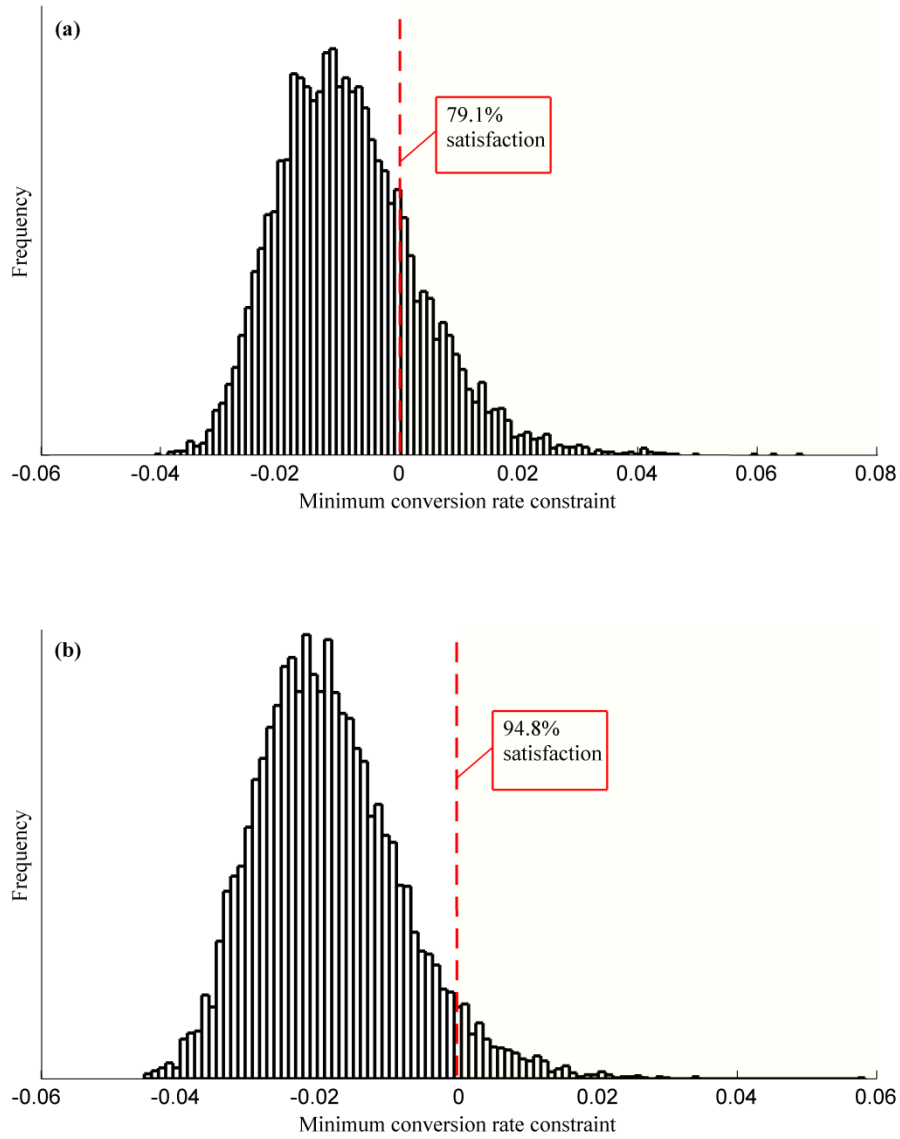

Figure 3.5 Frequency histogram for the minimum conversion rate constraint: (a) Case A, and (b) Case B.

Table 3.4 Optimal designs using different approaches for the worst-case problem.

	Pintarič et al.	PSE (*q=1*)
$V\ (m^3)$	171.2434	169.02
$A_t\ (m^2)$	6.5104	6.510
$T_1\ (K)$	389.00	389.00
$T_{w2}\ (K)$	329.94	329.94
Costs ($/yr)	29,038	28,807
CPU time(s)	2.025	1.887

3.4.2 Case study 2: Tennessee Eastman process

The Tennessee Eastman (TE) process is a widely used industrial problem proposed by Downs & Vogel [125] based on an actual process of Tennessee Eastman Co. The process consists of a reactor, recycle compressor, partial condenser and flash separator to produce two liquid products (G and H) and by-product F using four gaseous reactants, i.e. A, C, D and E, from the following reactions:

A (g) + C (g) + D (g) → G (liq)
A (g) + C (g) + E (g) → H (liq)
A (g) + E (g) → F (liq)
3 D (g) → F (liq)

The feed also contains an inert component B. The plant (shown in Figure 3.6) can operate at different production mix rates of G and H depending on market fluctuations. The base case is a 50/50 production in both G and H at a production rate of 7038 kg/h; this is the case considered in the present study. The four reactions in the reactor are defined as irreversible exothermic reactions; the reaction rates are temperature-dependent and can be described by an Arrhenius-like function. The reactions are approximated by first order kinetics with respect to the reaction concentrations. As shown in Figure 3.6, the reactants A, D and E in the feed stream enter the reactor unit together with the gaseous recycled stream where they react to form the desired liquid products G and H. A nonvolatile catalyst dissolved in the liquid phase is used to drive the gas phase reactions and the products exit the reactor along with some unreacted gases in a vapor phase. The liquid products are

condensed and separated from the gaseous mixture in the partial condenser and flash separator respectively, while the non-condensable components (unreacted gases) are recycled back to the reactor through a centrifugal compressor. The liquids collected at the bottom of the separator is pumped to the stripper which helps recover the remaining unreacted species D and E which would otherwise be lost in the product stream. This separation in the stripper is achieved by using a mixture of A and C as the solvent stream entering the base of the stripper (stream 4 in Figure 3.6), sending the vapor stream leaving the top of the stripper back to the reactor through the mixed recycle stream. The liquid stream at the bottom of the stripper is refined by heating with steam to obtain an acceptable purity of the desired products G and H. The separation of these two products is carried out in a downstream separation unit not shown in Figure 3.6. Non-condensable inert species B enters through stream 4, and thus a purge stream is introduced that prevents the buildup of this species as well as the by-product F.

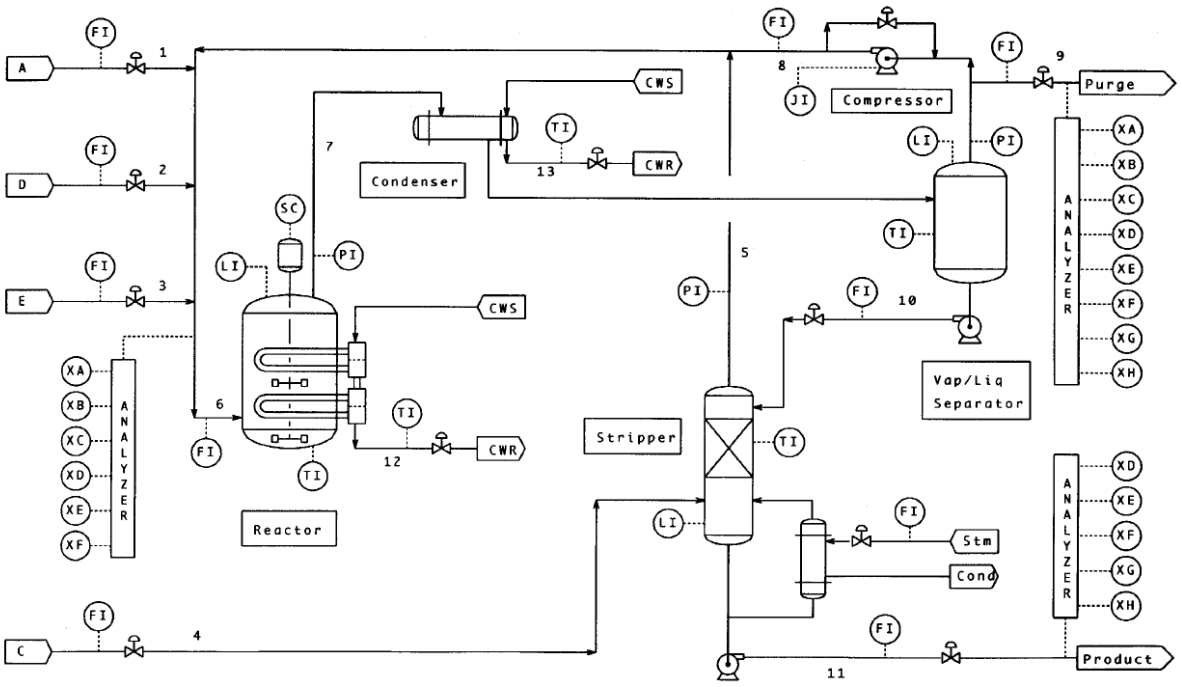

Figure 3.6 Schematic flowsheet of the Tennessee Eastman process [125].

This plant has 50 state variables, 12 manipulated (operating) variables, and 41 available output measurements. Six operational constraints are specified for the safe operation of the process. Detailed

descriptions of the TE process are given in the original problem formulation presented by Downs & Vogel [125]. However, a mathematical model describing the behavior of this process was not explicitly provided; instead these authors made available a FORTRAN code that simulates this plant under various operating conditions, i.e., a black-box model. This original FORTRAN code has been translated into several computing languages. The present work makes use of a MATLAB code provided by Ricker [133] to carry out the present analysis. The optimal steady-state operation of the TE problem has been previously studied by Ricker [133]. In that work, the optimization aimed to identify the nominal values in the system's states (**x**) that minimizes the plant's operating costs. Uncertainty in the model parameters or the system's states was not considered by Ricker [133]. At steady-state, the 12 manipulated variables **u** are represented by the last 12 states in **x** (i.e. x_{39} through x_{50}).

3.4.2.1 Scenario 1: Uncertainty in the model parameters

This scenario is similar to that presented by Ricker [133] in that it aims to determine the optimal steady-state operation of the TE process; however, the present analysis will explicitly account for uncertainty in one of the TE's model parameters. In this case, one of the states, i.e., the number of moles of liquid product G inside the reactor, will be assumed to be uncertain due to some model errors or lack of information that prevents the availability of accurate data. Hence, this uncertain parameter is described as follows:

$$x_7 \sim N(x_{7,nom},\ \sigma_7^{\,2}) \tag{3.16}$$

where $x_{7,nom}$ and σ_7 represent the state's mean value and standard deviation (i.e. $x_{7,nom}$=135.363, σ_7=1.8396), respectively. The same objective function for the TE process as that presented by Downs and Vogel and used by Ricker will be used in the present analysis, i.e.:

$$\begin{aligned}\phi_{TE} = \quad & 0.053m_3 + 0.0318m_{19} \quad + 0.44791m_{10}[2.209m_{29} + 6.177m_{31} + 22.06m_{32} + 14.56m_{33} \\ & + 17.89m_{34} + 30.44m_{35} + 22.94m_{36}] + 4.541x_{46}[0.2206m_{37} + 0.1456m_{38} + 0.1789m_{39}]\end{aligned} \tag{3.17}$$

The process constraints for the TE plant are as follows:

$$
\begin{aligned}
g_1 &= 1 - \frac{m_{12}}{50} = 0 \\
g_2 &= 1 - \frac{m_{15}}{50} = 0 \\
g_3 &= 1 - \frac{2.8153 x_{46} m_{40}}{p_G} = 0 \\
g_4 &= 1 - \frac{3.4510 x_{46} m_{41}}{p_H} = 0 \\
g_5 &= \frac{m_7}{P_{\max}} - 1 \le 0 \\
g_6 &= 1 - \frac{m_8}{L_{\min}} \le 0
\end{aligned}
\qquad (3.18)
$$

where m_i represents the i^{th} measurement in the plant (41 measured outputs total) whereas p_G and p_H are the desired production of products G and H, respectively. The first two constraints in (3.18) are the liquid level constraints in the flash separator and stripper whereas g_3 and g_4 are production targets for products G and H, respectively. $P_{\max}$ and $L_{\min}$ represent the reactor's maximum allowable pressure and the reactor's minimum liquid level, respectively. Accordingly, g_5 and g_6 represent the reactor's maximum pressure and minimum liquid level constraints, respectively. Following the methodology presented in this work, the above constraints were reformulated in the form shown in (3.8). Applying the PSE approximation analysis, the distribution (variability) in the process constraints due to uncertainty in x_7 is obtained by substituting sampled uncertainty data into each of the PSE-based expressions developed for each of the process constraints shown in (3.18). Following (3.7)-(3.8), the TE process constraints shown in (3.18) were reformulated as follows:

$$
\xi_{g(k)} \le 0 \qquad \forall k = 1,2,...,6 \qquad (3.19)
$$

where $\xi_{g(k)}$ represents the k^{th} process constraint in the TE process shown in (3.18) and that is evaluated using a PSE-based constraint function at a given probability of satisfaction Pb_h. Based on the above descriptions, the optimal operation problem of the TE process under uncertainty in x_7 can be formulated as follows:

$$
\begin{aligned}
&\min_{\mathbf{x}} \phi_{TE}(\mathbf{x},\mathbf{m}) \\
&\quad \text{s.t.} \\
&\quad \text{TE process model} \\
&\quad \xi_{g(k)} \le 0 \qquad \forall k = 1,2,...,6 \\
&\quad x_i \ge 0 \qquad \forall i = 1,2,...,38,\ i \ne 7 \\
&\quad 0 \le x_i \le 100 \qquad \forall i = 39,40,...,50
\end{aligned}
\tag{3.20}
$$

where the TE process model was developed by Ricker [133] as a MATLAB code and not discussed here for brevity. The present analysis assumes that a suitable control scheme can be designed to maintain the feasible operation of the TE process. Problem (3.20) aims to identify the optimal operation of the 49 states in the TE process (which also include the nominal values in the manipulated variables) in the presence of uncertainty in x_7, which follows the description shown in (3.16). For comparison purposes, problem (3.20) was solved using the mean (nominal) value in x_7 (i.e. optimal design using only $x_{7,nom}$) and using the uncertainty description shown in (3.16) for x_7. Also, the optimal operation of the TE plant was solved for different confidence levels in the process constraints and the model outputs. The results obtained for the available manipulated variables **u** and the output measurements **m**, which specify the TE's optimal steady-state operating conditions, are shown in Table 3.5. The present analysis shows that, for the nominal base case (i.e. $x_7=x_{7,nom}$), a total cost of 2% less than that reported by Ricker's [133] (114.31 $/h) was obtained with the present method. As shown in Tables 3.5, conservative (expensive) plant designs were specified by the present method to accommodate the uncertainty considered in x_7. For the present analysis, a first order PSE approximation was found to be sufficient to describe the output constraint distributions. A 13% increase in the total costs was observed for the case of compliance of the constraints under uncertainty (Pb_h=0.9973) as opposed to the case when $x_7$is fixed to its nominal value. As shown in Table 3.5, the optimal TE process operation requires more purging when x_7 is assumed to be uncertain, which leads to high economic losses due to wasted products in the purge stream. Table 3.5 also shows that in the purged stream, the concentration of the more expensive components (according to (3.17)), which are reactant D, products G and H, are higher when the uncertainty in x_7 is considered in the analysis. This also results in higher losses in the purge stream than in the case of fixing x_7 to its nominal (mean) value. Since x_7 represents the number of liquid moles of the product G in the reactor, this state has a direct effect on the reactor's pressure and liquid level, which results in a reduction in the condenser coolant flowrate.

Table 3.5 Optimal operation of the TE plant, Scenario 1.

Manipulated variables	$x_7=x_{7,nom}$		*Pb=0.6827*		*Pb=0.9545*	*Pb=0.9973*
		PSE	*MC*	*Halton*		
D feed flow, %	62.781	62.781	62.782	62.782	62.796	62.816
E feed flow, %	53.216	53.403	53.375	53.368	53.873	53.990
A feed flow, %	27.594	27.786	27.851	27.844	27.442	26.933
A+C feed flow, %	60.503	60.528	60.510	60.508	60.647	60.550
Recycle valve,%	63.722	63.487	63.598	63.572	55.470	46.516
Purge valve,%	20.978	20.836	20.816	20.825	21.601	22.624
Separator valve,%	36.812	36.976	36.973	36.970	37.522	38.100
Stripper valve,%	46.615	46.687	46.675	46.671	46.841	46.841
Steam valve,%	1.000	1.000	1.000	1.000	1.000	1.000
Reactor coolant,%	37.641	37.862	37.839	37.832	38.400	38.587
Condenser coolant,%	100.000	100.000	100.000	100.000	52.640	38.300
Agitator speed,%	48.623	48.702	48.676	48.673	49.054	49.172
Key measured outputs						
Recycle flow, ksmch	20.834	20.909	20.896	20.892	21.708	22.387
Reactor pressure, kPa	2800.000	2788.400	2788.200	2788.100	2757.400	2726.000
Reactor level, %	65.001	65.241	65.226	65.220	65.846	66.377
Reactor temp., ^oC	125.180	124.770	124.800	124.820	123.930	123.400
Compressor work, kW	327.860	330.090	330.120	330.050	338.200	340.160
Cond. cool. temperature, ^oC	46.839	46.887	46.880	46.878	53.112	58.015
Purge %A, mol%	39.525	40.011	40.115	40.087	38.359	35.838
Purge %B, mol%	22.283	22.394	22.397	22.398	22.600	22.854
Purge %C, mol%	15.327	14.461	14.299	14.315	13.720	12.920
Purge %D, mol%	0.600	0.646	0.644	0.643	0.787	0.958
Purge %E, mol%	11.554	12.109	12.096	12.091	14.181	16.767
Purge %F, mol%	4.858	4.636	4.688	4.699	4.396	4.383
Purge %G, mol%	3.974	3.898	3.912	3.916	4.033	4.249
Purge %H, mol%	1.879	1.845	1.851	1.853	1.924	2.031
Product %D, mol%	0.013	0.014	0.014	0.014	0.017	0.020
Product %E, mol%	0.807	0.875	0.870	0.869	0.999	1.136
Product %F, mol%	0.329	0.325	0.327	0.327	0.300	0.288
Product %G, mol%	53.629	53.547	53.560	53.564	53.370	53.371
Product %H, mol%	43.749	43.767	43.756	43.754	43.844	43.719

Table 3.5 continues.

Costs breakdown	$x_7=x_{7,nom}$		*Pb=0.6827*		*Pb=0.9545*	*Pb=0.9973*
		PSE	*MC*	*Halton*		
Purge losses ($/h)	56.824	56.347	56.362	56.388	58.378	61.221
Product losses ($/h)	37.971	39.980	39.911	39.864	43.146	47.044
Compressor ($/h)	17.575	17.693	17.694	17.691	18.128	18.233
Steam ($/h)	0.209	0.212	0.212	0.212	0.210	0.207
Total Cost ($/h)	112.580	114.230	114.180	114.150	119.86	126.710
CPU Time(s)	5.706	32.108	16,295.361	7721.978	36.651	36.875

As shown in Table 3.5, the computational time needed to solve this problem was about half a minute when using the present PSE approach. However, the stochastic programming approaches using the standard MC sampling method and the efficient Halton-based sampling method required CPU times that are at least 500 and 240 times larger than that required by the present PSE-based method. This result shows the potential computational benefits of the present methodology to address the optimal design of large-scale processes under uncertainty.

3.4.2.2 Scenario 2: Uncertainty in multiple parameters

This scenario aims to further explore the effect of using high-order terms in the PSE approximation functions due to the use of multiple uncertain parameters in the analysis. Accordingly, the uncertain states considered for this scenario follow a normal distribution PDF with the following characteristics:

$$\begin{aligned} x_7 &\sim N(135.363, 1.8396^2) \\ x_2 &\sim N(7.522, 0.6133^2) \\ x_9 &\sim N(2.580, 0.62204^2) \end{aligned} \tag{3.21}$$

where the means are the nominal values for the TE optimal base case [133] and a variance of 2.5%, 5% and 15% were assumed as parametric uncertainty for states 7, 2 and 9, respectively. The rest of the specifications are the same as in Scenario 1. This scenario was solved using different orders q in the PSE approximation at a constant user-defined probability for all the constraints (Pb_h=0.6). As shown in Table 3.6, the computational time required for Scenario 2 is larger than for Scenario 1 even

for the case of a first order PSE approximation (Scenario 2, q=1). This increase in the computational costs is mostly due to the simultaneous consideration of multiple uncertainties occurring in the plant. Table 3.6 also shows that the first order PSE approximation does not provide accurate results when compared to the designs achieved with high order PSE approximations, i.e., using a first-order PSE approximation in the calculations resulted in plant costs that are 11% lower than that obtained from a second-order PSE approximation. Thus, high order PSE approximation functions needed to be considered in the calculations to accurately describe the variability in the constraints due to the uncertainty in states x_2, x_7 and x_9. As shown in Table 3.6, the operating costs obtained for the second-order (q=2) and the third-order PSE approximation (q=3) have a relative error less than 1%. Hence, the current scenario will adopt a second order PSE approximation as it identifies the optimal operating conditions of the TE plant in a CPU time that is about 5 times faster than using third-order PSE approximation functions for the process constraints and model outputs considered in the analysis.

As shown in Table 3.6 (Scenario 2, q=2), a total operating cost of 140.71 \$/h is needed to satisfy the TE process constraints at a probability limit of Pb_h=0.6. This operating cost is more than 20% higher than that obtained for Scenario 1, i.e., only one uncertain state (x_7) at Pb_h=0.687, and about 25% higher than that obtained when x_7 is fixed to its nominal mean value (see Table 3: x_7=$x_{7,nom}$). As shown in Table 3.6, the purge losses still dominates the total TE plant costs. Note that the concentration of the products lost in the purge stream is higher in Scenario 2 than in Scenario 1. Similarly, the estimates manipulated variables shown in Table 3.6 indicate that a larger purge valve opening (more purging) is needed when compared to the design obtained under perfect knowledge of all the system's states, i.e. x_7=$x_{7,nom}$ in Table 3.5. This result indicates that the specification of the optimal operation of the TE process under the assumption of system's states or model parameters that are assumed to be perfectly known results in inoperable plants under uncertainty. On the other hand, the present method identified (at minimum computational cost) an optimal operating condition for this process that remains feasible (at given probability of satisfaction, Pb_h) in the presence of uncertainty in multiple system's states.

Table 3.6 Optimal operation of the TE plant, Scenarios 2 and 3.

	Scenario 2	*Scenario 2*	*Scenario 2*	*Scenario 3*
Manipulated variables	*(q=1)*	*(q=2)*	*(q=3)*	*(q=2)*
D feed flow, %	62.89	65.88	65.88	62.89
E feed flow, %	53.72	54.34	54.35	56.72
A feed flow, %	26.71	27.26	27.25	26.45
A+C feed flow, %	60.50	62.03	62.03	61.62
Recycle valve,%	45.13	43.90	43.82	1.00
Purge valve,%	23.05	24.01	24.01	26.39
Separator valve,%	38.03	40.07	40.10	41.33
Stripper valve,%	46.75	48.16	48.17	47.78
Steam valve,%	1.00	1.00	1.00	41.30
Reactor coolant,%	38.33	38.90	38.91	40.80
Condenser coolant,%	37.27	100.00	100.00	18.78
Agitator speed,%	48.93	48.88	48.89	50.26
Key measured outputs				
Recycle flow, ksmch	22.24	20.84	20.85	31.87
Reactor pressure, kPa	2720.00	2678.70	2678.40	2800.00
Reactor level, %	66.11	65.83	65.86	70.00
Reactor temperature, ^{o}C	123.97	125.06	125.03	118.48
Compressor work, kW	336.94	323.55	323.56	269.33
Cond. cool. temperature, ^{o}C	58.30	47.20	47.20	81.65
Purge %A, mol%	34.65	31.66	31.64	32.39
Purge %B, mol%	22.90	23.85	23.85	21.31
Purge %C, mol%	13.40	12.47	12.44	11.02
Purge %D, mol%	0.92	1.05	1.06	1.80
Purge %E, mol%	16.68	19.16	19.23	24.62
Purge %F, mol%	4.86	5.47	5.44	2.61
Purge %G, mol%	4.47	4.36	4.35	4.17
Purge %H, mol%	2.13	1.98	1.98	2.08
Product %D, mol%	0.02	0.02	0.02	0.03
Product %E, mol%	1.06	1.35	1.36	1.45
Product %F, mol%	0.30	0.38	0.37	0.15
Product %G, mol%	53.53	54.44	54.43	52.33
Product %H, mol%	43.62	42.35	42.34	44.57

Table 3.6 continues.

	Scenario 2	*Scenario 2*	*Scenario 2*	*Scenario 3*
Costs breakdown	*(q=1)*	*(q=2)*	*(q=3)*	*(q=2)*
Purge losses ($/h)	62.44	64.25	64.24	74.74
Product losses ($/h)	44.85	58.91	59.23	53.33
Compressor ($/h)	18.06	17.34	17.34	14.44
Steam ($/h)	0.20	0.21	0.21	7.03
Total Cost ($/h)	125.54	140.71	141.02	149.54
CPU Time(s)	201.79	358.71	1,868.93	274.19

For this case study, it was not possible to compare the results presented in Table 3.6 with that of a stochastic programming approach because the solution of the optimal operation of the TE plant will require intensive calculations. That is, assessing the variability in the process constraints and model outputs at each optimization step using extensive simulations of the full TE plant model for a large set of realizations in the uncertain parameters may result in prohibitive computational times. In order to compare the computational costs while using the actual TE process model and different orders in the PSE approximation functions, the CPU time needed to obtain the distribution (frequency histogram) in the reactor's maximum pressure constraint was assessed. To perform this analysis, the specifications obtained for the second-order PSE approximation shown in Table 3.6 (Scenario 2, q=2) were used to generate the frequency histogram for this constraint via the MC sampling method applied to the full plant model. The same frequency histogram was generated using a first-order, second-order and a third-order PSE approximation function for that constraint. 10,000 realizations that follow the description in (3.21) for the uncertain parameters were used in this analysis. As shown in Figure 3.7, second-order and third-order PSE approximations accurately capture the distribution in the reactor's pressure due to the realizations considered for the uncertain parameters. The CPU time needed to generate this distribution using the full plant model and the different PSE approximations are shown in the legends of Figure 3.7. These results indicate that using a third order PSE approximation (q=3) returns accurate approximations in a CPU time that is about 80 times faster than using the complete TE plant model.

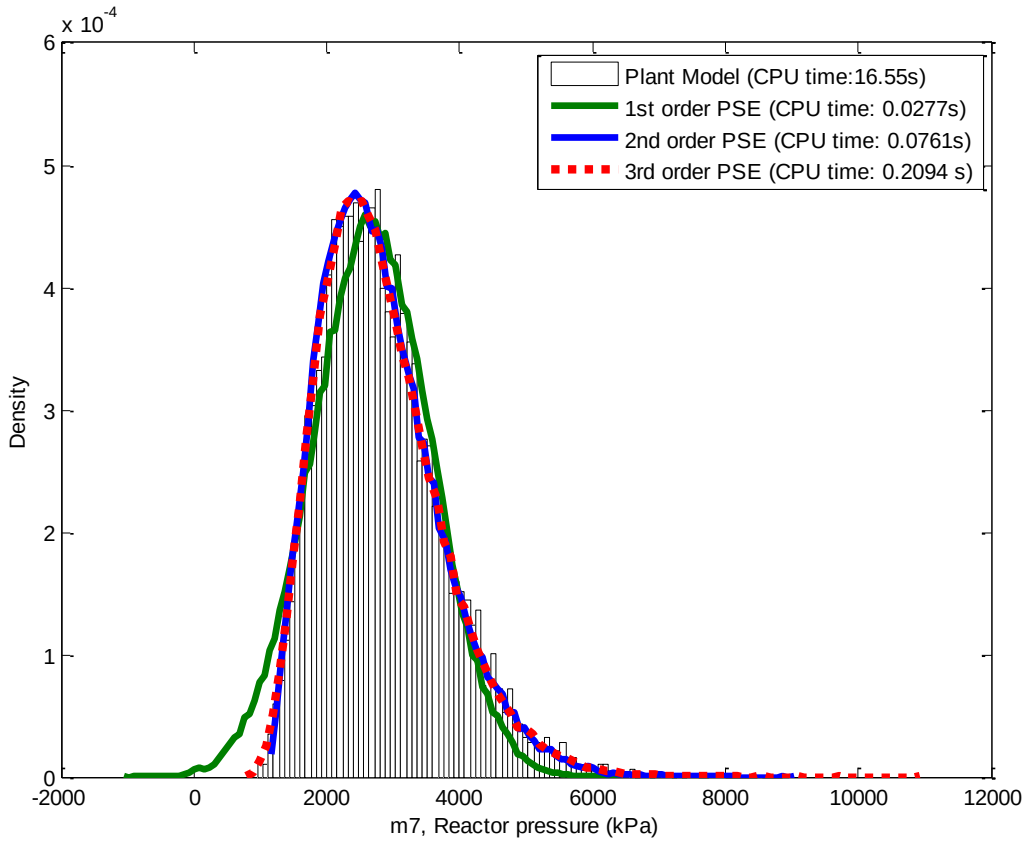

Figure 3.7 Frequency histogram for the reactor's pressure obtained via the Monte Carlo method applied to the full TE plant model and the PSE-based model using different approximation orders.

3.4.2.3 Scenario 3: Ranking-based designs

The present scenario aims to demonstrate the ranking-based feature of the proposed approach to address the optimal operation of the TE process. To perform this analysis, the results obtained from Scenario 2 will be compared to the case were the probability of satisfaction for the reactor's level and pressure constraints are set to 0.9 and 0.5, respectively, i.e. $\mathrm{Pb}_{g6} = 0.9$ and $\mathrm{Pb}_{g5} = 0.5$. The probability of satisfaction for the rest of the constraints considered for this plant, i.e., Pb_{g1}-Pb_{g4}, was set to 99.73%. The uncertainty in the parameters were assumed to be same as in Scenario 2 and shown in (3.21) whereas the order of the PSE approximation was set to q=2. Table 3.6 shows the results obtained for the present scenario (Scenario 3). Figure 3.8 shows the validation of the results

obtained for the present scenario by evaluating the distribution (variability) in the reactor's level and pressure constraints using the actual TE plant model.

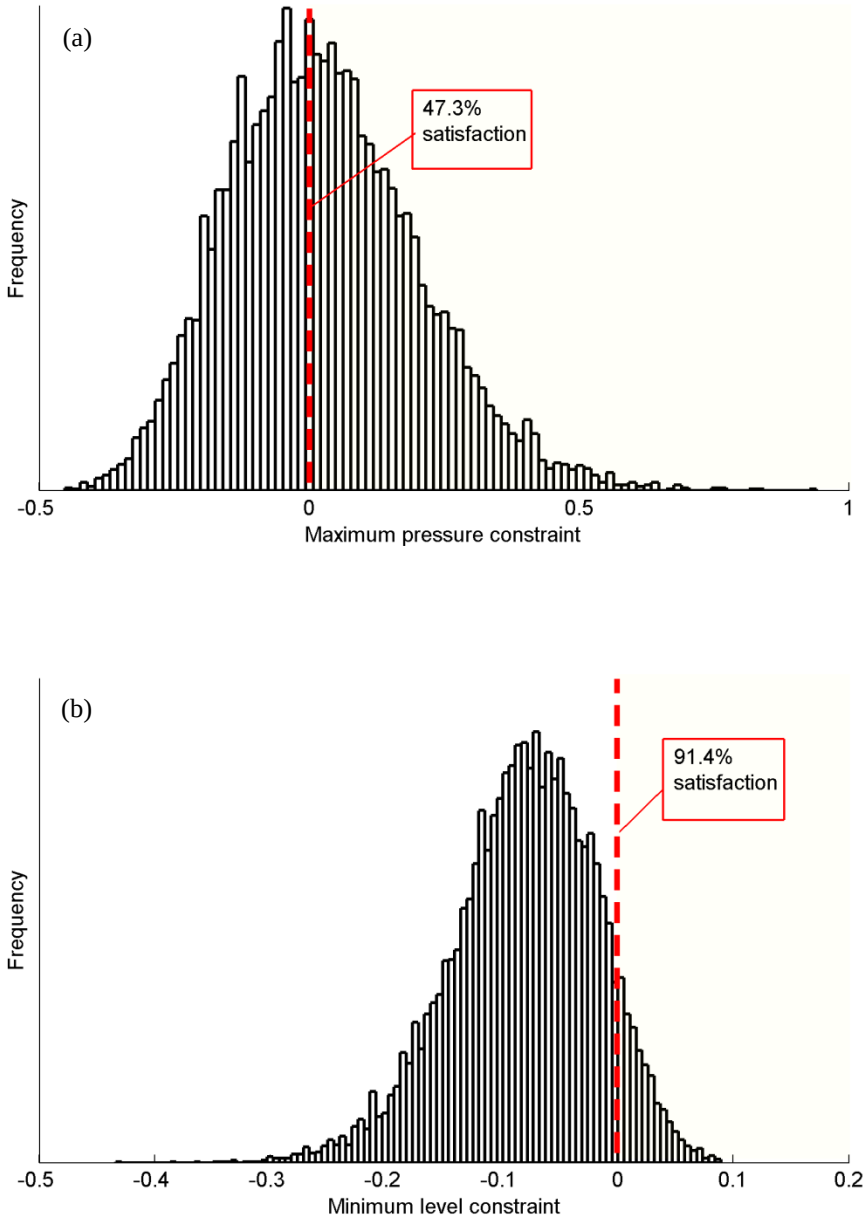

Figure 3.8 Frequency histogram for (a) the reactor's maximum pressure constraint, and (b) the reactor's minimum level constraint, obtained for Scenario 3 via the Monte Carlo sampling method applied to the full TE process model

As shown in this Figure, good approximations to the probability limits considered for the reactor's level and pressure are obtained while using the present ranking-based approach with as second-order PSE approximation. As shown in Table 3.6, the total costs specified for Scenario 3 are about 6% higher than those obtained Scenario 2 where the constraints were set to an equal probability of satisfaction of 60% (Pb_h=0.6). To ensure the high probability of satisfaction assigned to the reactor level constraint in the present scenario ($Pb_{g6} = 0.9$), the optimal operation requires the nominal value of the reactor level to be set at 70%, which is 4% higher than that specified for Scenario 2 (q=2). This increase in the reactor's nominal liquid level also increased the reactor coolant's flowrate by almost 2% with respect to Scenario 2 (q=2). Similarly, the reactor pressure constraint is not active at the solution for the Scenario 3 due to the low probability of satisfaction assigned to this constraint ($Pb_{g5} = 0.5$). Hence more violations were assumed to be allowed on this constraint for this Scenario. Moreover, the present scenario specified a nominal temperature in the reactor that is 7 ^{o}C lower than that obtained for Scenario 2. This decrease in temperature, combined with a high reactor working pressure, resulted in a decrease in the coolant flowrate in the condenser unit. Note that the computational time required to achieve a solution for the present Scenario is comparable to that required by Scenario 2 (q=2). These results show that the ranking-based approach proposed in this work is a computationally attractive practical tool that can be used to study different design alternatives that involve tradeoffs between profitability and robust (expensive) plant designs under uncertainty.

3.5 Chapter Summary

In this chapter, a new method that addresses the optimal process design under uncertainty was presented. A ranking-based approach is considered in the present study where the user can assign different probability limits to each of the safety, environmental and operational constraints considered in the analysis. Thus, critical constraints are enforced to be satisfied all the times by setting a high probability limit whereas less sensitive constraints to the process safety and economics may be allowed to be violated at an accepted level of confidence. This feature gives the flexibility to select between conservative (expensive) designs and economically attractive designs that allow constraint violations. An analytical expression for the process constraints in terms of the uncertain variables is obtained using a Power Series Expansion (PSE) approximation. The PSE expressions are then used to

compute (at minimum computational cost) the distribution (variability) in the process constraints and model outputs due to multiple realizations in the uncertain parameters, which are assessed using the MC sampling method. The proposed approach is computationally attractive because it avoids the need to simulate the complete plant model for each realization in the uncertain parameters as it is the case in stochastic programming-based approaches. The key computational effort in the present method relies in the identification of the sensitivity terms for each of the PSE approximations that need to be developed for the process constraints and model outputs considered in the analysis. However, the two case studies examined in this work indicate that the computational times needed by the present method to address the optimal design of a large-scale system is orders of magnitude shorter than those required by the traditional stochastic programming-based methods, which rely on extensive simulations of the complete process model.

Chapter 4
Optimal design of a post-combustion CO_2 capture plant under process uncertainty

This chapter presents a study on the effect of process uncertainty on the optimal design of CO_2 capture plants. The work presented in this chapter employs the novel method described in Chapter 3 [126], for the optimal design of large-scale chemical processes (such as the CO_2 capture plant) under uncertainty, which uses a Power Series Expansion (PSE) approximation to the actual nonlinear process in computing the output distribution of the process constraints in the presence of uncertainty. The motivation behind implementing the developed approach on a CO_2 capture plant is to demonstrate the applicability of the approach on an actual large-scale chemical process as well as to provide insights on the optimal design of CO_2 capture plants under uncertainty. The organization of this chapter is as follows: The process description of a post-combustion CO_2 capture process along with the implementation and formulation of the problem is presented in Section 4.1. Two case studies involving the optimal design of the CO_2 capture plant under single and multiple process uncertainties are presented in Section 4.2. The effect of process uncertainty on the optimal design of CO_2 capture plants is summarized in Section 4.3.

4.1 Post-combustion CO_2 capture process design problem

Post-combustion using chemical absorption with amine solvents (such as MEA) is by far the most common and developed technique to capture CO_2 from flue gas with low CO_2 concentrations. Figure 4.1 presents a schematic diagram of a typical amine-based carbon capture unit, consisting mainly of an absorber and a stripper column with the required heating and cooling equipment. The flue gas enters through the bottom of the absorption column and comes in contact with the lean amine solvent (such as MEA) flowing downwards from the top of the absorber column, selectively absorbing CO_2 from the flue gas. The treated flue gas leaves the top of the absorber column and is discharged from the process in the vent gas stream; the bottoms of the absorption process represent rich amine solvent with all the absorbed CO_2. This rich amine solvent is then pre-heated in a cross heat exchanger using

the recycled lean amine solvent stream coming from the stripping section of the plant. The heated rich amine stream enters the stripper column for solvent regeneration (removal of absorbed CO_2). Desorption of CO_2 from the amine solvent is an endothermic process, requiring additional heat supplied by the reboiler steam unit located at the bottom of the stripper column (Figure 4.3). Desorbed CO_2 leaves the top of the stripper in a vapor stream, which is then passed through a reflux condenser to obtain a CO_2-rich product gas. On the other end, regenerated lean amine solvent is cooled down before it is recycled back to the absorber column to remove the incoming CO_2 in flue gas stream. Since solvent will be lost in the regeneration process, make-up streams consisting of water and MEA are needed to maintain the operation of this plant.

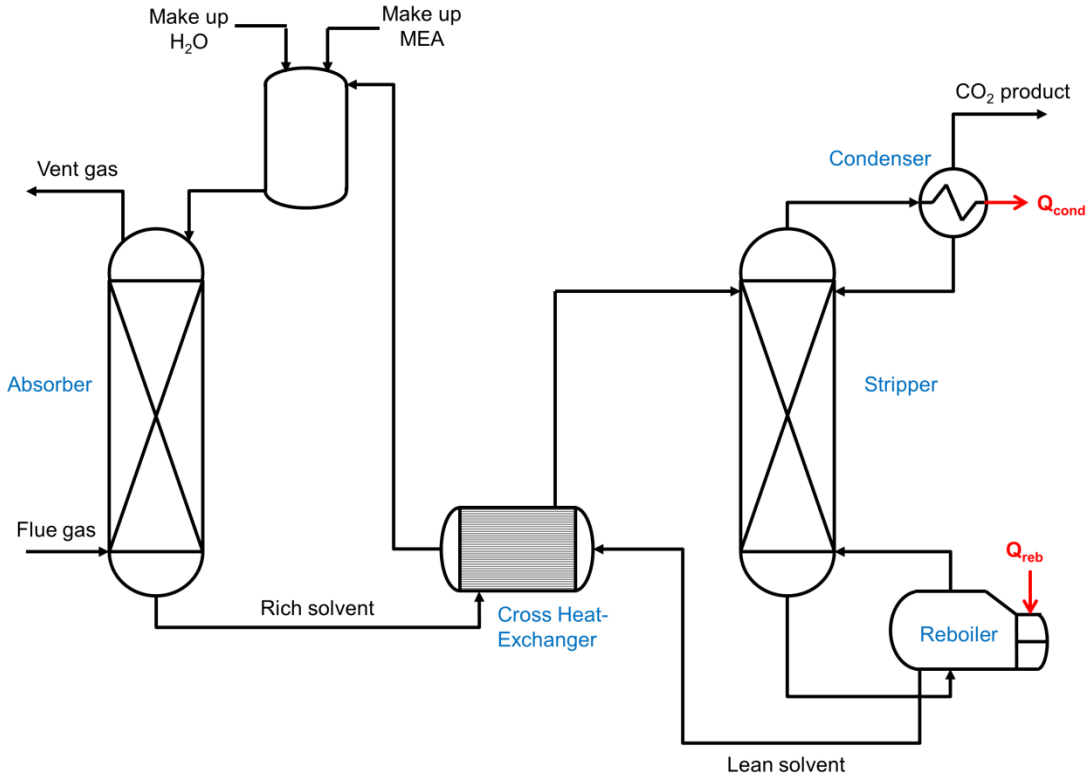

Figure 4.1 Schematic diagram of the main units of a typical amine-based carbon capture unit.

A previous study presented by Dugas [134] on a CO_2 capture pilot plant using MEA has been used as the design basis for this work because of the availability of the actual design and operating conditions

data. In addition to the process flowsheet reported by Dugas [134], the present work adds a condenser unit (as shown in Figure 4.1-state process was modelled in Aspen HYSYS using the base case operating conditions of the pilot plant process data reported by Dugas [134]. A rate-based model was adopted to model the absorption/stripping columns as opposed to the equilibrium-based model. The assumptions of theoretical stages and phase equilibrium are insufficient to describe the behaviour of the absorption process where reactions are taking place inside the packed column. Thus, the rate-based method, which uses a reaction mechanism model, has gained more acceptance over traditional equilibrium-based approaches [6,7,135], and is adopted in the present work. The mechanism that describes the reaction between CO_2 and MEA used in the present model is the Zwitterion mechanism, which is the most accepted kinetic model for absorption of CO_2 in aqueous MEA [136]. For this model, the kinetic data presented in [137,138] were used. NRTL was implemented as the base equation of state for this process while the Kent-Eisenberg thermodynamic model is used for the aqueous amine solutions. Table 4.1 shows the validation of the developed plant model in Aspen HYSYS. As shown in that Table, the developed model is in reasonable agreement with the experimental data reported in the literature for this CO_2 capture plant [12,13,134]. Note that some of the operating conditions and equipment sizes were compared with other references in the literature since those parameters were not reported by Dugas [134].

Table 4.1 Validation of the developed plant model in Aspen HYSYS.

	Plant model	Specification	[Source]
Flue-gas flowrate			
Temperature (K)	319.70	319.71	[134]
Molar flowrate (mol/s)	4.01	4.01	[134]
Mole fractions:			
CO_2	0.175	0.175	[134]
H_2O	0.025	0.025	[134]
N_2	0.8	0.8	[134]
Absorber			
Height (m)	6.1	6.1	[134]
Internal diameter (m)	0.43	0.43	[134]
Temperature (K)	325	314–329	[134]
Pressure (kPa)	102	101.3-103.5	[134]
Stripper			
Height (m)	6.1	6.1	[134]
Internal diameter (m)	0.43	0.43	[134]
Temperature (K)	358	350–380	[134]
Pressure (kPa)	160	159.5–160	[134]
Process variable			
Reboiler Temperature (K)	386.9	383-393	[12]
Reboiler Pressure (kPa)	160	160	[12]
Condenser Temperature (K)	314.3	312-315	[13]
Condenser Pressure (kPa)	159.5	159	[13]
CO_2 recovery (mole %)	95.04	95.9	[13]
CO_2 product (mole %)	95	95	[13]
Lean solvent temperature (K)	314	312.8	[13]
Vent gas CO_2 content (mole fraction)	0.0010	0.0055-0.0085	[12]

4.2 Optimal design under uncertainty framework

This section presents the implementation of the optimal design methodology presented in Chapter 3 on the post-combustion CO_2 capture plant described in the previous section. The objective function and the process constraints are explained first followed by the optimization variables selected for the present analysis.

4.2.1 Objective function

The aim of this work is to optimize the CO_2 capture (*CCap*) plant's design based on an economic objective function. The annualized objective function for this plant is defined in terms of the capital costs (CC) and the operating costs (OC) and is as follows:

$$\begin{aligned} \Phi_{CCap} &= \mathrm{CC}_{CCap} + \mathrm{OC}_{CCap} \\ \mathrm{CC}_{CCap} &= C_{abs} + C_{strp} + C_{HX} + C_{cond} \\ \mathrm{OC}_{CCap} &= C_{reb} \end{aligned} \tag{4.1}$$

where the capital costs include the costs of the main process equipment, i.e., absorber (C_{abs}), stripper (C_{strp}), cross heat exchanger (C_{HX}) and condenser (C_{cond}), whereas C_{reb} denotes the operating costs associated with the reboiler heat duty (Q_{reb}). In this work, only the cost of reboiler heat duty will be considered in the operating costs since the heating consumption for solvent regeneration dominates all other operational costs [9]. The cost function Φ_{CCap} will be used as the objective function in the formulation (3.9) presented in Section 3.3 of the previous chapter.

The detailed expressions for the cost functions in (4.1) are calculated using Guthrie's [139] correlations and are as follows:

Capital costs:

1. Heat exchanger costs (2011 US$/y) = *ROR*(Purchased Cost + Installed Cost) (4.2)

Purchase Cost, \$ = $\left(\frac{\text{M \& S}}{280}\right)(101.3A^{0.65}F_c)$ (4.3)

Installed Cost, \$ = $\left(\frac{\text{M \& S}}{280}\right)101.3A^{0.65}(2.29+F_c)$ (4.4)

$F_c = (F_d + F_p)\, F_m$ (4.5)

A=heat transfer area, ft^2

F_c is a correction factor due to design (F_d), pressure (F_p) and material (F_m) of the equipment.

Correction factors: F_d =0.85, F_p =0.25, F_m =1.

2. Column costs, (2011 US\$/y) = *ROR*(Purchased Cost + Installed Cost) (4.6)

Purchase Cost, \$ = $\left(\frac{\text{M \& S}}{280}\right)(101.9D^{1.066}H^{0.82}F_c)$ (4.7)

Installed Cost, \$ = $\left(\frac{\text{M \& S}}{280}\right)101.9D^{1.066}H^{0.82}(2.18+F_c)$ (4.8)

$F_c = F_m F_p$ (4.9)

D = diameter of absorber (or stripper), ft H = height of absorber (or stripper), ft

F_c is a correction factor due to material (F_m) and pressure (F_p) of the equipment

Correction factors: F_m = 1, F_p = 1.

ROR=20% (rate of return)

M&S = 1, 536.5 (Marshall & Swift equipment cost index, 2011 4th Q) [140]

Operational Costs:

C_{reb} (2011 US\$/y) $= \Theta\left(Q_{reb} \big/ \Delta H_{vap}\right) C_{steam}$ (4.10)

$C_{steam} = \$0.003/kg$, [16] $\Delta H_{vap} = 2257 kJ/kg$, $Q_{reb} = \text{reboiler duty}, kW$

$\Theta = 0.42857\,(\text{conversion factor})$

4.2.2 Process constraints

The optimal process design of a CO_2 capture plant is subject to operational and performance constraints that needs to be satisfied in the presence of process uncertainties. The percentage of CO_2 removed or captured (φ) from the flue gas stream is a metric typically used to measure the performance of these plants and is usually expected to be high enough for the process to be economically viable, with a recent study showing that a 95% CO_2 capture rate to be optimal [9]. The percentage of CO_2 captured φ is defined as follows:

$$\varphi = 1 - \frac{\text{moles of } CO_2 \text{ in vent gas}}{\text{moles of } CO_2 \text{ in flue gas}} \tag{4.11}$$

According to the optimization framework shown in (3.9), this performance metric will be used as a process constraint that targets the optimal design to achieve at least 95% CO_2 capture, i.e.,

$$0.95 - \varphi \leq 0 \tag{4.12}$$

The CO_2 product stream leaving the top of the stripper is desired to have high concentrations in CO_2; hence, a minimum of 95% CO_2 purity (ζ) in the product stream is defined as a constraint as follows:

$$0.95 - \zeta \leq 0 \tag{4.13}$$

In addition to constraints (4.12) and (4.13), operational constraints on the temperature in the reboiler and the lean solvent entering the absorber are included to ensure the feasible operation of this process, i.e.,

$$383 - T_{reb} \leq 0 \tag{4.14}$$

$$T_{reb} - 393 \leq 0 \tag{4.15}$$

$$313 - T_{lean} \leq 0 \tag{4.16}$$

$$T_{lean} - 315 \leq 0 \tag{4.17}$$

When heating the bottom stream of the stripper in the reboiler to regenerate amine solution, degradation of the MEA solvent can occur at high temperatures [15]. Hence, constraints (4.14) and

(4.15) are aimed to maintain the operating temperature range in the reboiler T_{reb} within 383-393 K [12,13]. The temperature of the lean amine solvent entering the absorber has a direct effect on the amount of CO_2 captured [141], and thus its operating temperature range is maintained at approximately 314 K [142]. In order to ease the optimal search, the formulation in (4.16)-(4.17) allows for a deviation of 1 K from the target value of 314 K.

To implement the ranking-based optimization framework proposed in the previous chapter, the constraints considered in the CO_2 capture plant have been reformulated using the PSE-based approach as shown in (3.8). Given the order q of the PSE approximation, the PSE-based function (h_{PSE}) is constructed first using the actual nonlinear CO_2 capture plant model described above. Then, N MC sampled realizations of the uncertain variables will be used in PSE-based function (h_{PSE}), to obtain a histogram of the distribution of each process constraint. Using a user-defined probability value (Pb_h), along with the obtained histograms, the extreme value (ξ_h) for each constraint is computed as shown in Figure 3.1. For example, the PSE-based constraint formulation for constraint (4.12) is as follows:

$$\text{P}(\varphi - 0.95 \le 0) \ge \text{Pb}_{\text{constraint(4.12)}} \quad \Leftrightarrow \quad \xi_{\text{constraint(4.12)}} \le 0 \tag{4.18}$$

The rest of the constraints are formulated in the same fashion and are not shown here for brevity. The probabilistic form of constraints (4.12)-(4.17) as shown in the right hand side of equation (4.18) will be used as the set of constraints for the optimization formulation shown in equation (3.9).

4.2.3 Optimization variables

The set of design and operating variables for the CO_2 Capture (*CCap*) plant ($\boldsymbol{\eta}_{CCap}$) that has been considered include the heights and diameters of both packed columns, the heat transfer areas of both the cross heat exchanger and the condenser, and the heat duty of the reboiler, i.e.,

$$\begin{aligned} \mathbf{d}_{CCap} &= [H_{abs}, H_{strp}, D_{abs}, D_{strp}, A_{HX}, A_{cond}] \\ \mathbf{u}_{CCap} &= [Q_{reb}] \\ \boldsymbol{\eta}_{CCap} &= [\mathbf{d}_{CCap}, \mathbf{u}_{CCap}] \end{aligned} \tag{4.19}$$

The base case design and operation of the CO_2 capture plant is given in Table 4.1 [12,13,134]. The cost of this base case design is evaluated using the capital and operating cost functions shown in (4.1). Detailed equipment specification and operating conditions of the CO_2 plant can be found in [12,13,134].

In the next section, the application of the present approach to address the optimal process design and operation of the CO_2 capture process is presented. The application of the optimization-based framework employed in this study has been implemented in MATLAB whereas the CO_2 capture process was modelled in Aspen HYSYS. This means that the optimization framework and all PSE computations were performed in MATLAB, with communications to and from the Aspen HYSYS whenever process simulations involving the plant model were needed. The studies presented in the next section were performed on an Intel Core i7 3770 CPU @3.4GHz (8GB in RAM).

4.3 Results and discussion

In this section, the formulation proposed to address the optimal design of the CO_2 capture plant has been tested under various scenarios. In this work, uncertainty is assumed in three input variables, i.e., the CO_2 content of the entering flue gas ($\%CO_2$), the temperature of this stream (T_{in}) as well as its flow rate (F_{in}). The results obtained for each scenario considered are presented next.

4.3.1 Scenario A: Steady state optimization without uncertainty

The first scenario considers the CO_2 capture plant's design under the assumption of perfectly known process parameters, i.e. all three input uncertain variables were assumed to be perfectly known and equal to their nominal steady state values, i.e.,

$$\begin{aligned} \overline{\%CO_2} &= 17.5 mol\% \\ \overline{T_{in}} &= 319 K \\ \overline{F_{in}} &= 4.01 mol/s \end{aligned} \tag{4.20}$$

where the overbar sign denote the nominal values of those variables. As shown in Table 4.2, the optimal design obtained for Scenario A is half the height of the stripper specified for the base-case design; also, the diameters of both packed columns are slightly smaller than those specified by the base-case design. Both the heat exchanger and the condenser were also slightly smaller than in the actual plant's design specified by Dugas [134]. To maintain the performance specifications and still satisfy the plant's process constraints, a higher reboiler duty was required when using smaller equipment sizes. This tradeoff, i.e. higher reboiler duty for lower equipment sizes, have resulted in a more economic design since the plant's capital costs dominates the process economics. Thus, although the present scenario has higher operational costs, the optimal design specified for this scenario is about 18% lower in total costs than that obtained with the base-case design.

Table 4.2 Base case plant design and the optimal steady-state plant design (Scenario A).

Decision variables	**Base-case design** [12,13,134]	**Scenario A**
Reboiler duty, Q_{reb} (kW)	153.6	172.12
Absorber height, H_{abs} (m)	6.1	6.1
Absorber diameter, D_{abs} (m)	0.43	0.3005
Stripper height, H_{strp} (m)	6.1	3.05
Stripper diameter, D_{strp} (m)	0.43	0.3011
Heat trans. area, A_{HX} (m^2)	22.47	19.80
Heat trans. area, A_{cond} (m^2)	14.40	11.10
Annualized Costs		
CC ($/y)	4.66E+04	3.58E+04
OC ($/y)	6.17E+03	7.42E+03
Total Costs ($/y)	5.27E+04	4.33E+04

4.3.2 Scenario B: Uncertainty in the flue gas stream's CO_2 composition

This scenario aims to search for the optimal CO_2 capture plant's design that remains feasible in the presence of uncertainty in the flue gas stream's CO_2 content. The uncertainty in this input variable is assumed to follow a Gaussian (Normal) distribution with the following mean and standard deviation parameters:

$$\%CO_2 \sim N(17.5mol\%, 0.175mol\%) \tag{4.21}$$

Based on the ranking-based approach, the user-defined minimum probability of satisfaction Pb_h was set to 85% for each of the constraints as shown in Table 4.3. This means that the optimal design will need to satisfy each constraint 85% of the time or more when subjected to the process uncertain description shown in (4.21).

Table 4.3 Input probability limits for the process constraints.

	Probability of satisfaction (%)		
Constraint	*Scenario B*	*Scenario C*	*Scenario D*
(4.12)	85	85	95
(4.13)	85	95	85
(4.14)	85	75	75
(4.15)	85	75	75
(4.16)	85	90	90
(4.17)	85	90	90

Table 4.4 Optimal steady-state plant designs under uncertainty; Scenario B.

Decision variables	**Scenario B** ***q=1***	**Scenario B** ***q=2***	**Scenario B** ***q=3***	**Scenario B** ***q=4***	**Scenario B** ***q=5***	**Scenario B** ***q=6***
Reboiler duty, Q_{reb} (kW)	184.5000	195.4961	194.2464	194.5281	197.2880	196.1544
Absorber height, H_{abs} (m)	6.1	6.1	6.1	6.1	6.1	6.1
Absorber diameter, D_{abs} (m)	0.3950	0.3794	0.3401	0.3390	0.3345	0.3371
Stripper height, H_{strp} (m)	3.05	5.3375	5.3375	5.3375	5.3375	5.3375
Stripper diameter, D_{strp} (m)	0.3150	0.4322	0.6365	0.6377	0.6382	0.6379
Heat trans. area, A_{HX} (m^2)	10.7991	10.8259	10.8553	10.8260	10.8259	10.8262
Heat trans. area, A_{cond} (m^2)	19.7984	19.7987	20.3930	20.3932	20.3935	20.3928
Cost						
CC ($/y)	3.76E+04	4.12E+04	4.43E+04	4.44E+04	4.43E+04	4.44E+04
OC ($/y)	7.42E+03	7.86E+03	7.81E+03	7.82E+03	7.93E+03	7.88E+03
Total ($/y)	4.50E+04	4.91E+04	5.21E+04	5.22E+04	5.22E+04	5.22E+04
CPU Time (h)	1.489	2.031	2.934	3.832	5.089	6.394

As discussed in Section 3.2.1 in the previous chapter, the method used in this work approximates the actual distribution of the process constraints due to the realizations of the uncertain process variables using a q^{th} order Power Series Expansion (PSE). Increasing the expansion order q improves the

distribution approximation and is needed when dealing with highly nonlinear systems. However, the higher the expansion order used, the more computationally intensive the problem becomes. Thus, an increase in the expansion order is only justified if it yields significant improvement in the resulting probability distribution of the process constraints. To further illustrate the convergence characteristics of the PSE-based method, and to also select the order q to be used in this problem, the present scenario was solved using different expansion orders (see Table 4.4). Figure 4.2 shows the convergence of the distribution while using different orders in the PSE expansion, i.e., from q=1 to q=6.

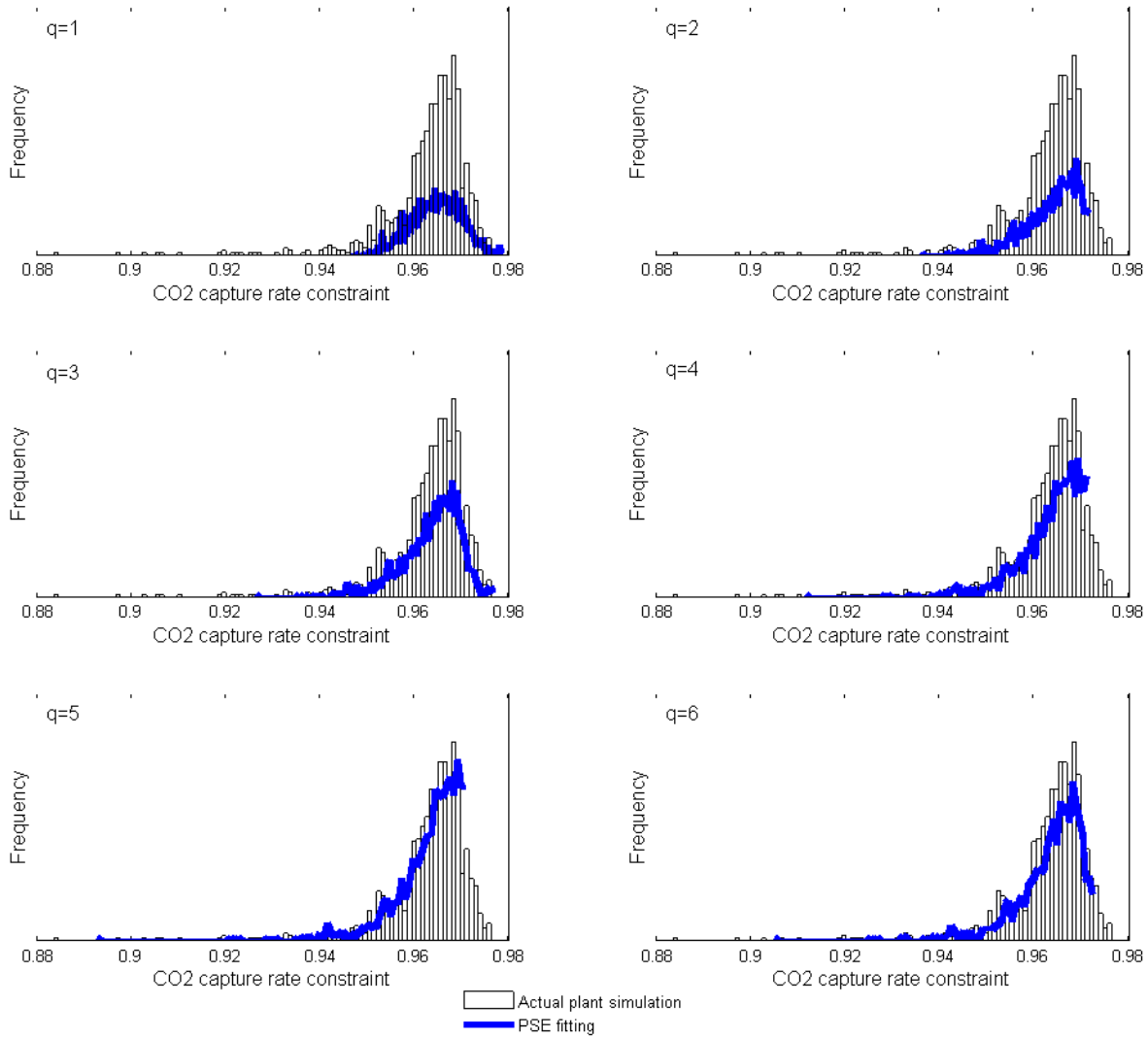

Figure 4.2 PSE fitting for the distribution of the CO_2 capture rate constraint using different expansion orders.

While Figure 4.2 may suggest that q=6 is the best approximation, Table 4.4 shows that the optimal solution converges at or near q=3, where the maximum difference with the solution of q=6 in both process design and plant's cost is less than 1%. As shown in Table 4.4, the computational effort for solving the optimal design problem is directly correlated with the expansion order used. Therefore, q=3 is sufficient enough to yield good accuracy and save computational time (23% faster than q=4 and 54% faster than q=6). As shown in Table 4.4 (Scenario B, q=3), uncertainty in the flue gas stream's CO_2 composition has affected the optimal design requiring larger columns (absorber's diameter and stripper height and diameter) as well as a larger heat duty than that required for Scenario A. Due to the presence of uncertainty, there will be instances where the CO_2 composition in flue gas will be higher than its nominal value, which demands larger columns and reboiler duty to capture the extra CO_2 contained in the flue gas stream as well as to regenerate the MEA from the rich amine solvent stream. As a result, this scenario yielded optimal designs that are 5% and 24% higher in operational and capital costs than that obtained from Scenario A's design; however, Scenario B's design satisfies the process constraints under uncertainty in $\%CO_2$ at least 85% of the time, which is the minimum probability of constraint satisfaction specified for this scenario (see Table 4.3). Process constraint (4.12), which is associated with the percentage of CO_2 captured φ, was found to be the only active constraint at the solution for Scenario B. The optimal design obtained for Scenario B was validated by running the actual plant model 1,000 times using sampled uncertain realizations in $\%CO_2$ for each simulation; as shown in Figure 4.3a, Scenario B's design is able to satisfy the active process constraint (4.12) according to the user-defined minimum probability limit, $\mathrm{Pb}_h = 0.85$. On the other hand, Figure 4.3b shows that the original base-case design is inoperable under uncertainty in $\%CO_2$ since process constraint (4.12) was found to be violated almost 82% of the time when using that design. Scenario A's design yielded similar high violations in the active constraint (4.12) when operating under the uncertainty description (4.21) and it is not shown here for brevity. Note that the cross heat exchanger and condenser areas were not significantly affected by the presence of uncertainty in this scenario.

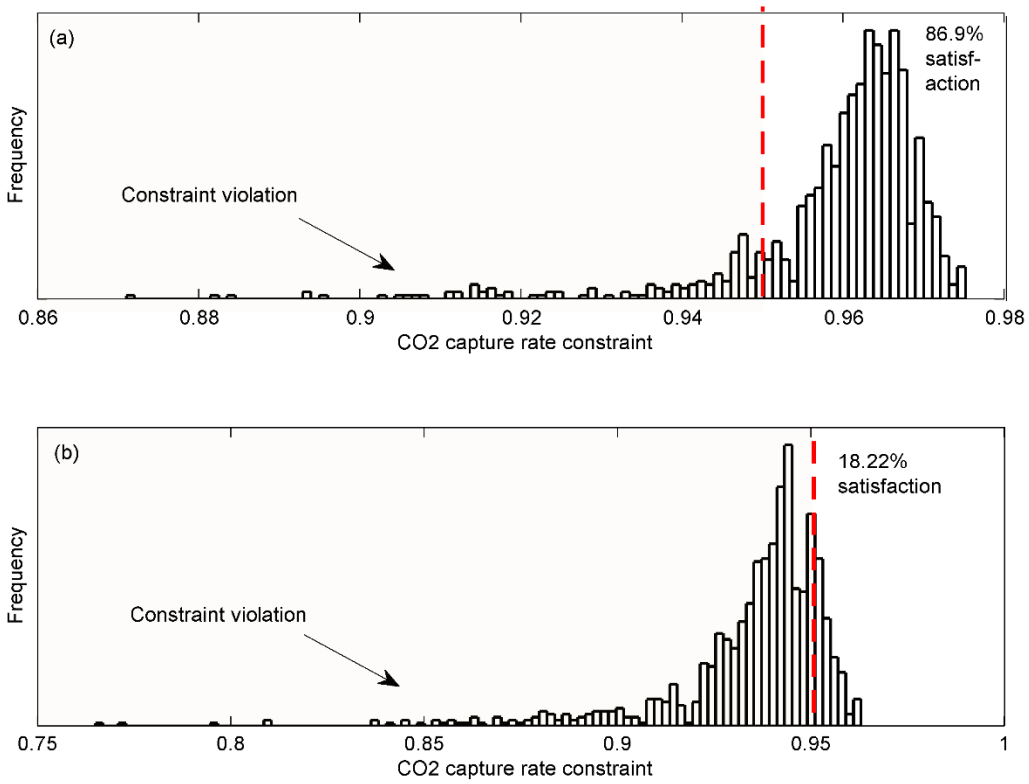

Figure 4.3 Frequency histograms for the CO_2 capture rate constraint under single uncertainty for (a) Scenario B design, and (b) the base-case design.

4.3.3 Scenario C: Ranking-based designs

In this scenario, the ranking-based feature of the optimal process design approach described in Section 2 has been explored for this process. Accordingly, each process constraint has been assigned to different probability limits Pb_h and it is shown in Table 4.3. Instead of the Gaussian distribution assumption shown in (4.21), a more conservative approach is used in this scenario; thus, the uncertainty in $\%CO_2$ was assumed to follow a uniform distribution with upper and lower bounds defined as follows:

$$\%CO_2 \sim U(15.75 mol\%, 19.25 mol\%) \tag{4.22}$$

Based on the results from the previous scenario, the order in the PSE expansion was set to q=3 for this scenario. Table 4.5 (Scenario C) shows the optimal design obtained for this scenario. With a uniform probability distribution describing the uncertainty (rather than Gaussian), a more expensive design was obtained; this was mainly due to the 16% increase in the plant's capital costs with respect to Scenario B's design. The optimal design for this scenario has larger absorber diameter and stripper height than that obtained for Scenario B's design; nevertheless, the stripper's diameter was the design parameter that changed the most, with a 37% increase in size with respect to Scenario B's design. Even though the larger sized plant required lower heat duty in the reboiler unit during the regeneration process of the amine solvent, the capital costs associated with the columns' size (diameter and height) dominate the process economic, and thus resulted in an overall increase of 13% in the total costs for this scenario as compared to Scenario B's design. The ranking-based structure of the input probability limits (shown in Table 4.3) did not change the active constraint of the problem, which remained to be the percentage of CO_2 captured φ (4.12).

Table 4.5 Optimal steady-state plant designs under uncertainty; Scenarios C and D.

Decision variables	**Scenario C** ***q=3***	**Scenario D** ***q=4***
Reboiler duty, Q_{reb} (kW)	180.5022	252.0000
Absorber height, H_{abs} (m)	6.1	7.625
Absorber diameter, D_{abs} (m)	0.3900	0.8370
Stripper height, H_{strp} (m)	6.1	6.1
Stripper diameter, D_{strp} (m)	0.8722	0.5550
Heat trans. area, A_{HX} (m^2)	10.8933	10.8855
Heat trans. area, A_{cond} (m^2)	20.4159	21.2527
Cost		
CC ($/y)	5.14E+04	5.76E+04
OC ($/y)	7.26E+03	1.01E+04
Total ($/y)	5.87E+04	6.77E+04
CPU Time (h)	2.943	3.901

4.3.4 Scenario D: Multiple process uncertainties

The present scenario extends Scenario B and considers the simultaneous occurrence of three uncertain realizations in the flue gas stream, i.e., CO_2 content, flow rate and temperature. The uncertainty description for this scenario is defined as follows:

$$\begin{aligned} \%CO_2 &\sim N(17.5\,mol\%,\ 0.175\,mol\%) \\ T_{in} &\sim N(319K,\ 16K) \\ F_{in} &\sim N(4.01\,mol/s,\ 0.2\,mol/s) \end{aligned} \tag{4.23}$$

The input probability limits assigned for the process constraints is shown in Table 4.3. Due to the increased degree of nonlinearity from the interaction of simultaneous occurrence of multiple uncertainties, an order of q=4 was found to be suitable to obtain reasonably good approximations to the process constraints' output distributions. Also note in Table 4.3 that a higher probability limit (compared to the previous scenarios) of 95% was assigned to the active constraint (4.12). This aspect, along with the simultaneous occurrence of multiple process uncertainties, makes this scenario even more challenging and computationally demanding. The simultaneous occurrence of multiple process uncertainties can lead to higher nonlinearities in the output of the process constraints, and thus may require higher PSE orders. From the computational point of view, this scenario requires the computation of higher order sensitivity terms of the process constraints with respect to 'three' different uncertain variables, as opposed to just 'one' as in the previous scenarios. In addition, the higher probability limit assigned to the active constraint in this scenario means that the optimal design has to satisfy the same constraint more frequently while subjected to more (multiple) uncertainties. The optimal design obtained for Scenario D is shown in Table 4.5 (Scenario D). For this scenario, a 25% increase in the absorber's height and more than double the diameter than that reported for Scenario B was specified. Likewise, the stripper column's overall volume was reduced by about 13% due to its smaller diameter, and only a slight increase in its height, when compared to Scenario B's design. As shown in Table 4.5 (Scenario D), a 30% increase in the reboiler heat duty than that obtained for Scenario B was necessary to achieve a feasible design. Overall, both the operation and capital costs are higher for this scenario which may be directly justified by the need to accommodate additional uncertainties; also, the present scenario is required to meet a higher demand of satisfying the active constraint with a minimum probability of 95% (rather than 85% as in the previous

scenarios). Moreover, the cross heat exchanger and condenser areas were not significantly affected by the presence of multiple uncertainties. Although the plant's costs for this scenario is 30% more than that obtained for Scenario B, this scenario specifies a CO_2 capture plant that can meet the desired specifications at the predefined minimum probability of satisfaction while using the uncertainty descriptions given in (4.23) (see Figure 4.4). Since a higher expansion order (q=4) was used in this scenario, a higher CPU time was needed to solve the optimal design problem under uncertainty than that required for Scenarios B and C where a lower order (q=3) was employed. Note that, the CPU time for this scenario is comparable to that in Scenario B when using q=4, even though more process uncertainty were considered in this scenario.

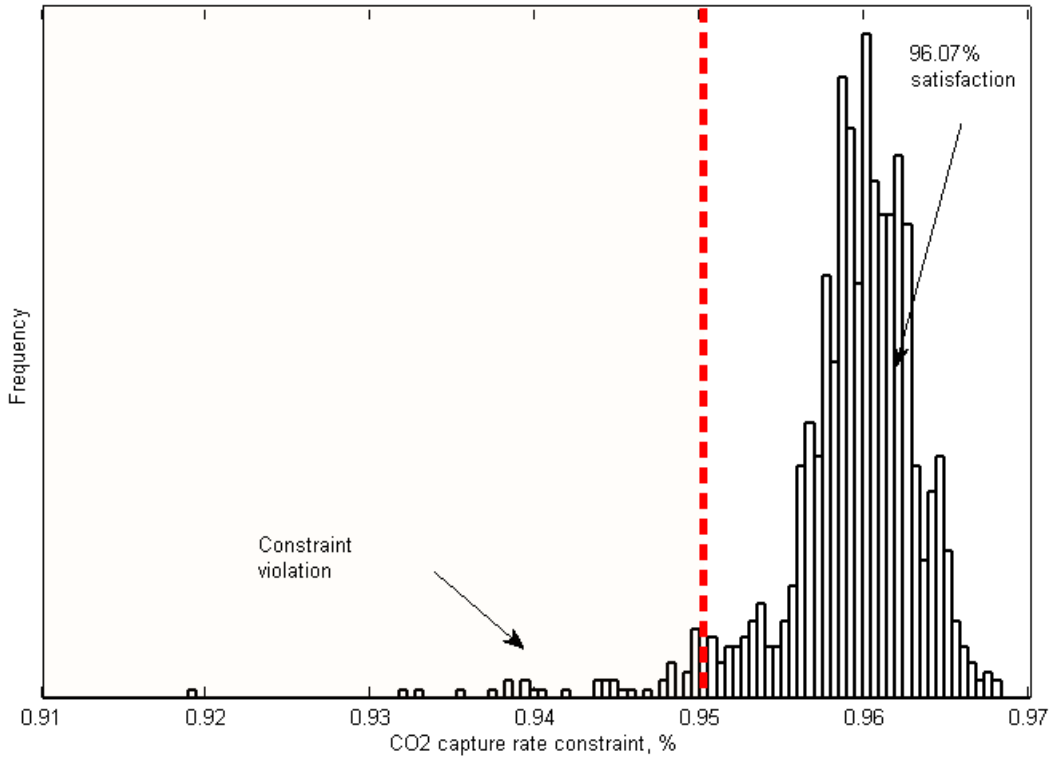

Figure 4.4 Frequency histogram for the CO_2 capture rate constraint under multiple uncertainty for Scenario D design.

4.4 Chapter summary

The optimal design of a CO_2 capture plant in the presence of process uncertainty has been studied in this chapter. The present work employed the proposed method for the optimal design of large-scale chemical processes under uncertainty in the previous chapter, which uses a Power Series Expansion (PSE) approximation to the actual nonlinear process to obtain the output distribution of the process constraints. The need to incorporate uncertainty in the optimal design procedure was justified by the fact that process constraints are usually violated more often for those designs that did not consider the effect of process uncertainty at the design stage. At steady-state, without consideration of uncertainty, the optimal feasible design specified an absorber that is double the height of the stripper column. In the presence of uncertainty in the flue gas stream's CO_2 content, the size of the stripper column (both diameter and height) increased significantly to satisfy the process constraints; the absorber size remained unchanged. The reboiler heat duty, which is an operating variable in the stripping section of the plant, is also higher when considering uncertainty in the flue gas stream's CO_2 content. With more uncertainties introduced in the flue gas input stream, the plant's absorber column increased more than the stripper. While the addition of uncertainties required higher reboiler heat duty, and therefore higher operational costs, the cross heat exchanger and condenser areas did not seem to be affected by the process uncertainty considered in this analysis. The optimal designs obtained under uncertainty specified larger sized plants and needed more utility (i.e., reboiler duty). As a result, these designs were more expensive than the steady state design (without considering uncertainty); with higher operational and especially capital costs which were the dominant term in the economic cost function. However, this increase in costs is justified by the fact that these designs satisfy the process constraints according to the user-defined probability of satisfaction, whereas the optimal steady-state design failed to satisfy the constraints most of the time when operating under uncertainty in the input flue gas stream.

Chapter 5
Simultaneous design and MPC-based control for dynamic systems under uncertainty: A stochastic approach

Although optimal process design is typically performed using steady-state optimization calculations, it has been shown that process dynamics play a significant role while searching for the optimal process design of a system under uncertainty. Therefore, the dynamic behavior of processes needs to be considered in the optimal design under uncertainty problem. This chapter presents a simultaneous design and Model Predictive Control (MPC)-based control methodology that gives the user the freedom of assigning priorities to the key goals of the system to be designed through the implementation of a stochastic approach. The key idea of the present probabilistic-based method is to determine the dynamic variability of the system that will be accounted for in the process design by assigning probability levels to each process variable (or combination of variables) according to their significance. The organization of this chapter is as follows: Section 5.1 presents the mathematical formulation of the MPC and its implementation in the optimization framework for the simultaneous design and control using the proposed probabilistic approach. The implementation of the proposed methodology to an actual wastewater treatment plant is presented next in Section 5.2. A comparison between the proposed MPC-based strategy and conventional multi-loop PI control, as well as a computational cost study of the proposed approach are also presented in this Section. A summary of this work is presented in Section 5.3. The content of this chapter has been published in Computers & Chemical Engineering [70] (see Appendix).

5.1 Simultaneous design and MPC-based control methodology

In this section, the details of the proposed simultaneous design and control methodology are presented. The mathematical description of the simultaneous design and control procedure that incorporates all the features included in this method is presented next. The key novelties of the present approach with respect to those published in the literature are explained at the end of this section.

A chemical process can be characterized by its nonlinear dynamic process model ($\mathbf{J}$), the process inputs ($\boldsymbol{\varepsilon}$), process outputs ($\boldsymbol{\delta}$), a control algorithm and its tuning parameters ($\boldsymbol{\Lambda}$). The process model of a system is represented by the set of differential equations that describe the behavior of the process in the transient domain. This work assumes that the process model ($\mathbf{J}$) is available for simulations. Process inputs ($\boldsymbol{\varepsilon}$) include the available manipulated variables (ς) that can be used by the control strategy to maintain stability and performance of the system within specifications, as well as the disturbances ($\boldsymbol{\lambda}$) affecting the process:

$$\boldsymbol{\varepsilon} = [\varsigma, \boldsymbol{\lambda}] \tag{5.1}$$

Both (ς) and ($\boldsymbol{\lambda}$) can be further classified into:

$$\varsigma = [\mathbf{u}, \boldsymbol{\rho}] \tag{5.2}$$

$$\boldsymbol{\lambda} = [\boldsymbol{\nu}, \boldsymbol{\omega}] \tag{5.3}$$

where $\mathbf{u}$ represents the manipulated variables used by the controller whereas $\boldsymbol{\rho}$ are the remaining available manipulated variables that are kept constant and unused by the controller; $\boldsymbol{\nu}$ represents the unmeasured disturbances while $\boldsymbol{\omega}$ represents those disturbances that are measured and can potentially be used for feedforward control. The process outputs are classified as follows:

$$\boldsymbol{\delta} = [\gamma, \chi] \tag{5.4}$$

where γ are the process controlled variables whereas χ represents the remaining output variables that are not in closed-loop. In this work, for any process variable, e.g., $\mathbf{S}$, its steady state value will be represented by an overbar ($\overline{\mathbf{S}}$) whereas a hat symbol ($\hat{\mathbf{S}}$) denote deviation form.

The present methodology implements the simultaneous design and control procedure using a probabilistic approach to handle the process constraints and cost function terms that depend on the system's dynamics. The disturbances are assumed to be stochastic (random) time-varying variables that follow predefined probability distribution functions defined by the user. The simultaneous design and MPC-based control methodology proposed in this work can be conceptually formulated as follows:

$$
\begin{aligned}
&\min_{\boldsymbol{\eta}=[\boldsymbol{\kappa},\boldsymbol{\Lambda}]} \ \Phi = \mathrm{CC} + \mathrm{OC} + \mathrm{DC} \\
&\quad \text{s.t.} \\
&\quad \text{Process nonlinear model } (\mathbf{J}) \\
&\quad \text{MPC scheme} \\
&\quad \text{Process Constraints} : \mathbf{h}(\mathbf{b}, \mathbf{u}(t), \boldsymbol{\rho}(t), \boldsymbol{\gamma}(t), \boldsymbol{\chi}(t)) \le \mathbf{a} \\
&\quad \text{Stability criterion} \\
&\quad \boldsymbol{\eta}^{l} \le \boldsymbol{\eta} \le \boldsymbol{\eta}^{u}
\end{aligned}
\tag{5.5}
$$

where the objective function Φ represents an economic measure of the plant costs incurred and thus need to be minimized by searching for the optimal values in the decision variables ($\boldsymbol{\eta}$) that minimize such function. The optimization variables $\boldsymbol{\eta}$ include the process design variables $\boldsymbol{\kappa}$, consisting of both fixed design parameters $\mathbf{d}$ (e.g. reactor's size) and continuous nominal (steady-state) operating conditions, $\bar{\mathbf{u}}$ and $\bar{\boldsymbol{\gamma}}$ (e.g. nominal flow rates in the outlet streams); and $\boldsymbol{\Lambda}$, which represent the MPC controller tuning parameters that will be defined below. The number of process design variables that can be considered as optimization variables is deduced from a degrees of freedom analysis. That is, once the values for the design variables $\boldsymbol{\kappa}$ have been specified by the optimization algorithm, then the nominal (steady-state) conditions for the rest of the process variables, $\bar{\boldsymbol{\rho}}$ and $\bar{\boldsymbol{\chi}}$, can be calculated by solving the first principle model equations at steady-state ($\bar{\mathbf{J}}$). Each of the terms included in the optimization problem (5.5) is described next.

5.1.1 MPC Scheme

The present methodology adopts a model-based control strategy such as a linear constrained Model Predictive Control (MPC) to maintain the manipulated and controlled variables within its feasible limits in the presence of disturbances. The mathematical formulation of a linear constrained MPC is as follows:

$$
\begin{aligned}
&\min_{\mathbf{\Delta u}} \sum_{r=1}^{R} (\hat{\boldsymbol{\gamma}}_{k+r|k} - \hat{\boldsymbol{\gamma}}_{\mathrm{sp}})^T \boldsymbol{\Gamma} (\hat{\boldsymbol{\gamma}}_{k+r|k} - \hat{\boldsymbol{\gamma}}_{\mathrm{sp}}) + \sum_{m=0}^{M-1} \Delta\hat{\mathbf{u}}_{k+m|k}{}^T \boldsymbol{\Omega} \Delta\hat{\mathbf{u}}_{k+m|k} \\
&\text{s.t.} \\
&\hat{\mathbf{x}}_{k+1} = \mathbf{A}(\mathbf{d}, \bar{\mathbf{u}}, \boldsymbol{\gamma}_{\mathrm{sp}}) \hat{\mathbf{x}}_k + \mathbf{B}(\mathbf{d}, \bar{\mathbf{u}}, \boldsymbol{\gamma}_{\mathrm{sp}}) \hat{\mathbf{w}}_k \\
&\hat{\boldsymbol{\gamma}}_k = \mathbf{C}(\mathbf{d}, \bar{\mathbf{u}}, \boldsymbol{\gamma}_{\mathrm{sp}}) \hat{\mathbf{x}}_k \\
&\hat{\mathbf{w}}_k = [\hat{\mathbf{u}}_k, \hat{\mathbf{v}}_k]^T \\
&\hat{\mathbf{u}}_{\min} \le \hat{\mathbf{u}}_k \le \hat{\mathbf{u}}_{\max} \\
&\Delta\hat{\mathbf{u}}_{\min} \le \Delta\hat{\mathbf{u}}_k \le \Delta\hat{\mathbf{u}}_{\max} \\
&\hat{\boldsymbol{\gamma}}_{\min} \le \hat{\boldsymbol{\gamma}}_k \le \hat{\boldsymbol{\gamma}}_{\max}
\end{aligned}
\tag{5.6}
$$

where $\hat{\boldsymbol{\gamma}}_{k+r|k}$ represents the predicted output controlled variables at the (k+r)th time interval, with the assumption that the corresponding value of each controlled variable in the vector $\hat{\boldsymbol{\gamma}}_k$ at the kth interval is available. The control moves needed at each time step to keep the controlled variables $\boldsymbol{\gamma}$ to their desired set points $\boldsymbol{\gamma}_{\mathrm{sp}}$, is represented by the vector $\Delta\hat{\mathbf{u}}_{k+m|k}$ where the subscript denotes the (k+m)th time interval. The set points $\hat{\boldsymbol{\gamma}}_{\mathrm{sp}}$, also known as the reference signals, remain constant during the calculation of the MPC formulation (5.6). The controller's prediction and control horizons are denoted by R and M, respectively. The internal model used by the MPC is represented by a discrete linear state space model that describes the process transient behavior around a nominal operating condition specified by the fixed design parameters $\mathbf{d}$, the nominal (steady-state) conditions of the manipulated variables $\bar{\mathbf{u}}$, and the process set points $\boldsymbol{\gamma}_{\mathrm{sp}}$. Since the linear MPC model depends on $\mathbf{d}$, $\bar{\mathbf{u}}$ and $\boldsymbol{\gamma}_{\mathrm{sp}}$, and these variables are included in the decision variables vector $\boldsymbol{\kappa}$ in the optimization framework (5.5), the MPC internal model needs to be identified (re-calculated) at each optimization step. The vector $\hat{\mathbf{x}}_k$ denotes the state variables of the system at the kth time interval which are estimated using the linear state-space model around the operating condition defined by $\mathbf{d}$, $\bar{\mathbf{u}}$ and $\boldsymbol{\gamma}_{\mathrm{sp}}$, respectively. Following (5.6), $\hat{\mathbf{w}}_k$ represents the inputs to the linear state space model and include the manipulated variables $\hat{\mathbf{u}}_k$ and the disturbances $\hat{\mathbf{v}}_k$. While $\hat{\mathbf{u}}_k$ is assumed to change up until the last control horizon M considered in the MPC formulation, the disturbances $\hat{\mathbf{v}}_k$ are assumed to remain constant for the entire control horizon M and equal to realization of the disturbances at the k^{th} (current) time interval. As shown in (5.6), estimates for the output variables $\hat{\boldsymbol{\gamma}}_k$ are obtained from the

linear MPC model and used to compute the control actions in manipulated variables $\mathbf{\Delta \hat{u}}$. To simplify the analysis, the system's states are estimated at each sampling interval from a linear discrete state observer computed from the internal linear MPC model [143]. Since a linear state space model is used to describe the process dynamics of the system (which is usually nonlinear), $\hat{\boldsymbol{\gamma}}_k$ will only be an approximation to the actual continuous controlled process outputs $\boldsymbol{\gamma}$. The MPC weights for the manipulated and controlled variables, i.e., the MPC controller tuning parameters, are represented in the MPC formulation (5.6) by the matrices $\mathbf{\Gamma}$ and $\mathbf{\Omega}$, respectively, which are assumed to be positive semi-definite diagonal matrices, i.e.,

$$\mathbf{\Lambda} = [\text{diag}(\mathbf{\Gamma}), \text{diag}(\mathbf{\Omega})]^T \tag{5.7}$$

Hence, the diagonal elements of the matrices $\mathbf{\Gamma}$ and $\mathbf{\Omega}$ represent decision variables that will be calculated from the simultaneous design and control methodology presented in (5.5). The linear constrained MPC problem formulation presented in (5.6) can be efficiently solved using numerical subroutines available on commercial software packages such as the MPC toolbox in MATLAB™.

5.1.2 Process constraints

To ensure feasibility, the process design variables $\boldsymbol{\kappa}$ and controller tuning parameters $\mathbf{\Lambda}$ selected by optimization algorithm must satisfy the process constraints **h**, which usually impose a physical limitation (e.g. valve saturation), a safety restriction or an operational constraint. These constraints are usually limited by critical values represented by the input limit **a**. As shown in problem (5.5), the constraints **h** can be a function of the design parameters, the process input and output variables. The present methodology evaluates the process constraints in a probabilistic manner using a stochastic-based worst-case variability (SB-WCV) index. A description of the process disturbances and the method used to compute the SB-WCV index are described next.

5.1.2.1 Process disturbances

Previous simultaneous design and control methodologies assumed that the time-dependent realizations in the disturbances follow a certain class of time-dependent functions, e.g., a sinusoidal function with uncertain (critical) parameters [21,24], or a series of step changes with unknown (but

bounded) magnitudes [25,26], or calculated from a worst-case scenario formulation [27,28]. The present approach differs from the previous methods in the sense that the disturbances are assumed to be stochastic (random) time-varying perturbations that follow a user-defined probability distribution function, i.e.,

$$\mathbf{v}_c(t) = \{\mathbf{v}_c \mid \mathbf{v}_c \sim \mathrm{PDF}(\boldsymbol{\alpha}_c)\}; \quad 0 \le t \le t_f \tag{5.8}$$

where $\mathbf{v}_c$ represents the c^{th} disturbance included in $\mathbf{v}$ whereas $\boldsymbol{\alpha}_c$ represents the parameters of the c^{th} disturbance's probability distribution function (e.g. mean and standard deviation for a normal distribution). Description (5.8) assumes that the disturbances are stochastic; its actual value at any time t is not specified but given by the probability distribution function PDF. To simplify the analysis, the disturbances' time-dependence is relaxed by discretizing the disturbances' estimates at specific time intervals, i.e.,

$$\mathbf{v}_c(t) \approx \sum_{k=1}^{K} \mathbf{v}_c(k) \qquad \mathbf{v}_c(k) \sim \mathrm{PDF}(\boldsymbol{\alpha}_c); \qquad t = k\Delta t,\ t_f = K\Delta t \tag{5.9}$$

where k and Δt represent the sampling period and the sampling interval, respectively. The disturbance description shown in (5.9) is an input to the present methodology. The choice of probability distribution function to represent the stochastic behaviour of the disturbances needs to be specified by the user. A common assumption is to use Gaussian or Uniform distributions if no prior knowledge is available; however the present method is not restricted to the form of the disturbance's probability distribution function and can take symmetric and non-symmetric probability distributions, e.g., lognormal distributions. The information about the disturbances' dynamic characteristics is usually not available at the design stage. Despite of that, the current approach of using a PDF such as a normal PDF is suitable since it provides a more general description of the disturbances, than other assumptions made at the design stage, e.g., the use of a sinusoidal function or series of steps, especially when the process to be designed is a new process for which plant experience is not available.

5.1.2.2 Stochastic-based worst-case variability (SB-WCV) index

The use of stochastic disturbances and analyzing its effect on the constrained variables has previously been studied by [144]. In the present work, a probabilistic-based approach is employed to evaluate the

process constraints $\mathbf{h}$ shown in problem (5.5). The closed-loop nonlinear process model ($\mathbf{J}_{\text{closed}}$) is simulated using multiple stochastic realizations of the disturbances that comply with (5.9) and the dynamic response of the process constraints $\mathbf{h}(t)$ is analyzed. The worst-case (largest) deviation observed in any constraint $h(t)$ for a particular realization in the disturbances $\boldsymbol{\nu}$ is called the *stochastic-based worst-case variability* (SB-WCV), ψ_h, and can be obtained as follows:

$$\begin{aligned} \psi_h = \arg\max\, & h(t) \\ & \text{s.t.} \\ & \text{Process nonlinear model}(\mathbf{J}) \\ & \text{MPC scheme (5.6)} \\ & \boldsymbol{\eta} = [\boldsymbol{\kappa}, \boldsymbol{\Lambda}] \end{aligned} \tag{5.10}$$

where ψ_h refers to the largest deviation in the positive direction observed in the process constraint $h \in \mathbf{h}$. The largest (worst-case) deviation in the negative direction can be obtained by replacing the 'max' argument in (5.10) with a 'min' for minimum. Since random (stochastic) time-dependent realizations of the disturbances $\boldsymbol{\nu}$ generated from (5.9) were used to obtain ψ_h, there is no guarantee that other disturbances' realizations that also comply with the disturbance description (5.9) can result in larger variability in h, i.e. ψ_h may not be the actual worst (largest) value that process constraint *h* can assume during the dynamic operation of the system. Accounting for all possible realizations in the disturbances $\boldsymbol{\nu}$ can be computationally intensive or even prohibitive. To address this issue, the present method uses a Monte Carlo (MC) sampling technique to generate *N* stochastic realizations of the disturbances that will be used in the nonlinear closed-loop process model ($\mathbf{J}_{\text{closed}}$), i.e. the process nonlinear model $\mathbf{J}$ engaged with the MPC control algorithm shown in (5.6), to obtain a set of *N* SB-WCV estimates for *h*, $\boldsymbol{\psi}_h = [\psi_{h1}, \psi_{h2} \ldots \psi_{hp}]$. The MC sampling in the present method consist of a set of random samples that were selected using a pseudo random number generator function. For example, the MATLAB built-in function 'randn', which implements the ziggurat algorithm [145], selects pseudo random numbers from a normal PDF with given mean and variance. This sub-routine in MATLAB was used in the present analysis to generate the disturbance realizations that follow a normal PDF. If *N* is sufficiently large, a frequency histogram of $\boldsymbol{\psi}_h$ will approximate to the true probability distribution of h around a nominal operating point defined by $\boldsymbol{\kappa}$, $\boldsymbol{\rho}$ and $\boldsymbol{\chi}$. The

resulting worst-case variability distribution function can then be approximated by a known probability distribution function, e.g., exponential, normal (Gaussian), lognormal. The distribution function that fits $\boldsymbol{\psi}_h$ to a known probability distribution is referred from heretofore as the *worst-case variability distribution function*, $\mathbf{g}(\boldsymbol{\psi}_h)$. In a previous work, a normal (Gaussian) distribution was used to fit the *N* worst variability estimates in the process variables, which was obtained from simulations of *N* random Monte Carlo disturbances [29]. In the current methodology, a lognormal probability distribution is adopted because it can describe a wider range of probability distributions relatively well, e.g., a lognormal distribution can fit both skewed and symmetric random distributions whereas a normal distribution poorly fits a skewed distribution [146]. Accordingly, the use of a lognormal distribution is expected to improve the accuracy in the description of the probability distribution function and will therefore improve the evaluation of the process constraints. Thus, the worst-variability distribution function $\mathbf{g}(\boldsymbol{\psi}_h)$ is calculated as follows [146]:

$$\mathbf{g}(\boldsymbol{\psi}_h) = \frac{1}{\psi_h \sigma_h \sqrt{2\pi}} \exp^{-(\ln \psi_h - \mu_h)^2 / 2\sigma_h^2}, \qquad \psi_h > 0 \tag{5.11}$$

where μ_h and σ_h are the mean and standard deviation of the lognormal distribution function, respectively. In order to improve the estimates of the mean and standard deviation for each process constraint *h*, the present method iterates over *N*, i.e., perform *N* disturbances realizations and compute the output probability distribution function at each iteration, up until the improvement in the estimates is less than a pre-specified criterion. The step-by-step procedure used to obtain the SB-WCV, $\boldsymbol{\psi}_h$, and then fitting to a probability distribution function $\mathbf{g}(\boldsymbol{\psi}_h)$, can be found in [29]. The distribution function $\mathbf{g}(\boldsymbol{\psi}_h)$ can then be used to evaluate the stochastic-based worst-case variability (SB-WCV) of constraint *h* at a given (user-defined) probability level (Pb_h), i.e., ψ_h^*, using the identified lognormal probability distribution function (5.11) with model parameters μ_h and σ_h:

$$\psi_h^* = \{\psi_h^* = CMF(\psi_h^*, \mu_h, \sigma_h) = \text{Pb}_h\} = CMF^{-1}(\text{Pb}_h, \mu_h, \sigma_h)$$

$$\text{Pb}_h = CMF(\psi_h^*, \mu_h, \sigma_h) = \int_{-\infty}^{\psi_h^*} f(\beta) d\beta = \frac{1}{\psi_h^* \sigma_h \sqrt{2\pi}} \int_{-\infty}^{\psi_h^*} \exp^{-(\ln \beta - \mu_h)^2 / 2(\sigma_h)^2} d\beta \tag{5.12}$$

Figure 5.1 presents a schematic of the computation of ψ_h^*. Using the calculated SB-WCV from (5.12), the process constraints shown in (5.5) can be reformulated in the present analysis as follows:

$$\mathbf{h}(\boldsymbol{\kappa}, \boldsymbol{\rho}, \boldsymbol{\chi}, \boldsymbol{\psi}_z^*) \leq \mathbf{a} \tag{5.13}$$

which is defined in terms of the design parameters, the steady-state inputs/outputs, and the corresponding SB-WCV index ($\boldsymbol{\psi}_h^*$) for each constraint *h* considered in problem (5.5). In the present analysis, algebraic manipulations need to be performed to ensure that *h* in (5.13) remains positive all the time.

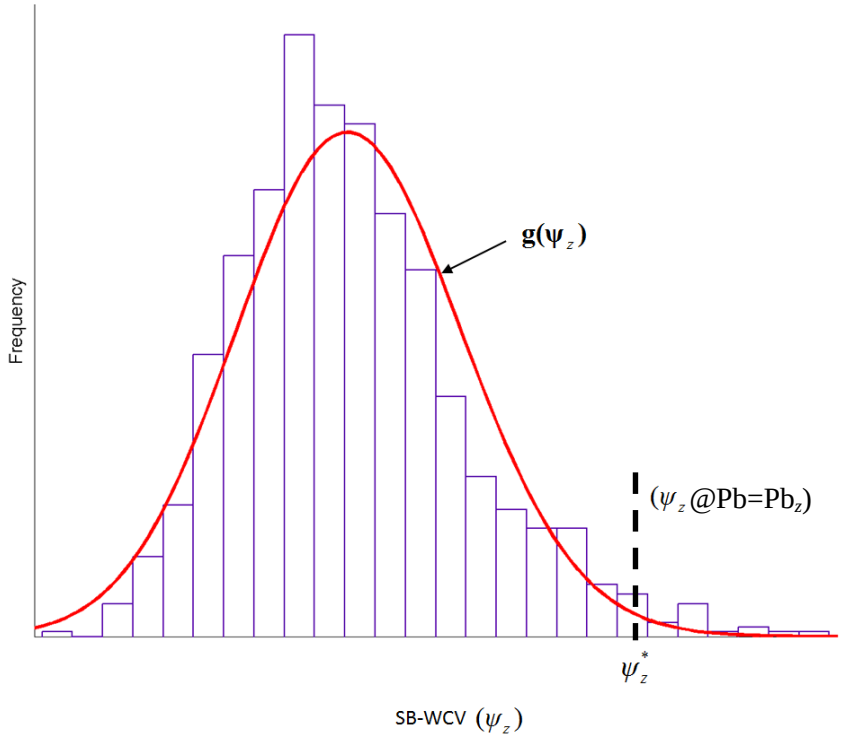

Figure 5.1 Schematic representation of the computation of the SB-WCV index.

The choice of (Pb_h) for each process constraint included in **h** depends on the significance of that constraint for the process design. That is, the present method allows 1-Pb_h violations for constraint *h*. Hence, process constraints that need to be satisfied at all times, e.g., a safety constraint, need to be evaluated using a relatively high probability limit, i.e., Pb→1, which will ensure that that constraints are only violated (almost surely) in a very few (rare) occasions. The selection of (Pb) also represents a

tradeoff between economically attractive process designs and conservative (expensive) designs. High probability limits (Pb) may be considered for critical systems to obtain conservative designs whereas low probability levels for (Pb) can be assigned to less critical variables for a more economic design. Accordingly, the present methodology offers the user the freedom in handling the process constraints, whether to follow a strict worst-case scenario approach by assigning high probability limits or attempt for a less expensive (economically attractive) design using low probability levels for all (or a few) of the process constraints.

The procedure described above to evaluate the process constraints using the SB-WCV index (ψ_h^*) can also be used to evaluate the process variables used to measure the system's dynamic performance. For example, the process dynamic performance costs can be calculated by assigning a dollar value to the process manipulated variables **u** or controlled variables $\boldsymbol{\gamma}$ that determine the dynamic performance of the system. The variability in these variables will be obtained from the SB-WCV indexes (ψ_u^* and ψ_γ^*) evaluated at a user-defined probability limit, i.e., Pb_u and Pb_γ. For simplicity, a general notation (ψ_z^*) would be used from heretofore to refer to the calculation of the SB-WCV index, where *z* may denote a process constraint *h*, a manipulated variable *u*, or a controlled variable γ.

5.1.3 Stability test

To ensure process stability, the current methodology makes use of local and global stability tests. Following the formulation presented in (5.5), a nominal stability test is embedded within the optimization problem (5.5) to ensure that the optimal design and control scheme obtained from that optimization problem is nominally stable. This test is carried out by calculating, at each optimization step, the eigenvalues of the sensitivity matrix $\mathbf{A}(x)$ from the closed-loop system evaluated at the nominal operating point specified by $\boldsymbol{\kappa}$ and the MPC controller parameters $\boldsymbol{\Lambda}$, which are the decision variables in problem (5.5). Therefore, the stability criterion shown in problem (5.5) is formulated as follows:

$$\mathrm{Re}(\mathrm{eig}(\mathbf{A}(x)|_{\boldsymbol{\kappa},\boldsymbol{\Lambda}})) < \mathbf{0} \qquad (5.14)$$

where nominal stability is ensured if the real part of all eigenvalues are negative. The sensitivity matrix $\mathbf{A}(x)$ can be computed using numerical methods such as finite differences; however, efficient methods that compute the sensitivity matrix of the system around a nominal operating point have been recently published in the literature, e.g., Kookos et al [147]. The addition of the stability criterion (5.14) ensures that the design obtained by the present method is nominally stable; however, it does not guarantee asymptotic stability. To this regard, a robust stability test based on the Quadratic Lyapunov (QL) function is considered in the present methodology to evaluate the system's asymptotic stability. The implementation of this test has been explicitly described in a previous study [20] and is not shown here for brevity. One drawback of the QL test is related to its computational costs for systems with a large number of states. For that reason, the present analysis only evaluates the asymptotic stability of those process design and control schemes obtained from the solution of present methodology's optimization formulation. In the case that the optimal design does not satisfy the QL stability test, this asymptotic stability criterion will need to be included in the formulation and therefore implemented at each iteration in the present optimization framework. Nevertheless, in the present work the latter case was never encountered since all the optimal designs obtained from the present method satisfied the QL stability test.

5.1.4 Cost function

As shown in problem (5.5), the objective function Φ can be defined as the addition of the annualized capital costs (CC), the operating costs (OC) and the dynamic performance costs (DC). The capital costs (CC) refer to the fixed annualized costs of purchasing and installing equipment and units in the process flowsheet. Estimates for the process units' costs can be obtained from empirical correlations available in literature [2,148,149]. The annual operating costs (OC) refer to the cost of the utilities used in the daily operation of the plant such as electricity or heating steam. Both capital (CC) and operating (OC) costs are normally calculated from the steady-state design and operating conditions, e.g., tank volume, cooling water duty or pumping power. On the other hand, the dynamic performance costs (DC) aim to measure the process variability in economic terms due to sudden fluctuations in the disturbances. The costs could be incurred due to loss profitability, e.g., off-spec product quality, or due to certain environmental costs implied on the discharge of wastes to the atmosphere or the surroundings. Thus, the dynamic performance costs are considered process specific. The specification of dynamic performance costs for different case studies and applications

can be found elsewhere [28,29,101,109]. The costs are annualized over an assumed plant life of 20 years.

5.1.5 Optimization framework and algorithm

Based on the above developments, the simultaneous design and MPC-based control methodology proposed in this work is formulated as follows:

$$
\begin{aligned}
&\min_{\boldsymbol{\eta}=[\boldsymbol{\kappa},\boldsymbol{\Lambda}]} \ \Phi = \mathrm{CC}(\boldsymbol{\kappa},\boldsymbol{\rho},\boldsymbol{\chi},\boldsymbol{\psi}_z^*) + \mathrm{OC}(\boldsymbol{\kappa},\boldsymbol{\rho},\boldsymbol{\chi},\boldsymbol{\psi}_z^*) + \mathrm{DC}(\boldsymbol{\kappa},\boldsymbol{\rho},\boldsymbol{\chi},\boldsymbol{\psi}_z^*,\boldsymbol{\Lambda}) \\
&\quad \text{s.t.} \\
&\quad \mathrm{Process\ nonlinear\ model}\,(\mathbf{J}) \\
&\quad \text{MPC scheme (5.6)} \\
&\quad \mathbf{h}(\boldsymbol{\kappa},\boldsymbol{\rho},\boldsymbol{\chi},\boldsymbol{\psi}_z^*) \le \mathbf{a} \\
&\quad \mathrm{Re}(\mathrm{eig}(\mathbf{A}(x)|_{\boldsymbol{\eta}})) < 0 \\
&\quad \boldsymbol{\eta}^l \le \boldsymbol{\eta} \le \boldsymbol{\eta}^u
\end{aligned}
\qquad (5.15)
$$

Due to the use of stochastic realizations to calculate the SB-WCV indexes for the constraints (ψ_h^*) and the dynamic performance costs (ψ_u^* and ψ_γ^*), the present problem is casted as a nonlinear constrained stochastic optimization problem. Stochastic optimization algorithms such as Genetic Algorithms [150], which is essentially a global optimization method, can be implemented to solve this type of optimization problems. However, GA is computationally intensive requiring multiple restarts to obtain a reliable solution of the decision variables. Nonetheless, the structure of the formulation presented in (5.15) allows the implementation of computer parallelization techniques which reduces the computational efforts required by the present method. To show the potential benefits of the present method while using multiple cores, a study on the computational costs of the proposed methodology while using computer parallelization techniques is presented later in Section 5.2.5. The step by step algorithm that needs to be followed to perform a single function evaluation of problem (5.15) is schematically shown in Figure 5.2 and it is described next.

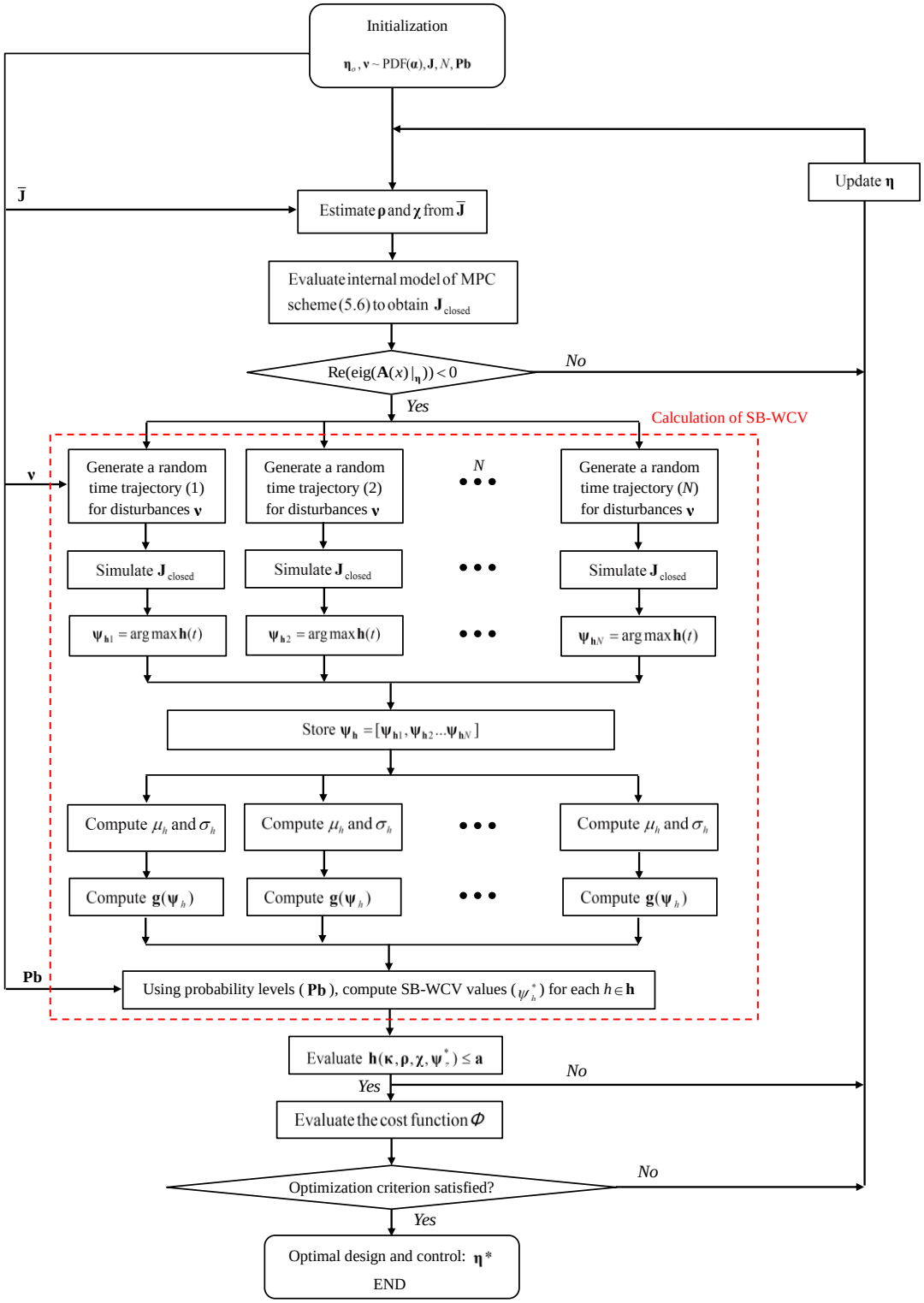

Figure 5.2 Algorithm for the MPC-based probabilistic approach in design and control.

Given, a set of decision variables $\boldsymbol{\eta}_o$, the nonlinear process model $\mathbf{J}$, a defined probability distribution function with its parameters for the disturbances ($\boldsymbol{\nu} \sim \text{PDF}(\boldsymbol{\alpha})$), the user-defined probabilities for the SB-WCVs ($\mathbf{Pb}$), and a maximum number of disturbance realizations (*N*), perform the following steps:

1. Estimate the nominal (steady-state) operating conditions for the process variables that are not included in $\boldsymbol{\eta}$ from the process (steady-state) nonlinear model ($\bar{\mathbf{J}}$).
2. Identify the internal linear state-space MPC model around a nominal operating condition specified by the design parameters $\mathbf{d}$ and nominal steady-state operating conditions ($\bar{\mathbf{u}}, \boldsymbol{\gamma}_{sp}$). This model can be obtained using analytical methods, e.g., Taylor series expansion, or from systems identification.
3. A set of *N* random realizations of the disturbances $\boldsymbol{\nu}$ is generated using Monte Carlo sampling from the particular probability distributions (PDFs) assigned to each disturbance (see description (5.9)).
4. The closed-loop process ($\mathbf{J}_{\text{closed}}$), i.e., the process model $\mathbf{J}$ and the MPC controller specified in (5.6), is simulated *N* times, with a different random realization of the input disturbances $\boldsymbol{\nu}$ used at each simulation. The process responses obtained from these simulations are used to obtain the worst-case variability from each of the *N* dynamic simulations (ψ_z) using the formulation presented in (5.10). The complete set of ψ_z values is lumped in a vector $\boldsymbol{\psi}_z$.
5. Fit $\boldsymbol{\psi}_z$ to a lognormal distribution function: $\mathbf{g}(\boldsymbol{\psi}_z)$.
6. Calculate the SB-WCV index, ψ_z^*, from equation (5.12) using $\mathbf{g}(\boldsymbol{\psi}_z)$ and the probability limit (Pb_z) defined by the user for each constraint or process variable *z*. The calculation of the SB-WCV index (ψ_z^*) represents the main calculation performed in this methodology and is explicitly shown by the enclosed dashed box in Figure 5.2.
7. Use SB-WCV (ψ_z^*) indexes to evaluate the process constraints $\mathbf{h}$ and process variability terms in the cost function Φ. If the optimization criteria are satisfied, then STOP, an optimal solution $\mathbf{d}^*$ have been found, otherwise update $\mathbf{d}$ and go to step 1.

5.1.5.1 Remarks

The methodology presented above is based upon a previous approach proposed by one of the authors for the simultaneous design and control of a chemical process with multi-loop PI controllers [29]. Further improvements have been made in the methodology to consider advanced (model-based) control schemes in the analysis and to improve the accuracy of the results. In the present method, a model-based control strategy such as Model Predictive Control (MPC) is considered in the analysis to maintain the system within specifications and stable in the presence of the stochastic disturbances. This improvement in the method will enable the specification of more economically attractive designs than those obtained with multi-loop (PI) control schemes since it offers the possibility to explicitly account in the control actions for constraints on the process inputs and outputs, e.g., saturation limits in the manipulated variables. Another improvement in the present methodology with respect to that shown in Ricardez-Sandoval [29] is the use of a lognormal distribution to describe the worst-case variability distributions in the process variables due to the fluctuations in the stochastic disturbances. A lognormal distribution can describe a wider range of probability distributions compared to the normal distribution. Therefore, it is expected that the adoption of a lognormal distribution will improve the accuracy in the results by providing better estimates for the worst-case variability distributions. To the authors' knowledge, this is the first stochastic-based methodology that proposes an MPC-based framework for simultaneous design and control of dynamic systems under uncertainty.

The methodology presented above assumes that the process flowsheet remains fixed during the course of the calculations. Although discrete decisions can be added into the present formulation to account for structural decisions in the analysis, and therefore obtain more attractive (economic) designs, the solution of those stochastic mixed-integer optimization problems is a challenging task that have been limited to small process systems [151]. Hence, the application of such highly demanding optimization methods to address the simultaneous design and control of large-scale systems is still an active area of research and is considered outside the scope of the present study.

The number of *N* input disturbance realizations used in this method determines the accuracy of the lognormal fit worst variability function $\mathbf{g}(\boldsymbol{\psi}_z)$. While a large number of disturbances realizations can improve the estimates of the index ψ_z^*, this also implies large computational costs. There is no clear

rule on the selection of N, the choice is normally decided after preliminary simulation tests to determine the optimal tradeoff between computational time and the desired accuracy in the calculations. The current methodology assumes stochastic disturbances with certain input probability distribution parameters. This description as shown in (5.9) can fit a wide range of applications where the disturbance is known to fluctuate randomly around a specific nominal value, e.g., raw material flowrate from a supplier usually incorporates variability around a certain agreed supply value. Unlike other simultaneous design and control methodologies that use a particular known function for the disturbance (e.g. sinusoidal), this stochastic disturbance description gives to the proposed methodology a more general and thus wider application. However, if the perturbations are known to follow a particular class of time-dependent functions, or is available from previous experiences with similar processes or from process design heuristics, such as the case of known deliberate changes to achieve different production levels, the current method may not adequately capture the actual dynamics of the process yielding less accurate (and perhaps more expensive) plant designs. Since the stochasticity in the disturbances is no longer considered in that case, deterministic dynamic optimization-based methods can be implemented to perform the integration design and control, e.g., Mohideen et al. [18], Bansal et al. [83], Swartz [26].

In principle the use of other type of models besides mechanistic process models to represent the actual process behavior can be also used as the process model $\mathbf{J}$ in the present methodology, e.g., empirical or black-box models obtained from systems identification. These empirical or black-box models need to be identified such that they provide a sufficiently accurate description of the transient behavior between the disturbances and manipulated variables and the system's outputs. Also, most of the empirical models are linear process models whereas the actual process behaves in a nonlinear fashion. Thus, the use of empirical linear models in the present methodology may introduce an error on the computation of the histograms for the constraint functions $\mathbf{h}$ since an approximated linear model is being used instead of the actual (typically nonlinear) process model. The latter may result in the specification of process design and control schemes that may not necessarily satisfy the process constraints $\mathbf{h}$ in the presence of random realizations in the disturbances. Another possible implication of using empirical process models is that the model parameters do not have a physical meaning as it is the case for mechanistic process models. The introduction of additional disturbances or uncertainties in the system's physical parameters is straightforward in the case of a mechanistic process model, i.e., assign a probability distribution function (PDF) to that disturbance or uncertain parameter and then

impose *N* stochastic realizations sampled from that PDF to that parameter and evaluate the process constraints and cost function under this scenario. On the other hand, an empirical model may not allow the user to alter physical parameters within the model other than the process inputs and outputs. This may result in the re-identification of a new empirical model while considering that new disturbance/uncertain parameter as an input. Nevertheless, the computational costs of using empirical models are relatively low when compared to the mechanistic process models. Thus, the implementation of empirical models in the present method may become computationally attractive to tackle large-scale nonlinear systems such as chemical plants.

5.2 CASE STUDY: Wastewater treatment industrial plant

To demonstrate the implementation of the present methodology, an actual industrial wastewater plant located in Manresa, Spain, has been used as a case study in this work. The real wastewater plant consists of six aeration tanks and two settlers as described by Gutierrez & Vega [152]. To simplify the analysis, the present study only considers the most significant units of that system, i.e., an aeration tank (bioreactor) and a clarifier/settler (see Figure 5.3).

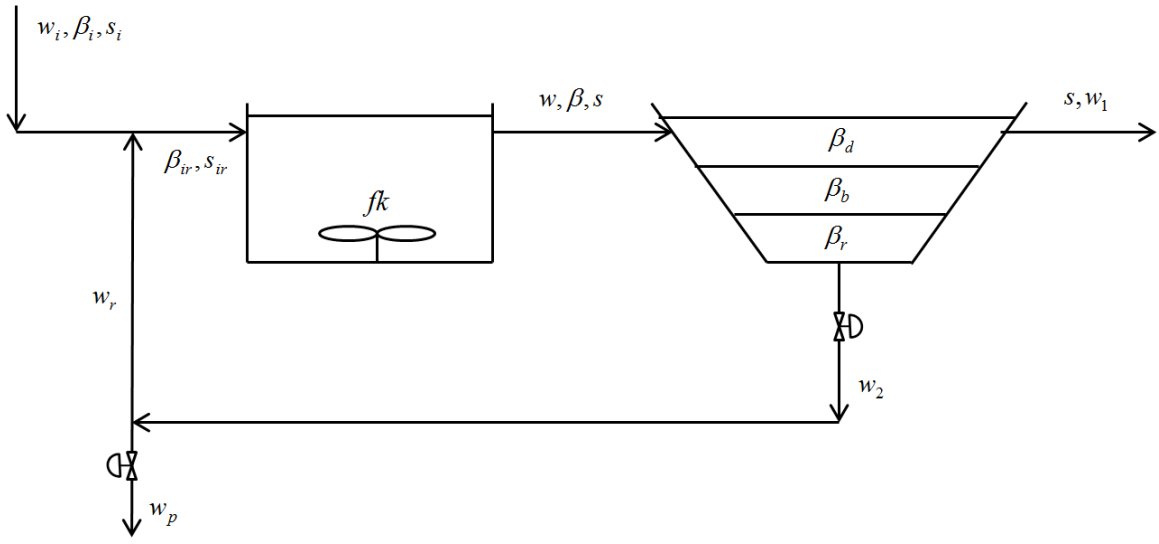

Figure 5.3 Schematic figure of the wastewater plant configuration considered for the case study.

The goal of the process is to remove biodegradable pollutants (substrate) from the wastewater that is fed to the aeration tank with the help of microbial population (biomass). The aeration turbine in the bioreactor supplies the necessary level of oxygen needed by the biomass to feed on the substrate, growing in size and forming an activated sludge. The water effluent is passed through a clarifier that is used to separate the activated sludge, which settles at the bottom of the tank by sedimentation, from treated water which is obtained at the top of that tank. The activated sludge is recycled back to the bioreactor to remove more substrate entering through the feed wastewater. As shown in Figure 5.3, a purge stream is needed to maintain the microbial biomass within specific limits inside the aeration tank. The mathematical model representing the rate of change of biomass and consumption of substrate inside the bioreactor is as follows [152]:

$$\frac{d\beta}{dt} = \vartheta \mu_y \frac{\beta s}{k_s + s} - k_d \frac{\beta^2}{s} - k_c \beta + \frac{w}{V_b}(\beta_{ir} - \beta) \tag{5.16}$$

$$\frac{ds}{dt} = -\vartheta \frac{\beta s}{k_s + s} + fk_d k_d \frac{\beta^2}{s} + fk_d k_c \beta + \frac{w}{V_b}(s_{ir} - s) \tag{5.17}$$

where β and s are the biomass and organic substrate concentrations (mg/L) inside the bioreactor, respectively. Similarly, β_{ir} and s_{ir} are the biomass and organic substrate concentrations (mg/L) entering the bioreactor, respectively. The volume of the reactor is denoted by V_b (m^3) whereas w (m^3/h) represents the bioreactor's outlet flow. Concentration gradients exist along the height of the clarifier. In this analysis, this gradient is approximated by breaking the clarifier into distinct layers that have different concentrations. The concentration within each layer is uniform. In this analysis, three layers are considered and are modeled as follows [152]:

$$\frac{d\beta_b}{dt} = \frac{1}{A_{cl} lb}(w_i + w_2 - w_p)(\beta - \beta_b) - \frac{1}{lb}(vs(d) - vs(b)) \tag{5.18}$$

$$\frac{d\beta_d}{dt} = \frac{1}{A_{cl} ld}(w_i - w_p)(\beta_b - \beta_d) - \frac{1}{ld} vs(d) \tag{5.19}$$

$$\frac{d\beta_r}{dt} = \frac{1}{A_{cl} lr} w_2 (\beta_b - \beta_r) + \frac{1}{lr} vs(b) \tag{5.20}$$

$$\frac{dc_o}{dt} = k_{la}\, fk(c_s - c_o) - OUR - \frac{w}{V_b} c_o \tag{5.21}$$

$$OUR = k_{01}\vartheta\beta\frac{\beta}{(k_s + s)} \tag{5.22}$$

$$w_1 = w - w_2 \tag{5.23}$$

$$w_r = w_2 - w_p \tag{5.24}$$

$$w = w_i + w_r \tag{5.25}$$

where β_d, β_b and β_r are the biomass concentrations (mg/l) at the different layers in the clarifier unit, i.e., surface, intermediate and bottom, respectively. The cross-sectional area of the settler is denoted by A_{cl} (m^2) whereas *ld*, *lb* and *lr* represent the height (depth) of the first, the second and the bottom layer in the settler, respectively. The terms *vs(d)*, *vs(b)* and *vs(r)* refer to the rate of settling for the activated sludge, which varies from layer to layer depending on the concentration of biomass. Dissolved oxygen, originally supplied to the system by the aeration turbines, is denoted by c_o, whereas *fk* represents the aeration turbine speed. The rest of the model parameters shown in (5.16)-(5.25) are described in Table 5.1.

Table 5.1 Description of the model parameters in Equations (5.16)-(5.25)

Symbol	Value (unit)	Description
ϑ	0.1824 (h^{-1})	specific growth rate
μ_y	0.5948	fraction of converted substrate to biomass
k_s	300 (h^{-1})	saturation constant
k_d	5.0000E-05 (h^{-1})	biomass death rate
k_c	1.3333E-04 (h^{-1})	specific cellular activity
k_{la}	0.7 (h^{-1})	oxygen transfer into the water constant
k_{01}	1.0000E-04 (h^{-1})	oxygen demand constant
c_s	8.0 (h^{-1})	oxygen specific saturation
fk_d	0.2	fraction of dead biomass (to substrate)

The control objectives for this case study are: 1) maintain the level of organic substrate leaving the system s below a certain maximum allowable value, 2) keep the biomass concentration β in the

bioreactor, and 3) maintain the dissolved oxygen concentration c_o, at pre-specified targets. The first objective is needed to meet environmental regulations regarding the quality of treated water (w_1) discharged to the effluents, i.e., with less organic substrates (pollutants). The biomass concentration is desired to be at a certain target because higher concentrations may lead to activated sludge to settle to the bottom of the clarifier, which may lead to additional operational costs needed to remove the sludge from the tank. The third objective of maintaining an oxygen concentration inside the bioreactor is important to maintain the biomass organisms alive, as they are needed to remove the organic substrate from the feed (control objective 1). These control goals need to be achieved in the presence of possible disturbances in the feed flow rate (w_i), inlet substrate concentration (s_i) and inlet biomass concentration (β_i). As shown in Figure 5.3, the available manipulated variables for the present system are the recycle flow rate (w_2), purge flow rate (w_p) and the aeration turbine speed (fk).

The stochastic-based simultaneous design and control methodology presented in the previous section has been implemented for the water treatment process described above. Process disturbances (w_i, s_i and β_i) were assumed to be stochastic and follow the description shown in (5.9). A linear constrained MPC algorithm such as that shown in (5.6) is used in this case study as the multivariable control scheme. The goal of this analysis is to obtain the optimal design parameters for this process and the MPC input and output weights that will minimize the plant's economics, while maintaining the dynamic operability of the process within its corresponding limits (up until a certain user-defined probability limit) in the presence of stochastic time-varying disturbances that follow a particular (user-defined) probability distribution. The simultaneous design and control optimization framework shown in (5.15) was applied to this process. The design variables selected for this case study are $\boldsymbol{\kappa}_{WW} = [\overline{w}_2, \overline{w}_p, \overline{fk}, V_b, A_{cl}]$ whereas the MPC tuning weights are $\boldsymbol{\Lambda}_{WW} = [\Gamma_{w2}, \Gamma_{wp}, \Gamma_{fk}, \Omega_\beta, \Omega_s, \Omega_{co}]$. In the design variables ($\boldsymbol{\kappa}_{WW}$), $\overline{w}_2, \overline{w}_p$ and $\overline{fk}$ represent the nominal (steady-state) operating conditions for the corresponding manipulated variables. In the tuning weights vector $\boldsymbol{\Lambda}_{WW}$, Γ_{w2}, Γ_{wp} *and* Γ_{fk} are the weights on the corresponding manipulated variables whereas Ω_β, Ω_s and

Ω_{co} are the weights on the controlled variables, respectively. The cost function defined for the present case study is as follows:

$$\Phi_{WW} = \mathrm{CC}_{WW} + \mathrm{OC}_{WW} + \mathrm{DC}_{WW} \tag{5.26}$$

The annualized capital costs are calculated as follows:

$$\mathrm{CC}_{WW} = 0.16(3500V_b + 2300A_{cl}) \tag{5.27}$$

That is, the capital cost depends only on the steady-state design variables: volume of the bioreactor (V_b) and cross-sectional area (A_{cl}) of the clarifier. The operating costs for this process are those associated with the electricity used by the aeration turbines in the bioreactor and pumps for the purge flow, i.e.,

$$\mathrm{OC}_{WW} = 870(\psi^*_{fk} + \psi^*_{w_p}) \tag{5.28}$$

where stochastic-based worst-case variability (SB-WCV) indexes for the aeration turbines and the pumps for the purge flow are used here instead of the steady-state operating conditions ($\overline{fk}$ and $\overline{w}_p$). This has been done to account for the variability of these process variables due to changes in the process disturbances. With regards to the dynamic performance cost, an economic value has to be assigned to those process variables that measures the system's dynamic performance or to those variables that has economic significance when its variability exceeds pre-specified limits. In this case study, the deviation of both the organic substrate and biomass concentrations from their target values in the bioreactor represent economic losses. This is because high substrate concentrations in the discharge effluent can have environmental penalty costs, whereas removing settled excess activated sludge in the tank due to high biomass concentrations may lead to additional operational costs. Therefore, the dynamic performance cost for this process is defined as follows:

$$\mathrm{DC}_{WW} = 10^5(\psi^*_s - \bar{s}) + 10^3(\psi^*_\beta - \bar{\beta}) \tag{5.29}$$

where $\bar{s}$ and $\bar{\beta}$ are the nominal steady-state values of the organic substrate and biomass concentrations respectively, and the SB-WCV indexes, ψ^*_s and ψ^*_β, are used to measure the variability in the substrate and the biomass concentrations due to fluctuations in the process disturbances, respectively. Note that a higher dynamic performance cost is assigned to the variability

in organic substrate (10^5 (\$/yr)/(mg/L)) because of the environmental significance and restriction in having high concentrations of substrate in the treated water discharged to the effluents. Variability in biomass concentrations incurs a dynamic performance cost (10^3 (\$/yr)/(mg/L)) because large biomass concentrations requires additional pump power to remove the activated sludge accumulated at the bottom of the clarifier. Moreover, the present case study considers the following dynamic path feasibility constraints:

$$
\begin{aligned}
&0.03 \le \frac{w_p(t)}{w_2(t)} \le 0.2 \\
&0.8 \le \frac{V_b \cdot \beta(t) + A_{cl} \cdot lr \cdot \beta_r(t)}{w_p \cdot \beta_r(t) \cdot 24} \le 10 \\
&s(t) \le 58
\end{aligned}
\tag{5.30}
$$

The first two constraints represent the restrictions on the ratio between purge-to-recycled flow rates and in the purge age in the decanter, respectively. The last constraint in (5.30) refers to the maximum allowable organic substrate concentration in the treated water that leaves the clarifier. These inequality constraints need to be satisfied during the entire operation of the plant (transient and steady-state) up to a certain probability limit. Therefore, the inequality constraints (5.30) can be reformulated using the proposed SB-WCV indexes with a defined probability level to test the compliance of these constraints with their corresponding limits, i.e.,

$$
\begin{aligned}
&\psi^*_{\min(c1)} \ge 0.03 \\
&\psi^*_{\max(c1)} \le 0.2 \\
&\psi^*_{\min(c2)} \ge 0.8 \\
&\psi^*_{\max(c2)} \le 10 \\
&\psi^*_{\max(s)} \le 58 \\
&\text{where:} \\
&c1 = \frac{w_p(t)}{w_2(t)} \\
&c2 = \frac{V_b \cdot \beta(t) + A_{cl} \cdot lr \cdot \beta_r(t)}{w_p \cdot \beta_r(t) \cdot 24}
\end{aligned}
\tag{5.31}
$$

where $c1$ and $c2$ denote the ratio between purge-to-recycled flow rates and the purge age in the decanter, respectively. The ‘max’ and ‘min’ notations in the subscripts of (5.31) indicate that the SB-WCV indexes are calculated with respect to the worst-case variability in the positive and in the

negative direction, respectively. Note that each SB-WCV (ψ_z^*) is evaluated around a nominal operating point defined by the process decision variables vector $\boldsymbol{\kappa}_{WW}$ and MPC controller tuning parameters $\boldsymbol{\Lambda}_{WW}$, respectively. Based on the above, the optimization framework described in (5.15) can be adapted for the present case study as follows:

$$
\begin{aligned}
&\min_{\boldsymbol{\eta}_{WW}=[\boldsymbol{\kappa}_{WW},\boldsymbol{\Lambda}_{WW}]} \Phi_{WW} = \mathrm{CC}_{WW} + \mathrm{OC}_{WW} + \mathrm{DC}_{WW} \\
&\quad \text{s.t.} \\
&\quad \text{Process model}(\mathbf{J}) \qquad [\text{Equations}(5.16)-(5.25)] \\
&\quad \text{MPC scheme}(5.6) \\
&\quad \text{constraints}(5.31) \\
&\quad \mathrm{Re}(\mathrm{eig}(\mathbf{A}(x)|_{\boldsymbol{\eta}})) < \mathbf{0} \\
&\quad \boldsymbol{\eta}^l \le \boldsymbol{\eta} \le \boldsymbol{\eta}^u
\end{aligned}
\tag{5.32}
$$

This simultaneous design and control formulation was coded and solved using the Genetic Algorithm (GA) method in MATLAB for the different scenarios considered in this work. At each optimization iteration, a linear discrete state-space model (as shown in (5.6)) obtained from $\mathbf{J}$ and evaluated around the nominal conditions defined by $\boldsymbol{\kappa}_{WW}$ is obtained and used by the MPC to estimate the control actions $\mathbf{\Delta u}$ needed to maintain the system within limits in the presence of stochastic fluctuations in the disturbances. The linear MPC model was obtained using Taylor Series expansion methods; however conventional systems identification methods can also be implemented in the present scheme to obtain a linear process model. To calculate the SB-WCV indexes (ψ_z^*) needed to evaluate the constraints and the terms in the cost function, the nonlinear closed-loop process model $\mathbf{J}_{\text{closed}}$, which consists of $\mathbf{J}$ (Equations (5.16)-(5.25)) engaged with the MPC algorithm (5.6), is simulated with *N* realizations in the disturbances (w_i, s_i and β_i), to obtain *N* dynamic responses for each process constraint formulated in (5.31), as well as for the input (w_p, fk) and the output variables (β, s) that are used to calculate the operational and dynamic performance costs. From each response to a single disturbance realization, the worst-case deviation, which may be the highest or lowest value according to the formulations presented above, is recorded to yield a set of *N* worst-case values. For example, for the minimum purge-to-recycled flow ratio constraint, a set of *N* lowest values obtained from the system's responses to the disturbances was obtained ($\boldsymbol{\psi}_{\min(c1)} \in \Re^{1\times N}$). This

set is fit to a lognormal distribution function ($\mathbf{g}(\boldsymbol{\psi}_{\min(c1)})$). The SB-WCV index ($\psi^*_{\min(c1)}$) is obtained by evaluating $\mathbf{g}(\boldsymbol{\psi}_{\min(c1)})$ at the given probability level assigned by the user for that particular constraint ($\mathrm{Pb}_{\min(c1)}$). The rest of SB-WCV indexes are estimated in a similar fashion and then used to evaluate either the process constraints or some of the economic costs in the objective function shown in problem (5.32). In addition, the nominal stability criterion is implemented on $\mathbf{J}_{\text{closed}}$ at each optimization step to ensure local stability. The aim of optimization problem (5.32) is to select the design variables ($\boldsymbol{\kappa}_{WW}$) and MPC controller tuning ($\boldsymbol{\Lambda}_{WW}$) that will yield a feasible solution, with the least (minimum) plant costs. Next, a few scenarios tested with the proposed approach to obtain the optimal design and control for the wastewater plant case study are presented.

5.2.1 Scenario A: Disturbance in the inlet flow rate (w_i)

In the first scenario, the inlet flow rate (w_i) is assumed to be a stochastic disturbance that follows a Gaussian (normal) distribution with standard deviation $\sigma_{wi} = 70$ m^3/h and mean (nominal) value of $\overline{w}_i = 1492$ m^3/h. The other two disturbances were assumed to remain constant and equal to their corresponding nominal (steady-state) operating values ($\overline{s}_i = 366$ mg/l, $\overline{\beta}_i = 80$ mg/l). In this scenario, each process constraint needs to be satisfied 50% of the time, i.e., Pb_h was set to 0.5 for each of the process constraints shown in (5.31). Similarly, the SB-WCV indexes for the maximum biomass concentration (ψ^*_{β}), substrate concentration (ψ^*_{s}), turbine speed (ψ^*_{fk}), and purge flowrate ($\psi^*_{w_p}$), which are needed to evaluate the cost function terms in (5.32), will also be evaluated at Pb=0.5. A set of $N = 100$ disturbance time-dependent realizations that fits the probability description specified w_i were used to simulate the closed-loop nonlinear process model $\mathbf{J}_{\text{closed}}$ for each set of decision variables $\boldsymbol{\eta}_{WW}$ selected by the optimization algorithm used to solve problem (5.32). The disturbance realizations for q_i were generated randomly (at each optimization step) using MC sampling techniques. The results obtained from the simulations were used to compute the SB-WCV indexes for the process constraints and the process time-dependent process variables that appear in the cost function in (5.32) following the procedure explained above. The feasible and stable optimal process design and MPC control scheme obtained for this scenario is presented in Table 5.2 (Scenario-A).

Table 5.2 Optimal design and control schemes.

	Optimal sequential design w_i ~N(1492,70) s_i=366 mg/L β_i =80 mg/L (Dynamically infeasible)	**Scenario-A** (MPC) w_i ~N(1492,70) s_i=366 mg/L β_i =80 mg/L	**Scenario-B1** (MPC) w_i ~N(1492,70) s_i ~N(366,20) β_i =80 mg/L	**Scenario-B2** (PI) w_i ~N(1492,70) s_i ~N(366,20) β_i =80 mg/L	**Scenario-C1** (MPC) w_i ~N(1492,70) s_i ~N(366,20) β_i =80 mg/L	**Scenario-C2** (PI) w_i ~N(1492,70) s_i ~N(366,20) β_i =80 mg/L	**Scenario-D** (MPC) w_i ~U(1268,1716) s_i ~U(312,422) β_i ~U(68,92)
Decision Var.							
$\overline{w}_2$	458.41	1507.00	532.26	804.90	555.82	380.96	1161.90
$\overline{w}_p$	13.75	46.64	25.95	35.80	36.59	20.04	39.83
$\overline{fk}$	0.05	0.87	0.95	0.30	0.98	0.26	0.55
V_b	4458.70	8414.80	8875.40	9109.90	8766.30	11397.49	9700.50
A_{cl}	4445.20	3278.40	3406.50	3309.80	3708.30	4819.49	3503.20
Γ_{w2}	--	8.94	3.11	$Kc_{w2-\beta}$ =3.20	3.61	$Kc_{w2-\beta}$ =4.86	0.70
Γ_{wp}	--	9.32	9.06	$Kc_{wp-\beta}$ =0.20	9.06	$Kc_{wp-\beta}$ =0.43	3.63
Γ_{fk}	--	0.48	1.66	Kc_{fk-c} = 0.80	1.66	Kc_{fk-c} = 1.29	2.10
Ω_s	--	3.178	1.85	$\tau_{I_{w2-\beta}}$ = 4.90	1.85	$\tau_{I_{w2-\beta}}$ = 7.39	1.07
Ω_β	--	0.330	11.57	$\tau_{I_{w_p-\beta}}$ =21.50	12.95	$\tau_{I_{w_p-\beta}}$ = 3.04	0.10
Ω_{co}	--	0.020	0.32	$\tau_{I_{fk-c}}$ = 1.20	1.32	$\tau_{I_{fk-c}}$ = 1.93	2.99
Costs ($/yr)							
CC_{WW}	4.13E+06	5.92E+06	6.22E+06	6.32E+06	6.27E+06	8.16E+06	6.72E+06
OC_{WW}	1.21E+04	4.25E+04	5.527E+04	3.27E+04	6.26E+04	2.116E+04	3.555E+04
DC_{WW}	--	5.79E+05	1.21E+06	1.26E+06	1.177E+06	9.40E+05	1.59E+06
Total costs	4.14E+06	6.54E+06	7.49E+06	7.61E+06	7.51E+06	9.12E+06	8.34E+06

A bioreactor volume of 8414.8 m^3 and a clarifier cross-sectional area of 3278.4 m^2 were selected as the optimal design that complies with the process constraints considered for this scenario in approximately 50% of the time, i.e. Pb_h=0.5. To validate this result, 1,000 disturbance realizations in the inlet flow rate (w_i ~N(1492,70)) were generated and used to simulate the nonlinear process model (Equations (5.16)-(5.25)) and the MPC algorithm (5.6) using the process design parameters and MPC weights obtained for this scenario (Table 5.2, Scenario-A). Figure 5.4 displays a frequency histogram of the worst-case realizations identified for the maximum substrate concentration (s), which was the

only active constraint identified for the present process design and MPC-based control configuration. As shown in this Figure, approximately 50% of the time the substrate concentration exceeds the constrained limit of 58 mg/L, which agrees with the restriction imposed for that constraint, i.e., Pb_s=0.5. The rest of the constraints considered for this scenario remained within their corresponding operational limits at all times in the presence of changes in the feed flow rate, w_i.

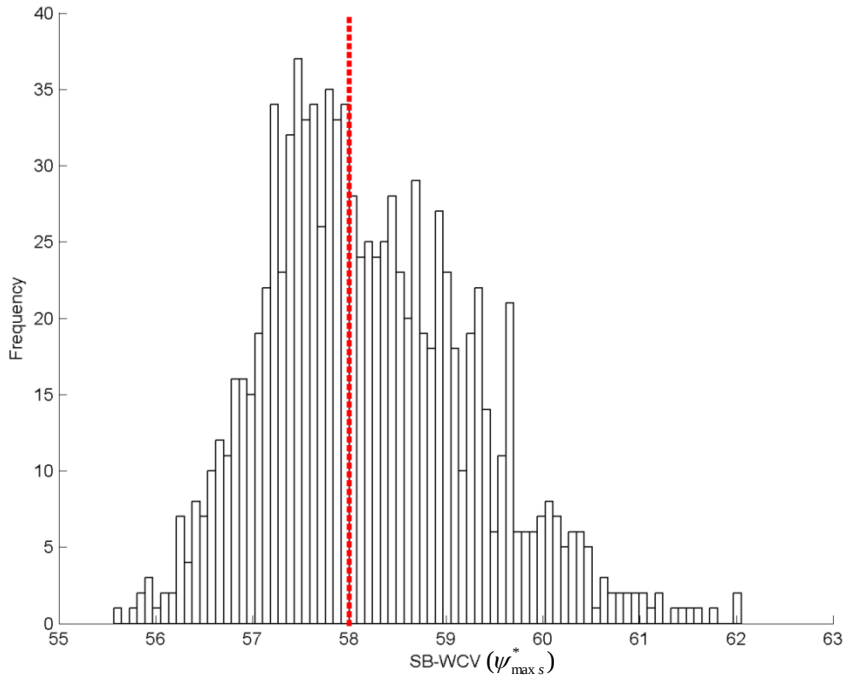

Figure 5.4 Frequency histogram of the SB-WCV distribution of organic substrate concentration (s), Pb=0.5. Dashed line represents the maximum constraint limit.

In order to compare the results obtained for the present scenario, a sequential optimal steady-state process design followed by the optimal tuning of an MPC controller was considered. In this case, the steady-state design optimization function to be minimized is the addition of the plant's capital costs (CC_{WW}) and the plant's operating costs (OC_{WW}) evaluated at steady-state. As shown in Table 5.2 (Optimal sequential design), the steady-state design specifies a bioreactor volume and a clarifier cross-sectional area that are 50% and 35% smaller than those obtained by the present scenario (Table 5.2, Scenario-A). To perform the controllability analysis, problem (5.32) was solved under the

assumption that the process design parameters obtained from the optimal steady-state design ($\boldsymbol{\kappa}_{WW}$) remained fixed in the calculations, i.e., only the weights of the MPC ($\boldsymbol{\Lambda}_{WW}$) were considered as decision variables in problem (5.32). The implementation of such optimal MPC tuning strategy was not able to return a feasible solution. The volume of the bioreactor has an inverse relationship with the substrate concentration; larger volume means more substrate is removed in the bioreactor and hence lower substrate effluent. The optimal steady-state design provided a small bioreactor volume since it did not take into account the variability of the process inputs (disturbances). Therefore, it was not possible for the MPC control strategy to maintain the effluent substrate concentration below its feasible limit (58 mg/L) in the presence of stochastic time-dependent realizations in the disturbances, giving an infeasible process design. The costs reported in Table 5.2 for the sequential design method correspond to those obtained from the optimal steady-state design formulation.

The analysis performed on this case scenario shows that the sequential design approach returned a process design and control configuration that is 30% less expensive than that specified by the present methodology. However, the sequential design is not dynamically feasible since it does not satisfy the process constraints in the presence of changes in the inlet flow rate w_i as described above. On the other hand, the simultaneous design and control methodology proposed in this work specified a plant's design that remained feasible (up to a 50% chance of compliance) and stable in the presence of sudden (stochastic) fluctuations in w_i. Note that fewer violations in the process constraints can be obtained by setting higher values to the probability of occurrence of the worst-case variability (Pb). The economic costs shown in Table 5.2 for the present scenario indicate that the capital cost (CC) dominates the plant economics ($5.92E+06), followed by the dynamic performance costs (DC), which aims to keep the substrate concentration below the specified maximum ($5.79E+05), whereas the operational costs (OC) are much lower than both capital and dynamic performance costs having no significant effect on the plant's costs ($4.25E+04). The larger bioreactor volume of Scenario A means that it can accommodate more biomass in the system, which is directly used to remove the organic substrates in the inlet stream. This means that the increase in the bioreactor's size provides better control on the substrate in the effluent, which is an active constraint and a key process variable that determines the performance of this process.

5.2.2 Scenario B: Simultaneous disturbance in the inlet's flow rate (w_i) and substrate concentration (s_i)

This scenario considers the simultaneous occurrence of sudden fluctuations in the inlet substrate concentration s_i and the inlet flowrate w_i. The disturbance description for the inlet flow rate is the same used in Scenario A, i.e., w_i ~N(1492,70), whereas the realizations in s_i are assumed to follow a normal probability distribution with mean $\bar{s}_i = 366$ mg/L and standard deviation $\sigma_{si} = 20$ m^3/h, i.e., s_i ~N(366,20). The inlet biomass concentration is assumed constant for this scenario at $\bar{\beta}_i = 80$ mg/L. In this case, the minimum purge-to-recycled flow ratio and maximum substrate concentration ($\psi^*_{\min(c1)}$ and $\psi^*_{\max s}$) were both assigned to a higher probability limit (Pb=0.9973). This means that optimal design and MPC-based control scheme specified by the present scenario need to comply with those two constraints approximately 99.73% of the time. The probability levels for the rest of the constraints as well as the time-dependent variables that appear in the cost function remained at Pb=0.5 as in the previous scenario. In order to compare different control strategies while using the present stochastic-based methodology, this scenario was solved using the MPC control scheme proposed in this work and a conventional multi-loop control structure composed of Proportional-Integral (PI) controllers. The wastewater treatment plant process involves removal of substrate in the inlet using biomass in the bioreactor. The outlet substrate concentration from the clarifier is a critical controlled variable that is required to remain below a certain specification. Also, the biomass concentration in the bioreactor is required to be maintained at a specific target. The transient behaviour of the biomass is sensitive to changes in the inlet stream and therefore will determine the relative performances of PI and MPC based on the degree of variability of this variable from its desired target and its degree of interactions with the other key process variables such as the substrate concentration at the outlet stream.

The results obtained with the MPC-based control scheme are shown in Table 5.2 (Scenario-B1). As shown in this Table, a larger reactor's volume (8875.4 m^3) and clarifier's area (3406.5 m^2) than that obtained for Scenario A were specified because of the additional disturbance considered in the present scenario. From an economic perspective, the additional disturbance increased the capitals costs by about 5% due to increased size of equipment (CC=$6.22E06), almost doubled the dynamic performance costs (DC=$1.21E06), and increased the operational costs by almost 30%

(OC=$5.53E04). The increase in the dynamic performance and operational costs are due to increased variability in the process outputs and in the manipulated variables used by the MPC scheme to maintain the system on target in the presence of simultaneous fluctuations in w_i and s_i, respectively. Figure 5.5 displays the frequency histogram of the worst-case realizations for the two active constraints ($\psi^*_{\min(c1)}$ and $\psi^*_{\max s}$), when the design was simulated for validation using the process design parameters and the MPC weights shown in Table 5.2 for this scenario (Scenario-B1). Note that the constraints comply with the predefined probability levels of 99.73% assigned to these constraints.

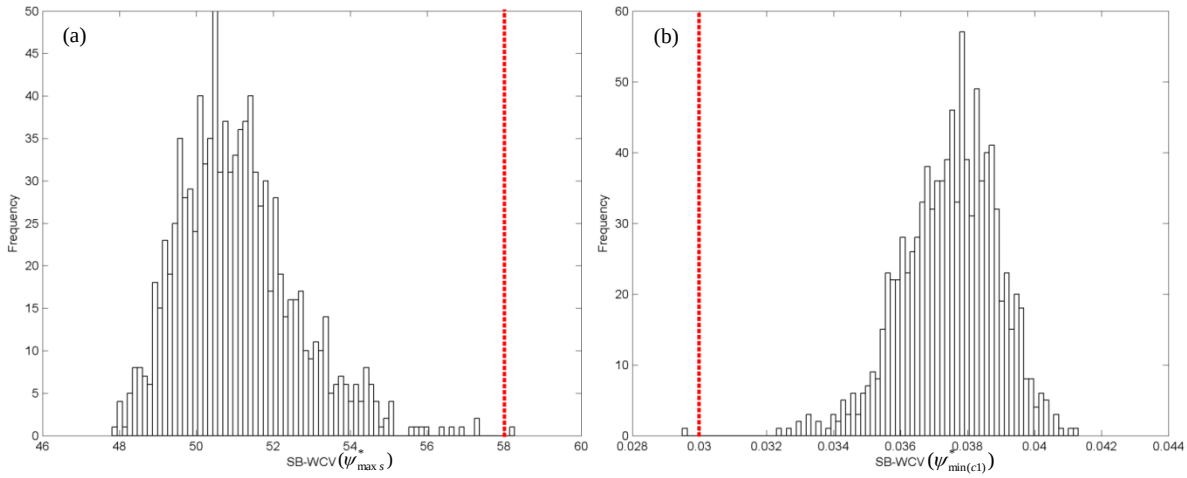

Figure 5.5 Frequency histograms of the SB-WCV distribution for (a) maximum organic substrate concentration and (b) minimum purge-to-recycled flow ratio, with Pr=0.9973. Dashed lines represent the maximum for (a) and minimum for (b) constraint limits.

Next, the MPC algorithm shown in (5.6) and that is used in problem (5.32) was replaced by a multi-loop control scheme composed of three PI control algorithms. In this case, the PI control algorithms will aim to control β, s and c_o independently by making changes in w_2, w_p and c_o, respectively. The control pairing is obtained from the RGA matrix shown in (5.33), which was computed around the steady-state optimal design obtained in the previous scenario. From the RGA matrix, it can be observed that the oxygen concentration controlled by aeration turbines' speed is decoupled from any interactions. However, the relatively large value of RGA for the other two control pairings suggests the presence of dynamic interactions between these control loops.

$$RGA = \begin{array}{c} \\ \beta \\ s \\ c_o \end{array} \begin{array}{c} \begin{array}{ccc} w_2 & w_p & fk \end{array} \\ \begin{bmatrix} 1.869 & -0.869 & 0 \\ -0.869 & 1.869 & 0 \\ 0 & 0 & 1.000 \end{bmatrix} \end{array} \tag{5.33}$$

The optimal design obtained from this control strategy is presented in Table 5.2 (Scenario-B2). Note that the controller tuning parameters for this case are the PI controller gains and integral time constants, i.e., Kc, τ_I. The results show that a multi-loop PI control scheme required a larger bioreactor volume (9109.9 m^3) with a slightly smaller clarifier area (3309.8 m^2) than that obtained using multivariable MPC-based control scheme (Scenario-B1). The larger reactor design specified by the multi-loop control scheme increased the capital costs by about 2% ($6.32E06) with respect to that obtained with the MPC-based control scheme. Although the operational cost is about 40% less for the case of the multi-loop PI control strategy to that obtained by the MPC-based control scheme, this allows the MPC scheme to reduce the variability in the key process outputs, i.e., biomass and substrate concentration, and therefore reduce the capital costs and the process dynamic performance costs, which are two orders of magnitude more significant than the operational costs. Figure 5.6 shows the dynamic responses of biomass concentration when the system is evaluated with 1,000 disturbance realizations, for the designs obtained using both the MPC and the multi-loop PI control strategies. Similarly, Table 5.3 shows the sum of squared errors of biomass and substrate concentrations with respect to their nominal steady-state values for both the MPC and the PI control schemes. As shown in that Table, higher sum of squared error values (especially for the biomass concentration) were obtained for the PI control scheme when compared to the MPC-based control strategy. This can also be observed by comparing Figures 5.6 a) and b). This superior performance observed for the MPC in controlling the key process variables are reflected in the 4% decrease in the MPC dynamic performance costs when compared to that obtained for the PI scenario (Table 5.2, Scenario-B2). Since the process economics in this case study are dominated by the capital and dynamic performance costs, the proposed MPC control-strategy produce a slightly more economically attractive optimal design, i.e., about 1.6% lower than the total costs incurred by the PI control design.

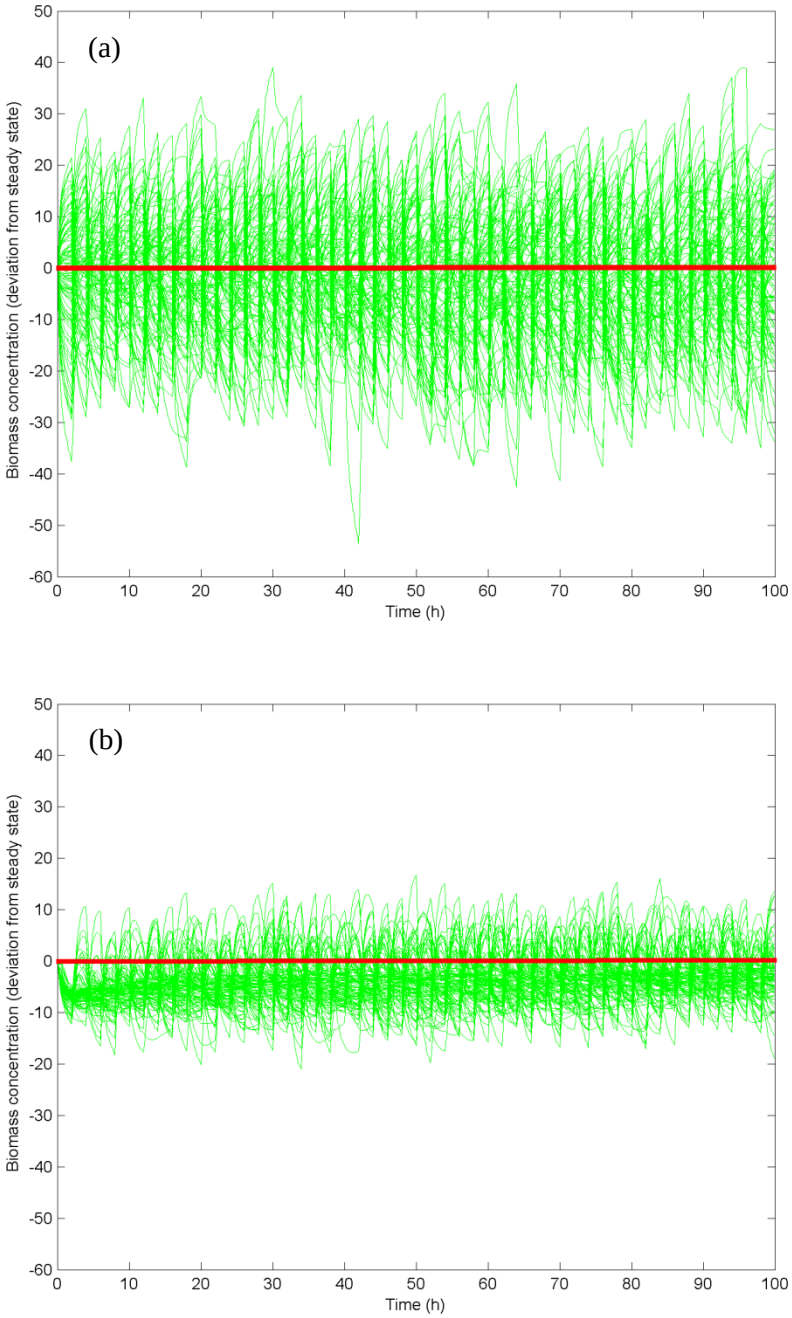

Figure 5.6 Dynamic response of the biomass concentration (a) Multi-loop PI control scheme, and (b) MPC control-strategy.

Table 5.3 Sum of squared errors for the deviation of controlled variables from their steady-state for both biomass and substrate concentrations, between PI and MPC control systems.

Controlled Variable	Sum of squared errors ($x10^3$)			
	Scenario B1 (MPC)	**Scenario B2 (PI)**	**Scenario C1 (MPC)**	**Scenario C2 (PI)**
Biomass	28.653	111.88	26.466	16.035
Substrate	6.7253	7.504	7.1312	4.1819
Oxygen	0.003307	0.000154	0.000717	9.47E-05

5.2.3 Scenario C: Constraints on the biomass concentration

Biomass concentration in the bioreactor, which is a key controlled variable in the present system, is sometimes desired to be maintained within certain upper and lower limits. High biomass concentrations may lead to sedimentation at the bottom of the clarifier tank which will increase operational costs, whereas low biomass concentrations may not be enough to remove the required amount of organic substrate causing an economic penalty to the water treatment plant's owner. In this scenario, biomass concentration is targeted at $\overline{\beta} = 2384$ mg/L with upper and lower limits $\beta^U = 2410$ mg/L and $\beta^L = 2360$ mg/L, respectively. Using the same disturbance specification as in Scenario B, optimal designs using both an MPC scheme (Scenario C1) and a multi-loop PI control strategy (Scenario C2) were calculated using the present simultaneous design and control methodology (Table 5.2). For the MPC scenario (Scenario-C1), these upper and lower limits were explicitly incorporated into the MPC algorithm in (5.6) as constraints on the controlled variables. For the multi-loop PI case, it is not possible to include these additional limits into the control algorithm. Nonetheless, these limits have been added into the main optimization framework (5.32) as process constraints for both cases. As shown in Figure 5.7, the optimal design obtained for Scenario C1 maintained the biomass concentration within its limits in the presence of changes in the inlet flow rate and the substrate inlet concentration. Table 5.2 shows that the capital and operating costs for Scenario C1 are 1% and 13% higher than those obtained for the case of no constraints on the biomass concentration (Table 5.2, Scenario-B1). On the other hand, in order for the multi-loop PI control

scheme to meet the biomass constraint, a bioreactor volume (11,397.5 m^3) and a clarifier area (4819.5 m^2) that are approximately 30% larger than that specified by Scenario C1 are required to accommodate the disturbances affecting the system. The total plant cost is more than 20% higher when using PI controllers as opposed to when implementing an advanced MPC control-strategy. Table 5.3 shows that for this scenario, the PI-based design (Scenario C2) provide slightly better control of the output variables with lower sum of squared errors than the MPC-based design (Scenario C1). However, this improvement in performance is possible at the expense of the 30% larger sized reactor volume and clarifier's area specified by the multi-loop PI control scheme, which caused the total costs to be 20% more than the MPC-based design. The results from Scenarios B and C show the improvements of the current methodology and the potential benefits when incorporating an MPC-based control scheme within a simultaneous design and control methodology.

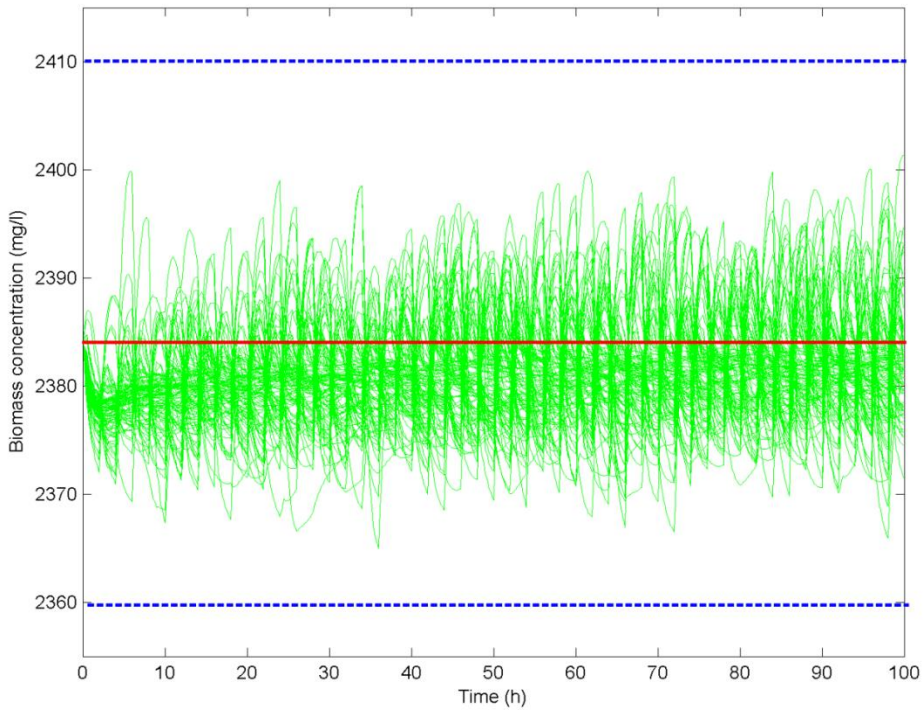

Figure 5.7 Biomass concentration response to disturbances for Scenario C1 with MPC-based control. Dashed lines represent the maximum and minimum constraint limits.

5.2.4 Scenario D: Multiple disturbances with a uniform distribution

This scenario considers the simultaneous occurrence of the three key input variables for this process, i.e., w_i, β_i, s_i. Also, each of these disturbances was assumed to follow a uniform distribution with specific lower and upper limits, i.e.,

$$\begin{aligned} w_i &\sim \mathrm{U}(1268,1716) \\ s_i &\sim \mathrm{U}(312,422) \\ \beta_i &\sim \mathrm{U}(68,92) \end{aligned} \tag{5.34}$$

Using the proposed simultaneous design and control approach, an optimal and feasible design is obtained that can accommodate the above disturbances into the system while maintaining the prescribed constraints (Table 5.2, Scenario-D). A high probability level (Pr=0.9973) was assigned to the two active constraints obtained from the previous scenarios ($\psi^*_{\min(c1)}$ and $\psi^*_{\max s}$) while the rest of the constraints as well as the dynamic performance measures are kept at Pb=0.5. Owing to the description considered for the disturbances, this scenario resulted in a larger plant's size (V_{cl}=9700.5 m^3, A_a=3503.2 m^2) than those obtained from the previous MPC-based scenario designs. The bioreactor volume specified for this scenario is approximately 15% and 9% larger than that obtained for Scenario-A and Scenario-B1, respectively. This increase in the plant's size also increased the plant's capital costs by approximately 12% and 8% with respect to the capital costs specified by Scenario-A and Scenario-B1, respectively.

5.2.5 Computational costs

In addition to the economic and operational analyses described above, the computational costs associated with the present simultaneous design and control methodology are discussed next. In the present approach, the calculation of the SB-WCV indexes (ψ^*_z) represent the highest computational burden since it involves the simulation of the nonlinear closed-loop process model for N disturbance realizations. Besides the computational cost involved in solving for the nonlinear process models, the MPC control actions are obtained from an optimization formulation that needs to be executed at each time interval. Nevertheless, the dynamic responses of the process constraints or process variables to the N disturbance realizations can be performed simultaneously in a parallel fashion. As shown in

Figure 5.2, this parallelization structure in carrying out the SB-WCV calculations reduces the computational costs associated with the present method. To show the benefits of implementing a parallelization technique, a study on the computational time required to perform a single evaluation of the proposed simultaneous design and control problem (5.32) for the Scenario D was conducted using a different number of disturbance realizations *N*, as well as different number of processor cores N_c. This study was performed on an Intel Core i7 3770 CPU @3.4GHz (8GB in RAM) with 4 physical cores and made use of the Parallel Computing Toolbox available in MATLAB™. Figure 5.8 presents the CPU times obtained from running one function evaluation of Scenario D's optimization problem using the proposed stochastic-based simultaneous design and control methodology.

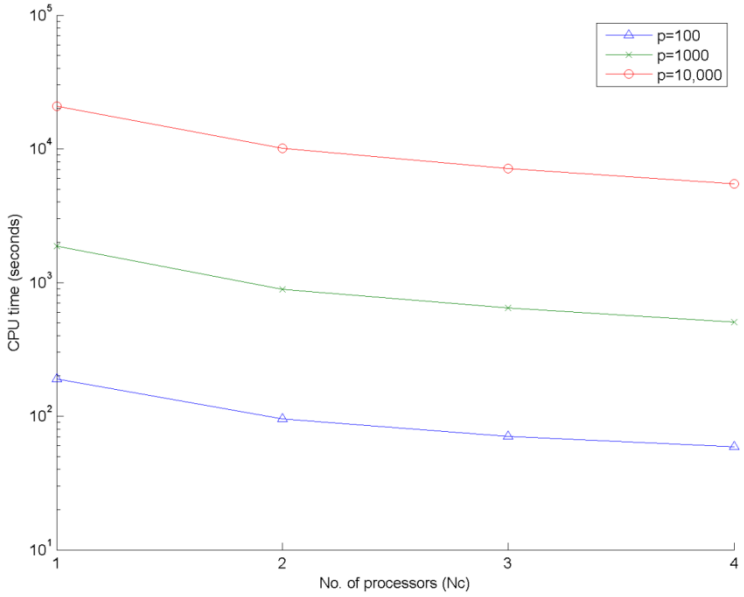

Figure 5.8 Computational times needed for a single function evaluation of problem (32) using different no. of processors.

This Figure shows that the CPU time is directly proportional to the number of disturbance realizations *p* used in the analysis, e.g. for N_c =1, if *N* increases by an order of magnitude from 100 to 1,000, then the CPU time also increases by approximately an order of magnitude, i.e. from 189 to 1,866 sec. The effect of parallelization is represented in Figure 5.8 by the use of different number of processor cores, from 1 (serial calculation) through 4. The trend shown in the Figure is that computational times are

reduced as the number of cores increases because the *p* simulations that need be executed are simultaneously performed in parallel. The current computational study requires the calculation of eight SB-WCV indexes at each optimization step (for constraints and dynamic performance measures).

A single function evaluation takes at most 3 minutes when using *N*=100 (1 core) and goes down to 59 seconds when engaging four processing cores for a total reduction of about 70% in CPU time. The same reduction in computational time is observed when *p* was set to *1000 and 10,000*, respectively. This significant improvement in the efficiency of the algorithm while using computer parallelization techniques allowed for the wastewater treatment plant problem to be solved in about 9 hours using 10 multiple initial conditions. While this cost may be significant, this calculation is performed offline.
A significant decrease in CPU time is observed when using 1 to 2 cores (almost 50% reduction). Figure 5.8 also shows an improvement of about 30% and 20% when going up from 2 to 3 cores and from 3 to 4 cores, respectively. A linear decrease in the CPU time when increasing the number of cores will not be observed because adding more cores also increases communication overheads and memory allocation requirements between the cores. Hence, an exponential decay in the CPU time is typically observed while using computer parallelization techniques [153,154]. However, the improvements observed while using the present case study are significant and shows the potential of the present methodology to address the optimal design of large-scale systems.

Increasing the number of differential equations in the problem will increase the computational costs of the proposed methodology. The actual increase in CPU time will depend on the specific problem to be considered, e.g., the size of the system in terms of the number of inputs, outputs and process constraints, the type for process models to be used (i.e. mechanistic or empirical models), the level of nonlinearity of the proposed process model, the degree of stiffness of the differential process model equations and the control strategy to be implemented in the system. These factors need to be considered for scalability. Nonetheless, the present analysis provides a base case of the wastewater treatment plant as a reference to estimate the computational costs that may be required to address the simultaneous design and control of large-scale systems while using the present methodology.

5.3 Chapter summary

This paper presented a stochastic-based simultaneous design and MPC-based control methodology that considers random stochastic disturbances in the analysis. Flexibility in the design stage is offered to choose between conservative expensive designs that ensure process feasibility at all times, and attractive economical designs that satisfies process constraints at a given user-defined probability limit. The novelties of the proposed method include the use of a multivariable MPC control scheme in the analysis and the computation of a stochastic-based worst-case variability (SB-WCV) index, which is the key calculation performed in this method and is used to evaluate the process constraints and the key time-varying process variables at a given probability of occurrence. The proposed method was implemented for the optimal design and control of an actual wastewater treatment industrial plant. The designs obtained by the present method satisfied the process constraints up to the user-defined probability levels assigned for each constraint. They were also able to maintain dynamic feasibility when the system was subject to single and multiple disturbances. A sequential steady-state design followed by optimal MPC tuning was performed for the present case study and shown to exhibit dynamic infeasibility. A comparison between the use of MPC or multi-loop PI control strategies embedded in the design and control approach has also been studied and presented in this work.

Chapter 6
Conclusions and Recommendations

The importance of optimal process design under uncertainty arises from the fact that they provide more reliable designs that ensure feasible operation of the process even under the presence of uncertain variability in the inputs. In order to apply systematic methods to design large-scale nonlinear chemical systems, there is a need to develop computationally efficient approaches for optimal design under uncertainty. A summary of the findings concluded from this work is presented in Section 6.1; recommendations for future work in this field are discussed in Section 6.2.

6.1 Conclusions

A practical ranking-based novel methodology to address the optimal design and operation of large-scale processes under uncertainty has been developed. The key idea in this method is to approximate the process constraint functions and process outputs using Power Series Expansions (PSE)-based functions. The ease of implementation of this novel method has been demonstrated through several case studies of different sizes: (i) reactor-heat exchanger system, (ii) Tennessee Eastman process, and (iii) a post-combustion CO_2 capture plant. The accuracy of the results obtained when implementing the proposed PSE-based approach can be improved by using higher expansion orders, and yet was shown to be computationally more efficient than traditional methods such as stochastic programming. The computational benefit of the proposed approach has been demonstrated when applied to address the design of large-scale systems such as the Tennessee Eastman and a post-combustion CO_2 capture plant. Solving those large-scale problems using the traditional stochastic programming approach would require the simulation of the actual plant model many times to obtain a probability distribution of the output process constraints. This task needs prohibitive computational times. The ranking-based feature of the approach developed in this work gives the user the flexibility to decide between high or low probabilities of satisfaction for the process constraints. Selection of low probabilities of satisfaction means that lower sized equipment design may be specified, which is more economically attractive at the expense of more violations in those less critical constraints. Thus the proposed

ranking-based method offers the option between conservative designs, which satisfies constraints most of the time, and economically attractive designs that allows for few violations in the constraints.

A study that evaluates the effect of process uncertainty on the optimal design of a post-combustion CO_2 capture plant using the novel ranking-based method developed in this work has been presented. The search for the optimal plant's design is carried out by searching for the sizes of the key process units included in the CO_2 capture plant (e.g., packed column's height and diameters, heat exchanger and condenser areas) that minimizes the process economics in the presence of uncertainty in the flue gas stream conditions. Case studies involving a single uncertain variable and all three (multiple) uncertain variables were studied. The optimal designs obtained under uncertainty yielded in general larger sized plants and needed more utility (i.e., reboiler duty). As a result, these designs were more expensive than the actual plant's design and the design obtained from optimization (without considering uncertainty) with higher operational and capital costs. However, while the present method yielded larger and thus more expensive designs, it ensures that the environmental and operational constraints are satisfied according to the user-defined probability of satisfaction, whereas the original plant base-case design did not meet the CO_2 removal rate target most of the time when operating under uncertainty. Therefore, the designs presented in this study will potentially lead to economic savings since the plant's CO_2 removal rate may not need to be reduced, or the plant itself may not need to be shut down, when changes in the flue gas stream's conditions may occur. Instead, the proposed designs will ensure that the plant can continuously operate at its design specifications since it can accommodate the potential changes that may occur in the fossil-fired power plant's operation due to varying changes in the electricity demands.

A stochastic-based simultaneous design and control methodology for dynamic chemical processes under uncertainty was developed. The key idea is to determine the dynamic variability of the system that will be accounted for in the process design using a stochastic-based worst-case variability (SB-WCV) index. The novelties of the proposed method include the use of a multivariable advanced Model Predictive Control (MPC) scheme in the analysis and the computation of a SB-WCV index, which is the key calculation used to evaluate the process constraints and the key time-varying process variables at a given probability of occurrence. A case study of an actual wastewater treatment industrial plant was used to evaluate the performance of the present methodology. A comparison between the use of MPC and conventional multi-loop PI control strategies embedded in the design

and control approach was also considered. The results have shown that the present MPC-based simultaneous design and control approach provided more economical designs owing to its superior control on the key process variables and thus handled the process constraints better than the multi-loop PI control-base strategy. A study on the computational costs of the simultaneous design and control methodology shows that the present approach can be considered for the optimal design of large-scale systems if multiple cores are available for simulation. Therefore, the present stochastic-based methodology represents a practical approach to address the integration of design and control while using advanced model-based control strategies such as Model Predictive Control.

6.2 Recommendations

The research presented in this work can be extended further to increase its contribution to the field of optimal process design under uncertainty. Some of the recommendations for the way forward of this research are discussed below.

- The ranking-based method developed in this work for optimal process design under uncertainty has proved to be computationally attractive even when dealing with relatively large chemical processes such as the Tennessee Eastman or a post-combustion CO_2 capture plant. The key benefit of the approach was the employment of Power Series Expansion (PSE) functions to replace the actual nonlinear process models with appropriate selection of the PSE's expansion order. Although this work has produced considerably accurate and validated optimal solutions in reasonable computational times, both the Tennessee Eastman and the CO_2 capture plant considered the simultaneous occurrence of up to three uncertain variables (or parameters). The problem of plant-wide process design involving many uncertainties (>10) has not been widely studied. Furthermore, the analysis presented in this work did not consider any integer decisions such as selecting the number of stages in a distillation column, or deciding between the installation of one large heat exchanger as opposed to employing two in series. These structural decisions can add the process synthesis aspect to the optimal design formulation. Thus, to further test the applicability of the proposed approach, a study on plant-wide design of a process plant involving multiple uncertain parameters with process synthesis decisions is recommended. The challenges of the proposed method in dealing with that many uncertain variables (>10) are in the computational burden of computing the sensitivity terms with respect to each uncertain variable.

More terms will appear in the PSE expression as the expansion order is increased to capture the higher nonlinearity. The development of more efficient ways of calculating the sensitivity terms in the PSE expression, such as the use of parallel computing, may need to be employed when dealing with such problems.

- The PSE-based method developed in this work was applied to perform optimal steady-state design processes. The extension of this approach to develop approximation methods to dynamic systems is recommended to gain the same computational benefits in the field of simultaneous design and control. The sensitivity terms in the PSE expression is constant at steady-state for a given equipment design. However, when introducing the time domain in analysis, these sensitivity terms will be also a function of time and thus change at each sampling interval. This means that instead of computing one sensitivity term for each set of design variables, it will have to be computed at different sampling intervals for that specific set of design variables. As a result, more sensitivity computations will be required to obtain a dynamic response of the output variables and constraint functions. Therefore, the use of other approximation methods may be necessary for nonlinear dynamical systems. One such promising approach may be the use of Polynomial Chaos Expansions (PCE), which is a method used to determine propagation of uncertainty in dynamic systems when there is probabilistic uncertainty in the system inputs.

- The study presented in this work on the effect of uncertainty on the design of a post-combustion CO_2 capture plant can be extended to consider more design parameters and uncertainties. In this work, uncertainty was assumed in only three variables of the input flue gas stream. As uncertainty is inherent in every process, the study of its effect on the design and operation of the plant is essential to understand the potential benefits of considering uncertainty in the design stage. Besides the flue gas stream, uncertainty may be considered in the reboiler duty as this study shows that this is a critical variable that affects the CO_2 loading of the recycled lean amine solvent stream. The effect of other uncertainties that could be studied include the heat transfer efficiency parameter of the heating and cooling equipment, condenser duty as well as the kinetic parameters that govern the mass transfer process in the absorber unit. Additional process equipment such as pumps, compressors can be included in the analysis to study its contribution (if any) to mitigate the effect of uncertainties. Thus, a more detailed study of the design of a post-combustion CO_2 capture plant in the presence of uncertainty is recommended for future work.

The study presented in this work made use of a steady-state model. Expanding the study to address the simultaneous design and control of this plant is recommended as part of the future work in this research.

Bibliography

[1] Biegler LT, Grossmann IE, Westerberg AW. Systematic Methods of Chemical Process Design. New Jersey: Prentice-Hall; 1997.

[2] Seider WD, Seader JD, Lewin DR. Product & process design principles: synthesis, analysis and evaluation. New York: Wiley; 2009.

[3] Nuchitprasittichai A, Cremaschi S. Sensitivity of amine-based CO_2 capture cost: The influences of CO_2 concentration in flue gas and utility cost fluctuations. Int J Greenh Gas Control 2013;13:34–43.

[4] Zhang X, Duncan IJ, Huang G, Li G. Identification of management strategies for CO_2 capture and sequestration under uncertainty through inexact modeling. Appl Energy 2014;113:310–7.

[5] Zhang X, Huang G. Optimization of environmental management strategies through a dynamic stochastic possibilistic multiobjective program. J Hazard Mater 2013;246-247:257–66.

[6] Zhang Y, Chen H, Chen C, Plaza JM, Dugas R, Rochelle GT. Rate-Based Process Modeling Study of CO_2 Capture with Aqueous Monoethanolamine Solution 2009:9233–46.

[7] Zhang M, Guo Y. Rate based modeling of absorption and regeneration for CO_2 capture by aqueous ammonia solution. Appl Energy 2013;111:142–52.

[8] Lawal A, Wang M, Stephenson P, Yeung H. Dynamic modelling of CO_2 absorption for post combustion capture in coal-fired power plants. Fuel 2009;88:2455–62.

[9] Mac Dowell N, Shah N. Identification of the cost-optimal degree of CO_2 capture: An optimisation study using dynamic process models. Int J Greenh Gas Control 2013;13:44–58.

[10] Leifsen H. Post-Combustion CO_2 Capture Using Chemical Absorption. M.S.E. Thesis, Norweigan University of Science and Technology; 2007.

[11] Rao AB, Rubin ES. A technical, economic, and environmental assessment of amine-based CO_2 capture technology for power plant greenhouse gas control. Environ Sci Technol 2002;36:4467–75.

[12] Harun N, Nittaya T, Douglas PL, Croiset E, Ricardez-Sandoval LA. Dynamic simulation of MEA absorption process for CO_2 capture from power plants. Int J Greenh Gas Control 2012;10:295–309.

[13] Nittaya T, Douglas PL, Croiset E, Ricardez-Sandoval LA. Dynamic modelling and control of MEA absorption processes for CO_2 capture from power plants. Fuel 2014;116:672–91.

[14] Metz B, Davidson O, de Coninck H, Loos M, Meyer L, editors. Special report on carbon dioxide capture and storage, Intergovernmental Panel on Climate Change. Cambridge University Press; 2005.

[15] Dooley JJ, Davidson CL, Dahowski RT. An Assessment of the Commercial Availability of Carbon Dioxide Capture and Storage Technologies as of June 2009. <http://www.pnl.gov/main/publications/external/technical_reports/PNNL-18520.pdf> [cited 01.05.14].

[16] Bansal V, Perkins JD, Pistikopoulos EN, Ross R, van Schijndel JMG. Simultaneous design and control optimisation under uncertainty. Comput Chem Eng 2000;24:261–6.

[17] Hamid MKA, Sin G, Gani R. Integration of process design and controller design for chemical processes using model-based methodology. Comput Chem Eng 2010;34:683–99.

[18] Mohideen MJ, Perkins JD, Pistikopoulos EN. Optimal design of dynamic systems under uncertainty. AIChE J 1996;42:2251–72.

[19] Ricardez Sandoval LA, Budman HM, Douglas PL. Simultaneous design and control of processes under uncertainty: A robust modelling approach. J Process Control 2008;18:735–52.

[20] Ricardez-Sandoval LA, Budman HM, Douglas PL. Simultaneous design and control of chemical processes with application to the Tennessee Eastman process. J Process Control 2009;19:1377–91.

[21] Sakizlis V, Perkins JD, Pistikopoulos EN. Recent advances in optimization-based simultaneous process and control design. Comput Chem Eng 2004;28:2069–86.

[22] Seferlis P, Georgiadis M. The integration of process design and control. Amsterdam: Elsevier Science; 2004.

[23] Luyben W. Chapter A1 The need for simultaneous design education. In: Seferlis, P., Georgiadis, M. C. (Eds.), The Integration of Process Design and Control, 17. Amsterdam: Elsevier Science; 2004. 264-270.

[24] Malcolm, Polan J, Zhang L, Linninger AA. Integrating Systems Design and Control using Dynamic Flexibility Analysis. AIChE J 2007; 53:2048-61.

[25] Bahri PA, Bandoni JA, Romagnoli JA. Integrated flexibility and controllability analysis in design of chemical processes. AIChE J 1997;43:997–1015.

[26] Swartz C. Chapter B3 the use of controller parametrization in the integration of design and control. . In: Seferlis, P., Georgiadis, M. C. (Eds.), The Integration of Process Design and Control, 17. Amsterdam: Elsevier Science; 2004. 239-263.

[27] Ricardez-Sandoval LA, Budman HM, Douglas PL. Simultaneous Design and Control: A New Approach and Comparisons with Existing Methodologies. Ind Eng Chem Res 2010;49:2822–33.

[28] Ricardez-Sandoval LA, Douglas PL, Budman HM. A methodology for the simultaneous design and control of large-scale systems under process parameter uncertainty. Comput Chem Eng 2011;35:307–18.

[29] Ricardez-Sandoval LA. Optimal design and control of dynamic systems under uncertainty: A probabilistic approach. Comput Chem Eng 2012; 43:91-107.

[30] Birge JR, Louveaux F. Introduction to Stochastic Programming. New York: Springer; 1997.

[31] Liu ML, Sahinidis NV. Optimization in Process Planning under Uncertainty. Ind Eng Chem Res 1996;35:4154–65.

[32] Acevedo J, Pistikopoulos EN. Stochastic optimization based algorithms for process synthesis under uncertainty. Comput Chem Eng 1998;22:647 – 671.

[33] Shapiro A. Monte Carlo sampling methods. In Ruszczynski A., Shapiro A. (Eds.), Handbooks in Operations Research and Management Science: Stochastic Programming, 10. New York: Elsevier Science; 2003. 353-425.

[34] Tawarmalani M, Ahmed S, Sahinidis N V. A finite branch-and-bound algorithm for two-stage stochastic integer programs. Math Program 2004;100:355–77.

[35] Norkin VI, Ch G, Ruszczyliski A. A branch and bound method for stochastic global optimization. 1998;83:425–50.

[36] Takriti S, Birge JR, Long E. A Stochastic Model for the Unit Commitment Problem.IEEE Trans Power Syst 1996;1:1497–508.

[37] Karuppiah R, Grossmann IE. Global optimization of multiscenario mixed integer nonlinear programming models arising in the synthesis of integrated water networks under uncertainty. Comput Chem Eng 2008;32:145–60.

[38] Paules G, Floudas C. Stochastic programming in process synthesis: A two-stage model with MINLP recourse for multiperiod heat-integrated distillation sequences. Comput Chem Eng 1992;16:189-210.

[39] Rooney WC, Biegler LT. Incorporating joint confidence regions into design under uncertainty. Comput Chem Eng 1999;23:1563–75.

[40] Rooney WC, Biegler LT. Design for model parameter uncertainty using nonlinear confidence regions. AIChE J 2001;47:1794–804.

[41] Rooney WC, Biegler LT. Optimal process design with model parameter uncertainty and process variability. AIChE J 2003;49:438–49.

[42] Raspanti CG, Bandoni JA., Biegler LT. New strategies for flexibility analysis and design under uncertainty. Comput Chem Eng 2000;24:2193–209.

[43] Zhu Y, Legg S, Laird CD. Optimal design of cryogenic air separation columns under uncertainty. Comput Chem Eng 2010;34:1377–84.

[44] Charnes A, Cooper WW. Chance-Constrained Programming. Manage Sci 1959;6:73–9.

[45] Wendt M, Li P, Wozny G. Nonlinear Chance-Constrained Process Optimization under Uncertainty. Ind Eng Chem Res 2002;41:3621–9.

[46] Li P, Arellano-Garcia H, Wozny G. Chance constrained programming approach to process optimization under uncertainty. Comput Chem Eng 2008;32:25–45.

[47] Arellano-Garcia H, Wozny G. Chance constrained optimization of process systems under uncertainty: I. Strict monotonicity. Comput Chem Eng 2009;33:1568–83.

[48] Ostrovsky GM, Ziyatdinov NN, Lapteva TV, Zaitsev IV. Optimization of chemical processes with dependent uncertain parameters. Chem Eng Sci 2012;83:119–27.

[49] Ostrovsky GM. Optimization Problem with Normally Distributed Uncertain Parameters. AIChE J 2013;59:2471–84.

[50] Ostrovsky GM, Ziyatdinov NN, Lapteva TV. Optimal design of chemical processes with chance constraints. Comput Chem Eng 2013;59:74–88.

[51] Padurean A, Cormos CC, Agachi PS. Pre-combustion carbon dioxide capture by gas–liquid absorption for Integrated Gasification Combined Cycle power plants. Int J Greenh Gas Control 2012;7:1–11.

[52] Hedin N, Andersson L, Bergström L, Yan J. Adsorbents for the post-combustion capture of CO_2 using rapid temperature swing or vacuum swing adsorption. Appl Energy 2013;104:418–33.

[53] Plaza MG, González AS, Pevida C, Pis JJ, Rubiera F. Valorisation of spent coffee grounds as CO_2 adsorbents for postcombustion capture applications. Appl Energy 2012;99:272–9.

[54] Wang M, Lawal A, Stephenson P, Sidders J, Ramshaw C. Post-combustion CO_2 Capture with Chemical Absorption : A State-of-the-art Review. Chem Eng Res Des 2011;89:1609–24.

[55] Nittaya T, Douglas PL, Croiset E, Ricardez-Sandoval LA. Dynamic Modelling and Evaluation of an Industrial-Scale CO_2 Capture Plant Using MEA Absorption Processes. Ind Eng Chem Res 2014; dx.doi.org/10.1021/ie500190p.

[56] Li H, Yan J, Anheden M. Impurity impacts on the purification process in oxy-fuel combustion based CO_2 capture and storage system. Appl Energy 2009;86:202–13.

[57] Chansomwong A, Zanganeh KE, Shafeen A, Douglas PL, Croiset E, Ricardez-Sandoval LA. Dynamic modelling of a CO_2 capture and purification unit for an oxy-coal-fired power plant. Int J Greenh Gas Control 2014;22:111–22.

[58] Nuchitprasittichai A, Cremaschi S. Optimization of CO_2 Capture Process with Aqueous Amines − A Comparison of Two Simulation − Optimization Approaches. Ind Eng Chem Res 2013;52:10236-243.

[59] Mofarahi M, Khojasteh Y, Khaledi H, Farahnak A. Design of CO_2 absorption plant for recovery of CO_2 from flue gases of gas turbine. Energy 2008;33:1311–9.

[60] Han C, Graves K, Neathery J, Liu K. Simulation of the Energy Consumption of CO_2 Capture by Aqueous Monoethanolamine in Pilot Plant. Energy Environ Res 2011;1:67–80.

[61] Rodríguez N, Mussati S, Scenna N. Optimization of post-combustion CO_2 process using DEA–MDEA mixtures. Chem Eng Res Des 2011;89:1763–73.

[62] J Khakdaman HR, Zoghi AT, Abedinzadegan M, Ghadirian HA. Revamping of gas refineries using amine blends. Int J Eng Sci 2008;19:27–32.

[63] Chang H, Shih C. Simulation and Optimization for Power Plant Flue Gas CO_2 Absorption-Stripping Systems. Sep Sci Technol 2005;40:877–909.

[64] Alie C, Backham L, Croiset E, Douglas PL. Simulation of CO_2 capture using MEA scrubbing: a flowsheet decomposition method. Energy Convers Manag 2005;46:475–87.

[65] Abu-Zahra MRM, Niederer JPM, Feron PHM, Versteeg GF. CO_2 capture from power plants. Int J Greenh Gas Control 2007;1:135–42.

[66] Abu-Zahra MRM, Schneiders LHJ, Niederer JPM, Feron PHM, Versteeg GF. CO2 capture from power plants: Part II. A parametric study of the economical performance based on mono-ethanolamine. Int J Greenh Gas Control 2007;1:37–46.

[67] Halemane KP, Grossmann IE. Optimal process design under uncertainty. AIChE J 1983;29:425–33.

[68] Grossmann IE, Sargent RWH. Optimum design of chemical plants with uncertain parameters. AIChE J 1978;24:1021–8.

[69] Ierapetritou MG, Acevedo J, Pistikopoulos EN. An optimization approach for process engineering problems under uncertainty. Comput Chem Eng 1996;20:703–9.

[70] Bahakim SS, Ricardez-Sandoval LA. Simultaneous design and MPC-based control for dynamic systems under uncertainty: A stochastic approach. Comput Chem Eng 2014;63:66–81.

[71] Sánchez-Sánchez K, Ricardez-Sandoval L. Simultaneous process synthesis and control design under uncertainty: A worst-case performance approach. AIChE J 2013;59:2497–514.

[72] Yang M, Blyth W, Bradley R, Bunn D, Clarke C, Wilson T. Evaluating the power investment options with uncertainty in climate policy. Energy Econ 2008;30:1933 – 1950.

[73] Geske J, Herold J. Carbon capture and storage investment and management in an environment of technological and price uncertainties. Available SSRN 1599564 2010.

[74] Fuss S, Johansson DJA, Szolgayova J, Obersteiner M. Impact of climate policy uncertainty on the adoption of electricity generating technologies. Energy Policy 2009;37:733–43.

[75] Szolgayova J, Fuss S, Obersteiner M. Assessing the effects of CO_2 price caps on electricity investments—A real options analysis. Energy Policy 2008;36:3974 – 3981.

[76] Li MW, Li YP, Huang GH. An interval-fuzzy two-stage stochastic programming model for planning carbon dioxide trading under uncertainty. Energy 2011;36:5677 – 5689.

[77] Han J-H. A multi-objective optimization model for sustainable electricity generation and CO_2 mitigation (EGCM) infrastructure design considering economic profit and financial risk. Appl Energy 2012;95:186 – 195.

[78] Cristóbal J, Guillén-Gosálbez G, Kraslawski A, Irabien A. Stochastic MILP model for optimal timing of investments in CO_2 capture technologies under uncertainty in prices. Energy 2013;54:343–51.

[79] Kim S, Koo J, Lee CJ, Yoon ES. Optimization of Korean energy planning for sustainability considering uncertainties in learning rates and external factors. Energy 2012;44:126–34.

[80] Georgiadis MC, Schenk M, Pistikopoulos EN, Gani R. The interactions of design control and operability in reactive distillation systems. Comput Chem Eng 2002;26:735–46.

[81] Luyben ML, Floudas CA. Analyzing the interaction of design and control—1. A multiobjective framework and application to binary distillation synthesis. Comput Chem Eng 1994;18:933–69.

[82] Alhammadi H, Romagnoli J. Chapter B4 Process design and operation incorporating environmental, profitability, heat integration and controllability considerations. In: Seferlis, P., Georgiadis, M. C. (Eds.), The Integration of Process Design and Control, 17. Amsterdam: Elsevier Science; 2004. 264-270.

[83] Bansal V, Perkins JD, Pistikopoulos EN. A Case Study in Simultaneous Design and Control Using Rigorous, Mixed-Integer Dynamic Optimization Models. Ind Eng Chem Res 2002;41:760–78.

[84] Kookos IK, Perkins JD. An Algorithm for Simultaneous Process Design and Control. Ind Eng Chem Res 2001;40:4079–88.

[85] Lopez-Negrete R, Flores-Tlacuahuac A. Integrated Design and Control Using a Simultaneous Mixed-Integer Dynamic Optimization Approach. Ind Eng Chem Res 2009;48:1933–43.

[86] Kookos IK. Control Structure Selection of an Ideal Reactive Distillation Column. Ind Eng Chem Res 2011;50:11193–200.

[87] Sharifzadeh M, Thornhill NF. Optimal selection of control structure using a steady-state inversely controlled process model. Comput Chem Eng 2012;38:126–38.

[88] Psaltis A, Kookos IK, Kravaris C. Plant-wide control structure selection methodology based on economics. Comput Chem Eng 2013;52:240–8.

[89] Zumoffen D, Basualdo M. Improvements on multiloop control design via net load evaluation. Comput Chem Eng 2013;50:54–70.

[90] Qin SJ, Badgwell TA. A survey of industrial model predictive control technology. Control Eng Pract 2003;11:733–64.

[91] García CE, Prett DM, Morari M. Model predictive control: Theory and practice—A survey. Automatica 1989;25:335–48.

[92] Lee J, Cooley B. Recent advances in model predictive control and other related areas. AIChE Symp Ser 1997; 93:201-16.

[93] Mayne DQ, Rawlings JB, Rao CV, Scokaert POM. Constrained model predictive control: Stability and optimality. Automatica 2000;36:789–814.

[94] Morari M, Lee JH. Model predictive control: past, present and future. Comput Chem Eng 1999;23:667–82.

[95] Lee JH. Model predictive control: Review of the three decades of development. Int J Control Autom Syst 2011;9:415–24.

[96] Huang H, Riggs JB. Comparison of PI and MPC for control of a gas recovery unit. J Process Control 2002;12:163–73.

[97] Stare A, Vrecko D, Hvala N, Strmcnik S. Comparison of control strategies for nitrogen removal in an activated sludge process in terms of operating costs: a simulation study. Water Res 2007;41:2004–14.

[98] Brengel DD, Seider WD. Coordinated design and control optimization of nonlinear processes. Comput Chem Eng 1992;16:861–86.

[99] Chawankul N, Ricardez-Sandoval LA, Budman H, Douglas PL. Integration of Design and Control: A Robust Control Approach Using MPC. Can J Chem Eng 2008;85:433–46.

[100] Francisco M, Vega P, Álvarez H. Robust Integrated Design of processes with terminal penalty model predictive controllers. Chem Eng Res Des 2011;89:1011–24.

[101] Gutierrez G, Ricardez LA, Budman H, Prada C. Integration of Design and Control using an MPC-based superstructure for control structure selection. Preprints of the 18th IFAC World Congress, Milan, Italy 2011:7648–53.

[102] Sanchez-Sanchez KB, Ricardez-Sandoval LA. Simultaneous Design and Control under Uncertainty Using Model Predictive Control. Ind Eng Chem Res 2013;52:4815–33.

[103] Lenhoff AM, Morari M. Design of resilient processing plants—I Process design under consideration of dynamic aspects. Chem Eng Sci 1982;37:245–58.

[104] Nguyen T, Barton GW, Perkins JD, Johnston RD. A condition number scaling policy for stability robustness analysis. AIChE J 1988;34:1200–6.

[105] Palazoglu A, Arkun Y. A multiobjective approach to design chemical plants with robust dynamic operability characteristics. Comput Chem Eng 1986;10:567–75.

[106] Flores-Tlacuahuac A, Biegler LT. Simultaneous mixed-integer dynamic optimization for integrated design and control. Comput Chem Eng 2007;31:588–600.

[107] Sharifzadeh M, Thornhill NF. Integrated design and control using a dynamic inversely controlled process model. Comput Chem Eng 2013;48:121–34.

[108] Gerhard J, Monnigmann M, Marquardt W. Constructive nonlinear dynamics foundations and application to robust nonlinear control. In: Meurer, T., Graichen, K., Gilles, E. D. (Eds.), Control and Observer Design for Nonlinear Finite and Infinite Dimensional Systems 2005; Berlin: Springer, 165-182.

[109] Ricardez-Sandoval LA, Budman HM, Douglas PL. Application of Robust Control Tools to the Simultaneous Design and Control of Dynamic Systems. Ind Eng Chem Res 2009;48:801–13.

[110] Trainor M, Giannakeas V, Kiss C, Ricardez-Sandoval LA. Optimal process and control design under uncertainty: A methodology with robust feasibility and stability analyses. Chem Eng Sci 2013;104:1065–80.

[111] Yuan Z, Chen B, Sin G, Gani R. State-of-the-art and progress in the optimization-based simultaneous design and control for chemical processes. AIChE J 2012; 58:1640-1659.

[112] Ricardez-Sandoval LA., Budman HM, Douglas PL. Integration of design and control for chemical processes: A review of the literature and some recent results. Annu Rev Control 2009;33:158–71.

[113] Sharifzadeh M. Integration of process design and control: A review. Chem Eng Res Des 2013;91:2515–49.

[114] McKay M, Beckman R, Conover W. Comparison of three methods for selecting values of input variables in the analysis of output from a computer code. Technometrics 1979;21:239-245.

[115] Florian A. An efficient sampling scheme: updated latin hypercube sampling. Prob Eng Mech 1992;7:123-130.

[116] Hammersley J, Morton K. A new Monte Carlo technique: antithetic variates. Proc Cambridge Phil Soc 1956;52:449-474.

[117] Freimer M, Linderoth J, Thomas D. The impact of sampling methods on bias and variance in stochastic linear programs. Comput Optim Appl 2012;51:51-75.

[118] Johnson M, Moore L, Ylvisaker D. Minimax and maximin distance designs. J Stat Plan Inf 1990;26:131-148.

[119] Diwekar UM, Kalagnanam JR. Efficient sampling technique for optimization under uncertainty. AIChE J 1997;43:440–7.

[120] Kim K-J, Diwekar UM. Efficient Combinatorial Optimization under Uncertainty. 2. Application to Stochastic Solvent Selection. Ind Eng Chem Res 2002;41:1285–96.

[121] Giannakoudis G, Papadopoulos AI, Seferlis P, Voutetakis S. Optimum design and operation under uncertainty of power systems using renewable energy sources and hydrogen storage. Int J Hydrogen Energy 2010;35:872–91.

[122] Mitra K. Multiobjective optimization of an industrial grinding operation under uncertainty. Chem Eng Sci 2009;64:5043–56.

[123] Li B, Peng L, Ramadass B. Accurate and efficient processor performance prediction via regression tree based modeling. J Syst Architect 2009;55:457-467.

[124] Gramacy R. tgp: an R package for Bayesian nonstationary, semiparametric nonlinear regression and design by treed Gaussian process models. J Stat Softw 2007;19.

[125] Downs JJ, Vogel EF. A plant-wide industrial process control problem. *C*omput Chem Eng 1993;17:245-255.

[126] Bahakim SS, Rasoulian S, Ricardez-Sandoval LA. Optimal design of large-scale chemical processes under uncertainty: A ranking-based approach. AIChE J 2014: doi 10.1002/aic.

[127] Pintarič ZN, Kasaš M, Kravanja Z. Sensitivity analyses for scenario reduction in flexible flow sheet design with a large number of uncertain parameters. AIChE J 2013;59:2862–71.

[128] Maly T, Petzold L. Numerical methods and software for sensitivity analysis of differential-algebraic systems. Appl Numer Math. 1996; 20: 57-79.

[129] Nocedal J, Wright SJ. Numerical optimization (2nd edition). New York: Springer; 2006..

[130] Grossmann IE, Halemane KP. Decomposition strategy for designing flexible chemical plants. AIChE J 1982; 28:686-694.

[131] Halton JH. On the efficiency of certain quasi-random sequences of points in evaluating multi-dimensional integrals. Numer Math 1960;2:84–90.

[132] Hammersley JM. Monte Carlo Methods For Solving Multivariable Problems. Ann N Y Acad Sci 1960;86:844–74.

[133] Ricker NL. Optimal steady-state operation of the Tennessee Eastman challenge process. Comput Chem Eng 1995;19:949–59.

[134] Dugas ER. Pilot Plant Study of Carbon Dioxide Capture by Aqueous Monoethanolamine. M.S.E. Thesis, University of Texas at Austin; 2006.

[135] Taylor R, Krishna R. Multicomponent Mass Transfer. New York: Wiley; 1993.

[136] Aroonwilas A. Effects of operating and design parameters on CO_2 absorption in columns with structured packings. Sep Purif Technol 2001;24:403–11.

[137] Versteeg GF, Van Dijck LAJ, Van Swaaij WPM. On The Kinetics Between CO_2 And Alkanolamines Both In Aqueous And Non-Aqueous Solutions. An Overview. Chem Eng Commun 1996;144:113–58.

[138] Hikita H, Asai S, Ishikawa H, Honda M. The kinetics of reactions of carbon dioxide with monoethanolamine, diethanolamine and triethanolamine by a rapid mixing method. Chem Eng J 1977;13:7–12.

[139] Guthrie KM. Data and techniques for preliminary capital cost estimating. Chem Eng 1969; 76: 114-42.

[140] Economic Indicators: Marshall and Swift Equipment Cost Index. Chemical Engineering, 2011;68.

[141] Aroonwilas A, Tontiwachwuthikul P. Mechanistic model for prediction of structured packing mass transfer performance in CO_2 absorption with chemical reactions. Chem Eng Sci 2000;55:3651–63.

[142] Lawal A, Wang M, Stephenson P, Koumpouras G, Yeung H. Dynamic modelling and analysis of post-combustion CO_2 chemical absorption process for coal-fired power plants. Fuel 2010;89:2791–801.

[143] Maciejowski, JM. Predictive Control with Constraints. London: Prentice Hall; 2002.

[144] Loeblein C, Perkins JD. Structural design for on-line process optimization: I. Dynamic economics of MPC. AIChE J 1999;45:1018–29.

[145] Marsaglia G, Tsang W. The ziggurat method for generating random variables. J Stat Softw 2000; 5:1-7.

[146] Montgomery DC, Runger GC. Applied Statistics and Probability for Engineers. New York: Wiley; 2010.

[147] Kookos IK. Optimal Operation of Batch Processes under Uncertainty: A Monte Carlo Simulation-Deterministic Optimization Approach. Ind Eng Chem Res 2003;42:6815–22.

[148] Peters M, Timmerhaus K, West R. Plant design and economics for chemical engineers. New York: McGraw Hill; 1968.

[149] Towler G, Sinnott R. Chemical engineering design: principles, practice, and economics of plant and process design. Oxford: Elsevier; 2012.

[150] Holland J. Adaptation in natural and artificial systems: an introductory analysis with applications to biology, control, and artificial intelligence Cambridge: MIT Press; 1992.

[151] Sahinidis N V. Optimization under uncertainty: state-of-the-art and opportunities. Comput Chem Eng 2004;28:971–83.

[152] Gutiérrez G, Vega P. Integrated design of activated sludge process taking into account the closed loop controllability. Proc ESCAPE 10 2000;63-69..

[153] Choy R, Edelman A. Parallel MATLAB: Doing it Right. Proc IEEE 2005;93:331–41.

[154] Dietrich S, Boyd ID. Scalar and Parallel Optimized Implementation of the Direct Simulation Monte Carlo Method. J Comput Phys 1996;126:328–42.

Appendix

The contents of Chapter 3 has been published in the AIChE Journal [126]. The author of this thesis is the first and main author of this publication and contributed all the technical aspects of the work as well as writing the manuscript. Permission to reuse the content of the article has been granted by the publisher (see Figure A.1).

The contents of Chapter 5 has been published in the Computers &Chemical Engineering [70]. The author of this thesis is the first and main author of this publication and contributed all the technical aspects of the work as well as writing the manuscript. Permission to reuse the content of the article has been granted by the publisher (see Figure A.2).

JOHN WILEY AND SONS LICENSE
TERMS AND CONDITIONS

Jul 18, 2014

This is a License Agreement between Sami Bahakim ("You") and John Wiley and Sons ("John Wiley and Sons") provided by Copyright Clearance Center ("CCC"). The license consists of your order details, the terms and conditions provided by John Wiley and Sons, and the payment terms and conditions.

All payments must be made in full to CCC. For payment instructions, please see information listed at the bottom of this form.

License Number	3431951038284
License date	Jul 18, 2014
Licensed content publisher	John Wiley and Sons
Licensed content publication	AIChE Journal
Licensed content title	Optimal design of large-scale chemical processes under uncertainty: A ranking-based approach
Licensed copyright line	© 2014 American Institute of Chemical Engineers
Licensed content author	Sami S. Bahakim,Shabnam Rasoulian,Luis A. Ricardez-Sandoval
Licensed content date	Jun 11, 2014
Start page	n/a
End page	n/a
Type of use	Dissertation/Thesis
Requestor type	Author of this Wiley article
Format	Print and electronic
Portion	Full article
Will you be translating?	No
Title of your thesis / dissertation	Efficient Ranking-Based Methodologies in the Optimal Design of Large-Scale Chemical Processes Under Uncertainty
Expected completion date	Aug 2014
Expected size (number of pages)	116
Total	0.00 USD
Terms and Conditions	

Figure A.1 License agreement copy from John Wiley and Sons to reuse content of article.

ELSEVIER LICENSE
TERMS AND CONDITIONS

Jul 18, 2014

This is a License Agreement between Sami Bahakim ("You") and Elsevier ("Elsevier") provided by Copyright Clearance Center ("CCC"). The license consists of your order details, the terms and conditions provided by Elsevier, and the payment terms and conditions.

All payments must be made in full to CCC. For payment instructions, please see information listed at the bottom of this form.

Supplier	Elsevier Limited The Boulevard,Langford Lane Kidlington,Oxford,OX5 1GB,UK
Registered Company Number	1982084
Customer name	Sami Bahakim
Customer address	230-350 Columbia St W Waterloo, ON N2L 6P2
License number	3431950916605
License date	Jul 18, 2014
Licensed content publisher	Elsevier
Licensed content publication	Computers & Chemical Engineering
Licensed content title	Simultaneous design and MPC-based control for dynamic systems under uncertainty: A stochastic approach
Licensed content author	Sami S. Bahakim,Luis A. Ricardez-Sandoval
Licensed content date	17 April 2014
Licensed content volume number	63
Licensed content issue number	None
Number of pages	16
Start Page	66
End Page	81
Type of Use	reuse in a thesis/dissertation
Portion	full article
Format	both print and electronic
Are you the author of this Elsevier article?	Yes
Will you be translating?	No
Title of your thesis/dissertation	Efficient Ranking-Based Methodologies in the Optimal Design of Large-Scale Chemical Processes Under Uncertainty
Expected completion date	Aug 2014
Estimated size (number of	116

Figure A.2 License agreement copy from Elsevier to reuse content of article.